Summer 8-7-2020

Snow-Albedo Feedback in Northern Alaska: How Vegetation Influences Snowmelt

Lucas C. Reckhaus
CUNY Hunter College

Snow-Albedo Feedback in Northern Alaska: How Vegetation Influences Snowmelt

By

Lucas C. Reckhaus

Submitted in partial fulfillment
of the requirements for the degree of
Master of Science Geoinformatics, Hunter College
The City University of New York

2020

August 6th, 2020

Dr. Wenge Ni-Meister
Thesis Sponsor

August 6th, 2020

Dr. Sean Ahearn
Second Reader

Reviewers' Page

City University of New York

Hunter College, 2020

Department of Geography and Environmental Science

MS Geoinformatics, Master's Thesis

By Lucas C. Reckhaus

Supervisor: Dr. Wenge Ni-Meister

Second Reader: Dr. Sean Ahearn

Abstract

This paper investigates how the snow-albedo feedback mechanism of the arctic is changing in response to rising climate temperatures. Specifically, the interplay of vegetation and snowmelt, and how these two variables can be correlated. This has the potential to refine climate modelling of the spring transition season. Research was conducted at the ecoregion scale in northern Alaska from 2000 to 2020. Each ecoregion is defined by distinct topographic and ecological conditions, allowing for meaningful contrast between the patterns of spring albedo transition across surface conditions and vegetation types. The five most northerly ecoregions of Alaska are chosen as they encompass three distinct geographic zones: the arctic permafrost, the Brooks Range which forms its southern boundary, and continental boreal forests and highlands beyond this. Findings indicate: 1) surface temperatures warming across all regions. 2) Albedo loss occurring earlier and faster. 3) vegetation growth occurring earlier and stronger. 4) A comparison of BSA and NDVI data shows an inverse relationship between the rate of snowmelt and the texture of a surface—influenced most heavily by vegetation cover. Overall, the snow albedo feedback mechanism of northern Alaska is in precipitous decline. This is reducing the process by which the terrestrial arctic contributes to the earth's cooling.

For the Hunter women in my family:

Claire,
Sylvia,
Jessica,

and Herb—who loved them all.

Forewords

There where the mighty mountains bare their fangs unto the moon,
There where the sullen sun-dogs glare in the snow-bright, bitter noon,
And the glacier-glutted streams sweep down at the clarion call of June.

There where the livid tundras keep their tryst with the tranquil snows;
There where the silences are spawned, and the light of hell-fire flows
Into the bowl of the midnight sky, violet, amber and rose.

There where the rapids churn and roar, and the ice-floes bellowing run;
Where the tortured, twisted rivers of blood rush to the setting sun—
I've packed my kit and I'm going, boys, ere another day is done.

—Robert W. Service (The Heart of the Sourdough, 1907)

Arctic Coastal Plain, Ecoregion 101, Looking eastward toward the Sag River off the Dalton Highway. 2011 Google Maps

The Arctic Foothills, Ecoregion 102, Looking eastward off the Dalton Highway. 2011 Google Maps

The Brooks Range, Ecoregion 103, Looking north off the Dalton Highway. 2011 Google Maps

Interior Forested Lowlands and Uplands, Ecoregion 104, Chatanika River. 2020 Google Maps

Interior Highlands, Ecoregion 105, Looking west off the Top of the World Highway. 2019 Google Maps

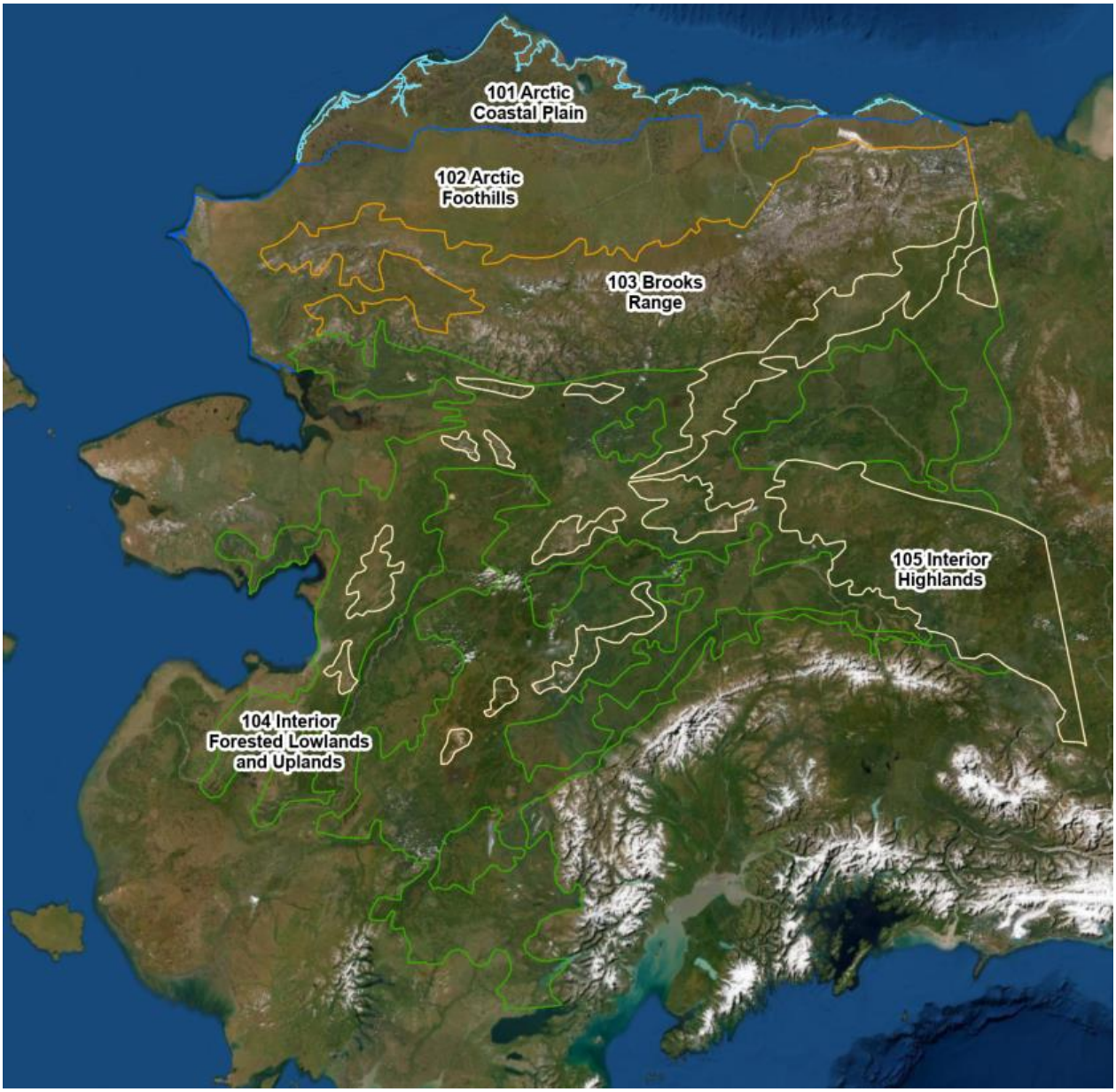

Figure 1: Five Northernmost Ecoregions of Alaska, EPA 2017

Table of Contents

List of Figures

List of Abbreviations

API—Application Program Interface

BSA—Black Sky Albedo

Eco-101—Arctic Coastal Plain

Eco-102—Arctic Foothills

Eco-103—Brooks Range

Eco-104—Interior Forested Lowlands and Uplands

Eco-105—Interior Highlands

EM—Electromagnetic

EPA—Environmental Protection Agency

GGE—Google Earth Engine

GIS—Geographic Information System

LiDAR—Light Detection and Reflection

LSA—Land Surface Albedo

MODIS—Moderate Resolution Imaging Spectroradiometer

NDVI—Normalized Difference Vegetation Index

PAF—Planetary Albedo Feedback

SAF—Snow Albedo Feedback

SCE—Snow Cover Extent

SNC—Snow Contrast

TEM—Temperature Changes

USGS – United States Geological Survey

1. Introduction

What is Albedo?

Remote sensing is based on the sun's electromagnetic (EM) energy. This is the radiation emitted by the sun's burning liquid plasma core. The combustion process is known as a "dynamo" and is to this date not yet fully understood. The process emits photon particles. These are massless, and travel as wave patterns out across the universe. Depending on the frequency at which these photons travel—determined by a temperature-to-energy ratio—different types of radiation are emitted. Most crucially for humans, visible light is created. Simultaneously are radio waves, micro-waves, infra-red, ultra-violet, x-ray, and gamma-rays (NASA Goddard Fight Center, 2013). Together, this makes EM radiation the most important life-giving source known to exist. The earth's constant exposure to EM energy presents a valuable scientific window through which to view the world, as every surface absorbs and reflects the EM spectrum differently. By using a lens that isolates for a specific EM frequency, insights are revealed otherwise unseen to the naked eye. Through the use of dedicated satellites this kind of information is now available.

Albedo is a way of measuring this interaction between terrestrial substances and EM energy. It describes how reflective a surface is to EM radiation. Data is measured on a scale of zero to one. Zero represents a surface with the characteristics of a black-body, absorbing all energy. One represents a perfect mirror, reflecting all energy. In nature, the closest thing to this is the albedo of pure snow, with an albedo of around 0.9. This simple concept has wide-ranging

applications, the foremost of which is its ability indicate how the global warming process is affecting the polar ice-caps (Kashiwase, H., Ohshima, K.I., Nihashi, S. *et al, 2017*). Put simply, as snow and ice melt, albedo decreases. This causes the region to absorb more EM radiation, which contributes to rising temperatures, causing melting snow, and so on in perpetuity. This cycle diminishes what is known as a region's *energy budget* (Hall, 2002). This is the overall ratio of the earth's energy absorption versus reflection and emission. At a global scale, the data to date shows high degrees of regional variation that does not currently point to a cohesive trend (Figure 1).

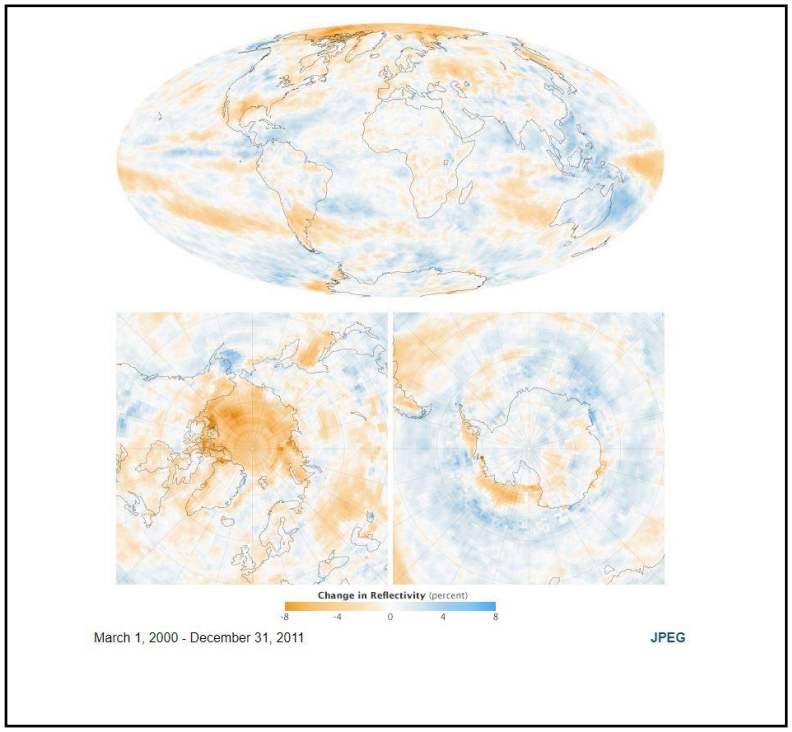

Figure 2: Global Albedo Change 2000-2011; NASA Earth Observatory, 2019

As global albedo data continues to be collected and observed for trends, regional albedo studies in pursuit of more accurate energy budget models are required. This extends beyond the poles to urban and rural settings as well.

First Mention—Johann Heinrich Lambert

The concept of albedo is credited to the famed enlightenment-era Swiss polymath Johann Heinrich Lambert. In *Photometria* (1760), he outlined what would become the founding principles of visual optics, describing how light travels in straight lines, the relationship of light to the mediums it passes through, and how to calculate illumination. Lambertian reflectance is known as the ideal diffuse reflectance (matt) surface, in which all light is equally reflected in different directions. He introduced the concept of Albedo (*latin*; "whiteness") to describe the overall measure of this diffuse reflectivity for a given surface (Coakley, 2003).

White Sky vs. Black-sky

There are two types of albedo. The one described by Lambert is today known as *white-sky albedo*, this describes a diffuse reflective effect, in which the incident beam of light is reflected off a surface in multiple directions, scattering the original beam. Visually this is the effect matt paint produces. White-sky albedo is not calculated for a single input ray of light. Instead it measures how much the surface scatters a ray of incoming light from any direction. Therefore, it is not influenced by solar zenith angle (Coakley, 2003). As a general rule an albedo reading refers to the full spectrum of EM radiation. A reading specific to a wavelength is known as *spectral albedo*.

The other is *black-sky albedo* (also known as directional hemispherical albedo). This describes an albedo "in the absence of a diffuse component" (UMass, 2019). In other words, a

scenario in which the beam of light is reflected out as a single ray with the same incidence angle heading in the opposite direction. This is also known as specular or direct reflectance, and is the effect produced by the clear surface of the lake reflecting a mirror image of the sky. Because black-sky albedo is a measurement of a single incidence beam of light, it is measured as a function of solar zenith angle. This means that for a given location, the solar zenith angle is used as the input angle. Therefore, black-sky albedo is sensitive to the location research site.

Measurement Devices & Frequencies

There are two principle dimensions to consider when studying albedo data. The first is time. This pertains to the interval of data collection. This can be as little as seconds (such as in the case of laser point-cloud data), to daily, monthly or annual average measurements. The second is space. This refers to the x, y, and in some cases z dimensions of the data field. Typically, albedo data trends toward the global scale, with individual pixels several hundred meters or larger, and a temporal resolution of several days to weeks. These parameters are dataset specific, and will continue to diversify as more data is collected on this subject.

Different Surface Examples

There are four dominant surface types on the earth today. Water (gas, liquid, solid); vegetation; bare earth/exposed rock; and impervious man-made structures. Of these, water and vegetation cover the majority of the planet, and are uniquely dynamic because they underpin the existence of life on earth as the foundations of every ecosystem.

H20 (water, vapor, solid)

The upper planetary atmosphere of earth has its own albedo, usually around 30 -35 percent. Most of this is the result of cloud cover, which absorbs significant amounts of EM radiation, notably in the infrared range. For this reason, it also changes dramatically over time and space. Terrestrially, fresh snow has the highest albedo of all surface types, scoring somewhere around 0.9 (equivalent to reflecting 90% of EM radiation. Ice is also highly reflective, though it varies between ice on rocks, fresh water, and sea). This demonstrates how the North and South Poles are crucially important as naturally occurring shields to radiation, producing a similar effect to sun screen. In this context the importance of albedo studies and the process of climate change comes into focus. Unlike H20 in its other states, liquid water has a very low albedo, and is sensitive to prolonged unmitigated exposure to EM radiation. This is one explanatory variable for the warming of global ocean temperatures.

Vegetation

Plants use sunlight to drive their process of photosynthesis, whereby they convert light into energy and release oxygen as bi-product. Therefore, by design all types of vegetation yield low albedo. Yet, there remains tremendous variation between plant types and their albedo characteristics. These differences result from the structural features of the plant species in question (Hovi, A., *et al*. , 2019; Kussinen, N., *et al*., 2015). For example, pine and other coniferous trees have small dense leaves and typically a taller and skinnier trunk and limb structure. This contributes to less overall surface area to interact with sunlight, and proportionally more sunlight directly penetrating the needles surface. The effect is a generally low albedo. Deciduous trees

are near opposite. They have broad leaves and wide limb structures. Many of their leaves have glossy membrane surfaces. These elements combined reflect a larger percentage of EM radiation, while the plants are simultaneously absorbing all they need to grow. Additional to consider for deciduous trees is their loss of leaves during half of the year. In such scenarios their albedo will change dramatically between seasons, in a way that a pine species or tree in a year-round temperate climate would not.

Drivers of Albedo Change

Vegetation Structure & Species

Forest structure has been shown to affect albedo, in terms of age, height distribution and species composition (Kussinen, N., et al. 2015). These are all parts of larger natural forest processes. There are different approaches to measuring this data, such as random sampling from the field and supervised or unsupervised classification. An even more granular scale has recently been enabled through the development of Light Detection and Reflection (LiDAR) technologies (Hovi, A., et al. 2019). These datasets are 3D point clouds of the surfaces that interact with a focused laser pulse, from which the exact structure and composition of a surface object can be determined. In this new light, the distinction between individual plant species is possible.

Mixed Vegetation & Snow

The coexistence of vegetation and snow over the same surface itself creates a unique set of albedo circumstances and challenges to measurement. Is the snow fresh and on the top layer of the vegetation? Has it settled onto the ground below? Has it frozen on the leaves petrifying

the forest? Is it thawing quickly and turning into melt-water? All of these are conditions that produce different albedo. In this way the seasonality of albedo studies is apparent (Essery, 2013).

Snow Grain Size & Geometry

At arguably the smallest scale, the individual grain size of the snowflakes will affect the albedo produced, similar to the way the size and shape of a leaf does for vegetation. Therefore, when analyzing snow albedo change, the coarseness of the snow is a variable of consideration.

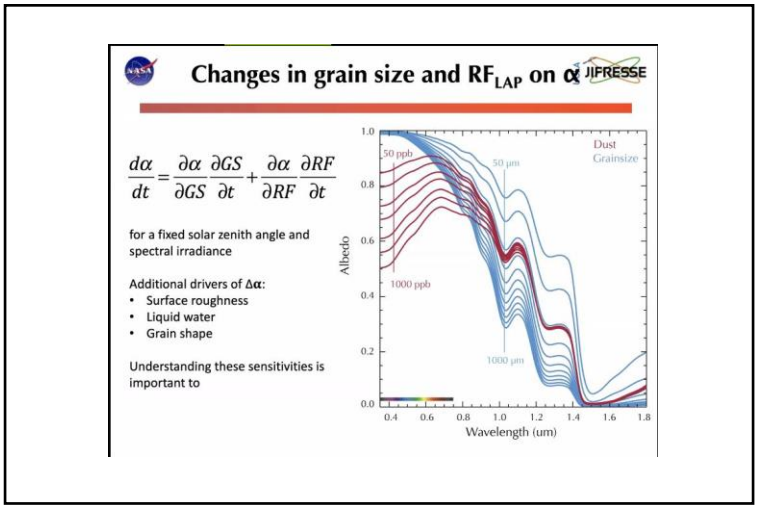

Figure 3: Snow Grain Size and Albedo. (NASA Earth Observatory, 2019)

Albedo, Climate Change & The Earth's Energy Budget.

For these reasons and others, albedo is a useful indicator of climate change. Albedo can be understood as a measure of resilience potential—how well a surface over an area is able to process the continuous EM radiation it is exposed to. This is analogous to household energy

consumption within an *urban metabolism* (Beatrice, J., 2019). There is an energy quota for every person in a city. At the household level, each unit can measured as a net receiver or contributor on a scale of 0 to 1. How well a city's energy grid is able to cope is indicative of the sustainability of the city. Likewise, when an environmental *energy budget* is described, it encompasses a net estimation of the collective processes that drive a region's ability to provide life. Recognizing a regions' historical albedo patterns, and understanding what surface processes are driving them, is an important variable of this macro energy budget; itself a key area of study in climate and environmental science. Of recognized concern to scientists is that these processes often create positive feedback loops, perpetuating the very causes which propagate them. Such is the case of snow and ice albedo feedback in the arctic (Curry, A., & Schramm, J.L., 1995).

2. Theoretical Framework

Define the Topic: Global Warming

2019 was the second warmest year globally on record, with temperatures 2.07 degrees F above pre-industrial levels (NOAA, 2020). One place where its effects are most exacerbated is in the far northern latitudes of the Arctic (approximate to the Northern Frigid Zone). Here temperatures are greater than 5 degrees F warmer than average, with terrestrial temperatures at record highs (climate.gov, 2015). Derksen and Brown (2012: 2) confirm these trends as "…consistent with the poleward amplification of SCE [snow cover extent] sensitivity to warming air temperatures…. A striking feature of the May and June series is the acceleration in snow cover loss evident since the early 2000's". This change in surface composition driven by air temperature is significant. Traditionally the Arctic is snow- and ice-bound for most of the year. As already discussed, the reflective properties of this cover are significant. As temperatures have warmed in the last century, the extent of this snow and ice has retreated. For example, Dery and Brown back in 2007 using linear regression show there is "…a significant dependence of the retreat of the spring continental SCE [snow cover extent] on latitude and elevation. The poleward amplification is consistent with an enhanced snow-albedo feedback over northern latitudes that acts to reinforce an initial anomaly in the cryospheric system" (Dery & Brown, 2007: 1). That is to say; high latitudes and elevations are more prone to warming, and the melt of snow in those regions has an exacerbated global impact. This is the so-called "snow-albedo feedback" by which EM radiation is reflected off the earth. Derry and Brown explain that "Because of its large

seasonal variability and distinctive physical properties, snow plays a major role in the climate system through strong positive feedbacks related to albedo … and other weaker feedbacks related to moisture storage, latent heat, and insulation of the underlying surface…" (Derry & Brown, 2007: 1) The retreat of this snow and ice cover has initiated a positive feedback loop, in which less and less EM radiation is being reflected, heating the planet further, thereby melting more snow and ice. Chapin et al. (2005: 358) visualize this feedback system to great effect (Figure 3).

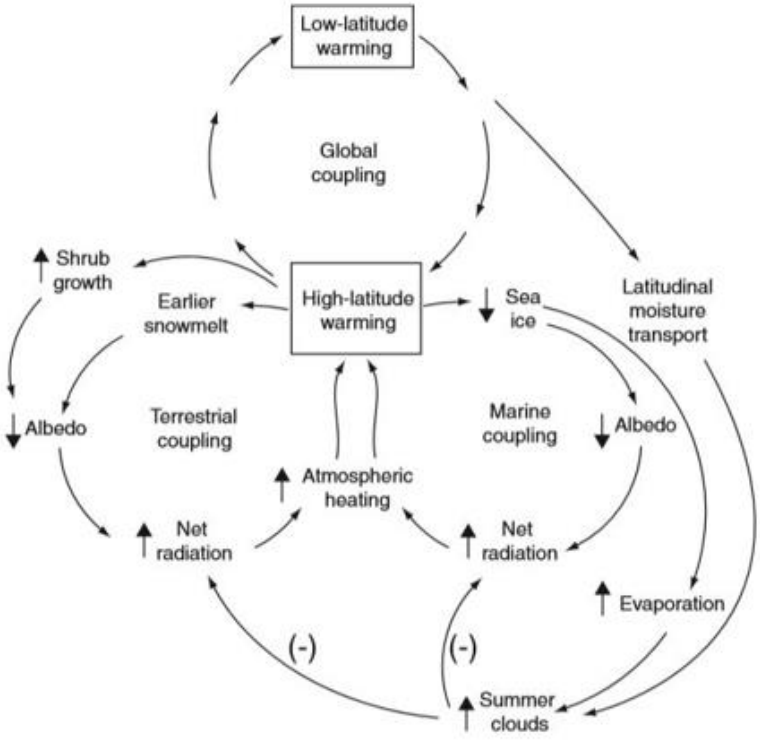

Figure 4: Global Coupled Climate Model (Chapin et al. 2005: 358)
[Arrows linking processes indicate a positive effect of one process on another unless otherwise indicated (by minus signs)]

Nested within the terrestrial coupling system is another important factor which has the potential to dramatically accelerate the warming process. This is the carbon deposit stored within permafrost across the Northern hemisphere.

Role of permafrost & other frozen bodies

Permafrost is predominantly frozen bog left behind from the last ice age. 25% of all land in the Northern hemisphere contains this surface. Largely this is frozen plant matter. Its decay at warmer temperatures releases a significant amount of carbon into the atmosphere. This increases the net radiation absorbed by the earth and causes further atmospheric heating. It is estimated that 1,400 gigatons of carbon is trapped beneath the earth's surface in this form (National Snow & Ice Data Center, 2020). This is equal to more carbon than is currently present in the atmosphere. To what extent this occurs is under discussion in the scientific community, but it is clear this is an active process the effects of which are increasingly felt. Chapin et al. (2005: 657) explain that: "many Arctic thresholds relate to abrupt physical and ecological changes that occur near the freezing point of water. Paleoclimate evidence, which is mostly indicative of summer conditions, shows that the Arctic in summer is now warmer than at any time in at least the past 400 years… This warming should have a large impact on the rates of water-dependent processes." Thus, as the water content of the permafrost thaws, organic matter begins to decay.

Albedo as a tool for measurement

The Arctic is in a period of profound climatological change. This affects sea ice, snow cover, vegetation, and permafrost, which in turn have cascading repercussions for the local ecosystems in these areas, and the earth's overall warming trend. A question for scientists is how to best measure these changes. Albedo offers one form of measurement that is highly versatile in its ability to produce a value across any surface type, which can be related back to its composition. As albedo is also highly sensitive to the presence of water content, it lends itself especially well to the study of snow, ice and vegetation (which has water content). Dery and Brown (2007) highlight how albedo can be related to snow cover season modeling: "The snow-albedo feedback, along with the ice-albedo feedback, is invoked as a leading cause of amplified warming in polar and mountainous regions…. Consistent with this hypothesis, changes in snow cover duration during the first and second halves of the hydrological year over 1967–2004 show a contrasting seasonal response, with the largest decreases occurring in spring over mainly NH [Northern hemisphere] high elevations…" (Dery & Brown 2007: 1). In other words, shifting snow cover extent and its seasonal distribution is correlated to albedo trends. These show the spring as a time when the most pronounced changes are occurring. Colman (2013) goes so far as to call this relationship a "special case". This is because feedback measured along one timescale will be of a magnitude stronger at another. For example, "…the sensitivity of snow albedo to climate change depended on the treatment of features such as vegetation canopy/surface interactions, with high albedo contrast implying greater climate change sensitivity. Processes such as this are likely to apply on other timescales, too." (*Colman 2013: 2832).* Again, this underscores the practical usefulness of albedo observation to inform climate studies in the Arctic. Not only is the

albedo feedback mechanism correlated to a larger global system, but albedo is a tangible measurement that can be taken from satellite data. Wang et al. (2015: 1) estimate daily mean land surface albedo from MODIS satellite data. They say reduced albedo caused by annual loses of net polar snow and sea-ice is believed to amplify global warming. Furthermore, they say contamination of snow in the form of soot and other particulate matter also reduces snow reflectivity, thereby accelerating the snowmelt process. The nexus of albedo between processes on the land and those in the climate make it a crucial input variable for climatological studies.

From a remote sensing perspective, the relationship between albedo and surface type presents an opportunity for classification as an index. Indexes are ways of standardizing and categorizing values. It should be possible to identify the unique albedo signature of individual ecoregions, composed of similar surface type. Once defined for a surface type at a specific time of year, comparisons can be made through time to inform models for the future. Moody et al. 2007 state clearly "The statistics demonstrate that each ecosystem classification has a discernible spectral albedo signature when accompanied by snow on the ground. This indicates that winter canopy and the underlying surface radiative properties are impacted by the presence of snow overlying these surfaces." (Moody et al. 2007: 337) While they speak of winter canopy, their statement can be extended to any type of surface cover in the Arctic or Northern hemisphere.

Thesis Statement

The ecoregion is a crucial scale of investigation in the Arctic because it represents a self-contained climatological system—influential at the local level, yet indicative of global trends. Because ecoregions are defined by a set of homogenous surface characteristics (such as foothills,

lowlands, highlands), each one should also have a discernible albedo signature. From this premise, this study proposes to visually model the albedo and vegetation indexes of five ecoregions through time. From this, insights can be drawn about the climatological changes occurring in the Arctic. These are important for use in climate models as explanatory variables.

Main debates

Having established the role of Arctic snow-albedo feedback within the global climate system, the main debate in the scientific community lies elsewhere. One question is whether there are albedo patterns at a regional scale, and if these are deviating from a reference trend. At the global scale, previous studies of annual albedo patterns have been inconclusive (NASA Earth observatory, 2019). They show albedo changing, but without any discernible coherency. At the macro-region scale, the Arctic has been shown to have annual patterns of albedo, such as *the snow-albedo feedback* mechanism. At a scale down, at the level of the ecoregion, there is room for exploration as to the significance of annual albedo patterns. There appear several avenues for research. First, do ecoregions demonstrate unique albedo signatures? Second, do they show annual patterns/are there indications of change? Third, how closely can albedo signatures of ecoregions be correlated to specific surface types? This last question is one of scale, and arguably an area inviting more research. It is within this perceived gap in the literature that this work places itself.

Is annual albedo changing in the Arctic?

Fernandes et al. (2009) *Controls on Northern hemisphere snow albedo feedback quantified using satellite Earth observations* conclude in agreement with several other studies that the snow albedo feedback (SAF) mechanism of the Arctic is the most significant explanatory variable for planetary albedo feedback (PAF). In turn, the cyclical expression of SAF in the Arctic is driven by changes in surface temperature, in turn driven by seasonal surface cover, predominantly snow and ice, and those elements' interaction with the vegetation types and surfaces they cover. Fernandes et al. (2009: 1) state that numerous studies have confirmed that changes in local SAF account for the majority of the variability observed in PAF.

At what rate is albedo changing in the arctic?

Fletcher et al. (2012) perform a review of multiple statistical climate-albedo models to discern the most influential factor in observed albedo change. They come up with a formula composed of net albedo feedback, albedo contrast (derived from snow vs. exposed surface), and albedo-temperature (temperature dependence dictating snow albedo) (NET, SNC, and TEM), predicting that NET = SNC + TEM (2012: 1). Overall, they conclude that "…SAF calculated from the seasonal cycle is a good predictor of SAF in climate change among a suite of coupled climate models" (2012: 1). More specifically breaking down the influence of the constituent components of SAF, they find that "…69% of the total observed feedback strength (1.11% change in surface albedo per unit surface warming) is due to SNC, and 31% is due to TEM" (2012: 8). Importantly, they conclude that the temperature term (TEM) albedo component is significant in the Arctic, showing the highest explanatory percentage in coastal regions. Of the models they evaluate, they

find 12 of 17 overestimate the net albedo feedback, indicating snow albedo sensitivity is commonly exaggerated (2012: 8).

What is driving this change?

Snow & Ice Composition & Distribution

Snow and ice have dominated the Arctic climate going back 2.6 million years to the Pliocene (Britannica, 2020). The snow-albedo feedback process is one way in which the Arctic has historically kept global temperatures in check. When looking for the cause of changing albedo in the Arctic, snow cover is shown to be the most influential component (Fletcher et al. 2012). Fernandes et al. (2009) say "The North American spatial pattern of SAF is chiefly explained by the snow cover component" (Fernandes et al 2009: 5). What follows next is a review of the physics of (snow) albedo, and the processes which affect its change.

In cases where snow albedo is in decline, it is the result of two related processes. Because snow is so highly reflective, most other surfaces beneath it represent a significant drop off in albedo value. Therefore, when snow retreats or shifts, newly exposed surfaces are overwhelmingly less reflective. As snow and ice in the Arctic have been in observed decline for decades, this is significant. The other process which reduces snow albedo is the age of the snow. Old snow is as a rule less reflective. It accumulates debris, melts, and loses its overall purity. Qu & Hall (2007: 3971) explain: "First snow cover shrinks, and where it does it generally reveals a land surface that is much less reflective of solar radiation. Second, the remaining snow generally has a lower albedo because its optical properties are sensitive to Ts [surface air temperature]. For example, wet melting snow, more common in a warmer climate, has a lower surface albedo

than dry frozen snow" (Qu & Hall, 2007: 3971). Therefore, in transition seasons where the temperature hovers around freezing, a shift of temperature by only a few degrees can drastically change surface composition and reflection. Additionally, as there is an inverse relationship between snow age and albedo, the resulting increased average age of snowfall in a warming climate causes lower average albedo. Thus not only is newly exposed snowmelt less reflective, but snow albedo is also highly sensitive to shifting patterns of snowfall and changes to seasonal temperatures.

Returning to the work of Fletcher et al. (2012), their study parallels the two categories put forward herein. They evaluate the weighted influence of albedo change from snow contrast (SNC) vs temperature changes (TEM) and conclude that "In observations, SNC dominates the total SAF at latitudes equatorward of 65 degrees N while TEM dominates over the Arctic, peaking in localized coastal regions. On average, the magnitude of SAF in… climate models is slightly larger than observed, due primarily to a positive bias in TEM at lower latitudes" (2012: 8). At first it is perhaps counterintuitive that contrast from snow cover retreat is less significant in the Arctic than temperature. However, if one considers that contrast is in large part a function of snowfall patterns, then it is reasonable that the Arctic snow cover remains extensive enough for contrast to be minimal, while at lower latitudes in North America and Eurasia, shifting patterns of snowfall will drastically differentiate the snow cover of an area between seasons and over years.

Changes in vegetation cover

While it is logical to give preeminent importance to snow and frozen surfaces in a study of Arctic albedo, the role of vegetated surfaces is important on its own. Differing species of plants and trees exhibit dissimilar albedo characteristics (Kussinen et al. 2015; Hovi et al., 2019), while

vegetation's interaction with snow creates a third mixed-surface dimension to consider. Moody et al. (2007: 337) address the nuances of this dynamic. They give as example that "the 0.47 µm albedo of winter snow-free evergreen needle leaf forests increase from 0.03 to 0.36 in the presence of snow, compared to an increase of 0.04 to 0.76 for croplands." Overall they confirm that the albedo of "snow covered ecosystems with some winter canopy" is less than those without a winter canopy "…for example, the 0.47 µm albedo of snow covered mixed forests is 0.39 compared to 0.87 for barren/deserts and 0.95 for permanent snow." Put most simply, vegetation has an overall low albedo, because plants are designed to absorb sunlight. Further nuances in leaf shape and composition can vary these albedo properties, but do not change the fundamental characteristic of vegetation. Interestingly, Moody et al. show that even when covered in snow, the vegetation underneath reduces the albedo of the snow above. Thus, mixed forest with snow in winter has a lower albedo than a barren prairie or permanent snow locations. On the other hand, the albedo of vegetated surfaces is increased significantly by the presence of snow, as shown in the evergreen needle leaf example. How the two opposite albedo forces of snow and vegetation interact is therefore subject to a wide range of local variables. These determine which of the two forces will be more dominant at a given time, and at a given scale.

Mechanisms of Albedo Change

Scale is key to this section, which considers the dominant macro processes affecting albedo. There are two scales of significance, very much each-other's opposite. Within each, there are three systems operating. On the one hand there is snow-albedo feedback and its role within the global climate system. This is at the largest macro-scale of global climate. On the other hand,

at the scale of the snowflake, are the physical mechanisms that define the strength of snow's albedo. As discussed prior by Fletcher et al. (2012), these are a) surface temperature, and b) snow age. Qu & Hall (2007) define these same two physical processes in a visual representation:

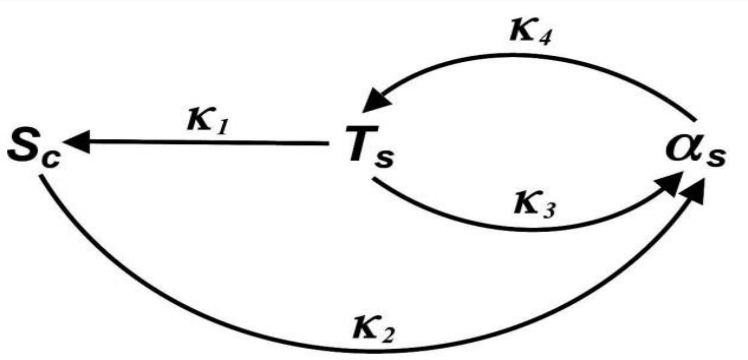

Figure 5: Snow Cover Feedback & Snowpack Metamorphosis Feedback
(Qu & Hall 2007: 3972)

> *An increase in surface air temperature (Ts) leads to a reduction in snow cover (Sc), which in turn leads to a reduction in surface albedo (αs). The second is the snowpack metamorphosis feedback: the increase in Ts, leads to a reduction in albedo of the snowpack itself. The reduction in surface albedo resulting from both feedbacks leads in turn to a further increase in Ts.*

Returning to Fletcher et al. (2012: 8), they conclude that albedo change from thermal impacts (TEM) on snow surface are declining as a cause, relative to the explanatory importance of albedo loss resulting from contrast between snow covered and non-snow covered surfaces (SNC). Yet, the weighted importance of the TEM term is significantly enhanced in the context of seasonal cycles. Because TEM is tied to physical process that affect the albedo of snow covered surfaces, and these processes occur at different timescales depending on their origin (seasonal foliage vs pollution), there is value in deconstructing the TEM to its underlying constituent physical processes. "For example, changes in the rate of black carbon or mineral deposition on the snowpack from industrial emissions would be likely to occur much more slowly than the buildup of debris on snow (e.g., leaf litter, pine needles) during the winter-spring transition" (2012: 8).

The thermal term is then very much a question of the processes by which particle matter accumulates on snow, thereby detracting from its high albedo value. What these processes are—industrial, seasonal, vegetation-based, or other—will be a local contextualization. This serves to further underscore the utility of studying albedo within an ecoregion, in which such a process can more accurately be assessed and traced back to a source of the thermal surface altering substance.

Conceptual Model

Graphic

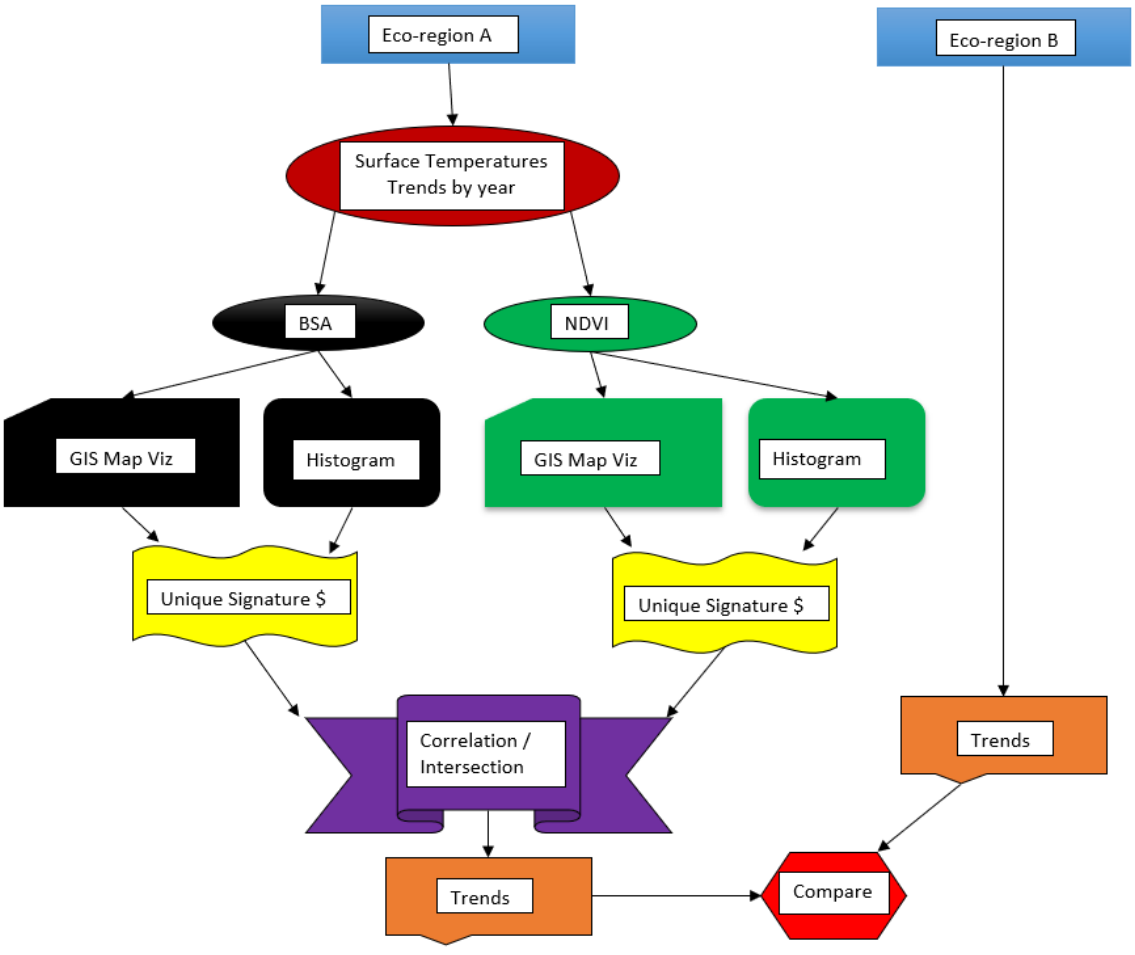

Figure 6: Conceptual Model

The preceding graphic was developed to represent the workflow of this study. It represents both the computational phases of this work and the conceptual linking of results. Step one is to calculate average daily surface temperatures within an ecoregion for the study period. From this data, identify years which present wet snow conditions, along with any other anomalous temperature events that can be used as signal markers to search for in the albedo and vegetation data. Next, calculate albedo values for the same area and output as a line graph. Then, visualize a map-based image that shows these average values spatially. Repeat the same graph and map process for vegetation. At this point compare the two pairs of visualizations (NDVI and BSA) and look for specific signatures of each corresponding to an ecoregion. Compare these signatures and results in search of possible correlations and intersections between the two datasets, and the larger snow-albedo feedback they play into.

Spatial Scale

As discussed, the primary scale of research is the ecoregion. For a given region, there are two subjects of measurement, Black-sky Albedo and vegetation index NDVI. For each of these respectively, there are two types of representations: a traditional line graph, and a spatial visualization using GIS. Each allows for a different evaluation: the GIS with a geographic context, the graph from an abstracted tabular perspective.

Temporal Scale

The temporal frequency of this study is the five-month period of March through July, from 2000, reaching forward every two years. The year 2019 breaks this rhythm but was included because it represents very recent data, and because the year 2020 was incomplete at the time of writing. These months represent the peak spring melt season in Alaska, while the years of study are from the beginning of this century to the most recent available data. The selection of this time range is informed by Derksen and Brown (2012: 4) who highlight the May to June span for its dynamic signature within the annual cycle. They say that the May to June period shows evidence of "profound" change. "The five lowest June SCE values in the satellite era (since 1967) have all occurred over the past five seasons (2008–2012)." Furthermore, "…successive records for the lowest June SCE in the satellite era were set each year for Eurasia since 2008, and in 4 of the past 5 years for North America, and the rate of terrestrial snow extent loss in June between 1979 and 2011 (17.8% decade) is greater than the loss of September sea ice (10.6% decade) over the same period" (Derksen et al., 2012: 4). From this it is clear the May to June period is of central importance to the study to changing snow cover patterns in the Arctic. It is during this time that some of the greatest mean temperature changes are being observed. Crucially, it is also a time of natural annual change, when snow and vegetation intermix, and the linkages between these two systems are most clearly demonstrable. Additionally (upon reviewing the data) it was observed that March and April are important in the measuring of albedo, as these show what the resting winter state is, while loss can occur as early as April.

In addition to the choice of temporal observation window, there is the more technical question of the specific means of data collection during that period. This pertains to the satellite itself, and how its sensors have been programmed. Regarding albedo, the question is: What is

used to represent a day's reading? Wang et al. (2015) explain the complexity of this determination:

> Even under the assumption that surface features are stable, LSA diurnal variations will occur because the illuminating conditions change throughout the day, and thus, the consideration of temporal mean albedos, such as daily mean albedos, is very important for adequately studying the energy balance … In fact, the use of local noon albedo in calculating daily upward shortwave radiation may produce negative bias as large as 10%, which is much larger than the accuracy requirement of 5% defined by Global Climate Observing System [2006]. (Wang et al., 2015: 4826)

For the purposes of this research, this question is essentially answered by the MODIS data itself. Wang et al.'s point regarding "daily mean" vs "local noon" is addressed by the creation of what is called a daily composite. This is when each pixel's value is an average of a sixteen-day time-period, in which that day of measure constitutes the mid-point. This minimizes the impact of data anomalies on individual days and produces the most statistically representative results. The same is true of the MODIS NDVI data used.

3. Methodology

Case Set

The eco region Is the natural case set for this thesis. These regions are delineated all over the world by geologic, landform, soil, vegetative, climatic, wildlife, water and built-area variables. While internationally there is variation as to their boundaries, at a national level (and between the US and Canada) there is usually a high degree of homogeneity within the assessment system. In this *case*, the ecoregions of Alaska were specifically developed by the US Geological Survey for Alaska and its unique characteristics. In all there are 20 defined ecoregions of Alaska to come out of the *Major Ecosystems of Alaska* project by the Joint Federal-State Land Use Planning Commission for Alaska, 1973. Each region in turn can have up to nine different classes within it. Furthermore, the variable of largest significant in the governments assessment "…is on the regional distribution of vegetation community type and structure" (1973: 2). As this thesis looks at the interplay between albedo, and surface cover/vegetation, this is ideal. Gallant et al. (1995: 4) advance this delineation further still. They offer insight into the decision-making process of the 1973 study. They say upfront the delineations are judgement calls contingent upon four key principles: (1) the environmental characteristics (observed as patterns) of a given place versus those of a neighboring place; (2) the geographic size of an area; (3) the resolution of the explanatory values used as criteria (i.e. the pixel scale satellite data used, or the time interval); the resolution and scale of analysis from which the analysis of the ecoregion is written. For a

specific example, consider the way they distinguished between the Arctic Coastal Plain (Eco-101) and the Arctic Foothills (Eco-102):

> …topographic data and physiographic maps show several extensive flat coastal plain areas that coincide with areas depicted as wet tundra on a map of major ecosystems. Among these coincidental areas, one occurs where arctic climate prevails, while several occur where subarctic climate prevails. Different climatic regimes result in different growing season lengths, different hydrologic cycles, and some variation in occurrence of plant species. Such differences led us to distinguish the Arctic Coastal Plain Ecoregion from the Subarctic Coastal Plains Ecoregion. Another example includes the montane areas in Alaska. (Gallant et al., 1995: 4)

The result of Gallant et al.'s study is a refinement of the borders of the ecoregions from the original 1973 study. Today these are the most current and in use by the USGS.

Specific Case Set

With this understanding, each of the five ecoregions selected for this study is presented in detail, from the perspective of its geology, topography, climate, vegetation, observable patterns, and role within Alaska.

Eco-101 Arctic Coastal Plain

Climate

The Arctic Coastal Plain is the most northerly geographic extent of the United States, and fully within the arctic circle. Therefore, its climate is dominated by marine weather patterns, which define and the ever-changing boundary between land and sea. However, because temperatures are so cold year-round, there is very low annual precipitation, as water overwhelmingly falls in the form of fog in the summer and snow in the winter. Temperatures here historically range between -22 degrees F (-30 degrees Celsius) to -5.8 degrees F (-21 degrees Celsius) in the winter, and hover around 46 degrees Fahrenheit (8 degrees Celsius) in the summer.

Thus, temperatures are usually below zero, with the potential to be so during any month of the year (A Gallant et al., 1995: 8). Recent years in the arctic are documented as the warmest on record. This applies here and is resulting in some of the most pronounced ecological change anywhere in the world.

Geology

This is one of the foremost regions of permafrost on the world. This is a layer of permanently frozen ground which resides underneath a layer of "active" top-soil (only 0.5 meters deep), and the snow which covers this most of the year. In the summer, the active layer will thaw but the permafrost will not. This itself is composed of frozen organic (mostly carbon) matter. Under tropical conditions, the area would be a swamp. The contents froze millennia ago. Historically, permafrost can reach depths of more than 300 meters. As soils here are rarely exposed, and drainage is poor, they are of a coarse and fibrous variety. This especially true in waterways and estuaries. Because conditions are so extreme, vegetation is closely linked to "microtopographic" features (Gallant et al.,1995: 8). Where one side of a ridge receives a trickle of melt-water and shelter from winds, the other does not. These nuances dictate the amount of sustainable life. Sedge-grass is the most common plant found. Moss is also common. Some of the larger plant species are dwarf scrubs, mountain-cranberry, four-angled cassiope, and bearberry.

Topography & Vegetation

The area is roughly 50,000—km2 and a poor natural drainage basin. Instead of streams, thaw-lakes form, which stay frozen most of the year and cover between 20 to 50 percent of the land surface. These increase by circa one meter per year and can be as shallow as a meter.

Interestingly, these lakes are often formed along a north-northwest axis; shaped by coastal winds. Large ice drifts over many years become covered in topsoil and shaped by the wind into cylindrical hills known as “pingos”. These are the tallest features on a landscape barren of any large vegetation. From coastal sand dunes, the rolling hills of the land itself rise almost imperceptibly from the coast at a gradient of less than 1 percent (continuing in this manner through the arctic foothills (Eco 102) until the Brooks Range (Eco 103). This area was not glaciated during the last ice age. At its southern-most extents in the highlands, streams emerge. The Colville River serves as a natural boundary between streams to the east which snake down to through deltas to the sea, and those to the west, which are of a slower pace and may not decisively flow into the ocean (A Gallant et al., 1995: 8).

Eco-102 Arctic Foothills

Climate

The Arctic Foothills signify the shift of influence from sea to land. Whereas the Arctic Coastal Plain is essentially a massive tidal plain, the Arctic Foothills are shaped by forces of the continental climate. The is on average slightly warmer than neighboring regions to both the north and south, where the ocean and the mountains respectively keep temperatures down. There are few physical weather stations here. Those that do exist document averages of between -20.2°F and -4°F in the winter, and 33.8°F to 59° in the summer. Precipitation rates here are comparable to those in the Coastal Plain around 140 mm per year. This accumulation is disproportionately centered on the Noatak Valley, to the west of the region. Here there is nearly twice as much precipitation than anywhere else. Snowfall is most constant on the southern boundary of this

region, where is transitions into the Brook's range. High altitudes and downward winds from the mountains provide this area with revolving fresh snow. As in most of the Arctic, freezing temperatures can occur at any given time, even in the peak of summer. During these weeks around the solstice, the sun never sets here (A Gallant et al., 1995: 11)

Geology

This region has two areas which are distinguished: north and south. To the north (towards the sea), east-west running ridges and table-top features define the landscape. They are the result of glacial movements depositing "unconsolidated Quaternary materials (glacial, alluvial, and aeolian)…" over a pre-existing set of continental deposits from the Lower Cretaceous period (A Gallant et al., 1995: 11). Elevations are limited to 600 meters above sea-level. The Northern section of the Arctic Foothills runs into the Brook's Mountain range. Here, Jurassic-Cretaceous era sandstone and quartz formations begin to rise up beneath the permafrost, which itself has an active layer of around 1 meter (deeper in rivers). Elevations here can now reach up to 800 meters, and the highest locations are now sporadic ridges and mesas, connected by rolling plains. This portion of the region was not glaciated in the last ice age. The ice features here are climate driven, such "…pingos, gelifluction lobes, ice-wedge polygons, stone stripes, and beaded drainage…" (A Gallant et al., 1995: 12).

Topography & Vegetation

The surface are of the Arctic Foothills is 124,000—km2. Hillside slopes average around 5°, and are steepest in areas transitioning to the Brook's range, which marks the southern boundary of this region. This region is devoid of any large forms of vegetation. Soils are predominantly of a

coarse variety, remnants of erosion of sedimentary rock. Lakes have muck sediment, with some exceptions of sand. Because of the poor natural drainage, materials build up in the shallow active layer. This creates an altogether hostile climate for plants. Grasses, and shrubs dominate. Mountain cranberry is perhaps the most recognizable vegetation here. Mosses and fungi are common in crevasses. While as a general rule it is said trees do not grow north of the Brooks Range to this region's south, there are irregular areas where trees are found. One such exception is the Noatak River Valley (in the south-west), where soil conditions are fine enough to support the roots of trees. The white spruce there follow the banks of the river, and in some places further inland balsam poplar can also be found. The headwaters of these rivers lie in the Brook's range, and they merge to the east, and to the far south-west. The larger of these are perennial, while the smaller freeze in winter. During the spring melt season, flooding and wash-out events are common. The chance of wildfires in this region is historically insignificant.

Eco-103 Brooks Range

Climate

Temperatures here are still categorized in the Arctic domain. The only USGS weather station is at an altitude of 770 meters at the Anaktuvuk pass and records annual daily mean temperatures of min -30° Celcius (-22°F) to max -22° Celcius (-7.6°F) in the winter and 3° Celcius (-37°F) to max -16° Celcius (60.8°F) in the summer. Freezing temperatures are expected In every month of the year. The stark difference in elevation changes, and differences in exposure to direct sunlight create a region with highly variable surface temperatures across time and space.

Average precipitation is measured between 280 mm, with around 160 cm of annual snowfall (A Gallant et al., 1995: 15).

Geology

The Brooks Range is the most northerly range in Alaska. These mountains are rugged, emerging swiftly from the lower-foothills preceding them to the north, and on their southern side rising above the tree line and serving as the boundary from which point further no large vegetation is expected to be found. They stretch across northern Alaska and into Canada. Technically these form part of the Rocky Mountains. The sedimentary rock in these areas is predominantly sandstone, shale, limestone deposits of marine and continental origin. These were formed during the Cretaceous period (79 million years ago). At higher elevations, glaciation from the Pleistocene ice-age is evident (above 1,800 meters), though these are documented in drastic retreat. Low valleys are around 500 meters, while peaks start at 800 meters and rise all the way up to 2,400 meters. Permafrost the ever present here as well, though it varies greatly in distribution between valleys, where it accumulates, and mountain slopes where soil is continuously eroded and thus has little foothold. While the highest elevations are snow covered all year, annual thawing creates outwash down the slopes of mountains which accumulates into the active layer of the soil above the permafrost. There is strong interplay between frozen and thawed states of surface here. These result in significant ice-formations (A Gallant et al., 1995: 15).

Topography & Vegetation

The Brooks Range comprises some 134,000—km2 extending from near the Chuckchi Sea to the Canadian Yukon. Slopes most commonly range between 5° and 15°. From the air, it looks as though pock-marked from above, with few if any flat surfaces to pick out. Though historically glaciated, there are fewer than expected lakes for a region of this configuration. Where they do exist, these closed water features are in rock basins or at the end of valleys with no clear route out. There are noteworthy patterns to the streams here. They are observed to run north-south when large, and east or west when they are tributary branches. Significant debris is carried down these rivers and streams, often collecting at the bottom. There are several thermal water features which have been documented in the region. Vegetation is reflective of the harshness of this terrain, and its role as a natural boundary between continental and arctic eco-systems. There is little vegetation to speak of on the sides of the mountains. Only stray shrubs which find root in the odd crevasse survive. At lower altitudes in the valleys to the south, trees are found such as willow and spruce and eventually the first signs of pine (A Gallant et al., 1995: 15).

Eco-104 Interior Forested Lowlands and Uplands

Climate

This regions' discontinuous geographic extent, stretched over the entire width of the Alaskan interior, results in a high degree of temperatures variation, especially from east to west, where inland micro-climates can emerge. Summers experience highs of 62 - 71°F, but are short lived, lasting only a few weeks. These temperatures peak (in 2019 at 80 °F) during the last week of June and the first week of July. Spatially there are two strong indicators of the climate variation

in this region: altitude and distance to the ocean. Low-altitude, inland areas experience the highest temperatures, while coastal proximity and elevation correlate to lower annual summer temperatures. The reverse is true of winter patterns. Average precipitation is between 250 mm and 550 mm. Of this, snowfall can account for nearly all of this under minimum drought conditions (205 cm). The weather patterns that contribute another source of water are most common in the summer. Snow cover is pervasive for roughly half the year, lingering longer at high altitudes, in receded areas, and north facing slopes. The heavy vegetation in this region, comprising both undergrowth and trees, offers a small layer of thermal insulation (A Gallant et al., 1995: 17).

Geology

Most of this region's geology is from the Mesozoic (252 to 66 BCA) and the Paleozoic (541 to 251.902 BCA). The sedimentary formations which formed then are punctuated by trails of volcanic deposit. There are few sources of spring water, and they are brief where they do occur. Most of the waterways emanate from neighboring regions, such as the Brooks Range (Eco-103) where meltwaters are annually released. There is scant exposed surface cover in the region. Most of the area is covered in dense forests. Soils vary depending on elevation. Those in high-up are formed be mountain debris, while in the lowlands they are the result of flooded plains. In these lowland areas, the shallow soil Is underlined by permafrost. (A Gallant et al., 1995: 19-20)

Topography & Vegetation

This is the largest region studied at 269,000—km2. It is also discontinuous. This region is closely related to the topography and vegetation which distinguish it from the adjacent interior

highlands (Eco- 105) and the interior bottomlands (Eco – 106). What defines this region are dense forests across wide low plains, undulating beneath the brush. There are occasional low-lying hillocks with flat tops (tree covered), and several plateaus. Where this region borders the Brooks Range in the north and the Alaska Range to its south, the transition is relatively direct, as the ridgelines of the mountains rise up quickly, exceeding the tree-line. Elevations for this ecoregion range from sea-level to 500m, with some outlier hilltops reaching 700meters. The angle of the surface is in the range of 0° to 5°. The USGS survey of this area defines five variables which result in a varied vegetation here. These are permafrost, surface water, fire, hillslope aspect, solid characteristics. Together these variables create a surface environment which changes significantly at a fine scale. These are the first conditions conducive to higher vegetation forms in northern Alaska. Coniferous trees are abundant here (white spruce, usually on insulated, arid, south-facing hills, and black spruce in floodplain areas). Deciduous species are also found, such as birch. Balsam poplar is another found along rivers and floodplains. The list of vegetation species goes on. Suffice to say that there are all the components of canopy, understory and brush, mosses, and fungi. (A Gallant et al., 1995: 19).

Eco-105 Interior Highlands

Climate

This region is defined by a completely continental climate. USGS report delineating this region (1995) says there was “no long-term weather data available”. Therefore, inferences are made from the environmental conditions. One is that this region receives higher annual and average precipitation than surrounding low-lying areas in the interior forested lowlands and

uplands. This is explained by the “orographic effect” by which the temperature and air-pressure changes which occur at altitude create precipitation in in the air that passes over. The second conclusion is that peak summer temperatures “decrease with elevation”. This is the result of exposure to sunlight on the higher slopes and the cooling shade produced by the forest canopy in lower areas (A Gallant et al., 1995: 21).

Geology

The geology of the Interior Highlands was formed in the Paleozoic (541 to 251.902 million years ago) and the Precambrian (the earths earliest phase). These pre-historic formations are metamorphic rocks, forged into their transformed state by the intense heat and pressure of the earth’s crust forming and the molten outflow of volcanos. In two known areas, the Kuskokwin Mountains and Nulato Hills, there are also formations dating to the Cretaceous (145 to 66 million years ago) and Lower Paleozoic (541 to 251.902 million years ago). Permafrost is found across the northern extent of this ecoregion, and in a discontinuous manner through the central and southern extents. Where there is permafrost year-round in the north, many natural ice formations can be found, such as gelifluction lobes, forstboils and stone stripes. Soils across this region are shallow, with little earthen content. Instead, rock is weathered off the side of these hills and ground to varying degrees of grain. Soil drainage is minimal and the permafrost itself not very deep. Because of this, the permafrost here has higher than average ambient temperatures (>-1.5c). Because of the thin layers of both permafrost and soil, there is a high chance of erosion and “organic mat disturbances” when wildfires or other warming events significantly raise the surface temperatures (A Gallant et al., 1995: 21).

.

Topography & Vegetation

The Interior Highlands are 115,000--km2 in size and discontinuous. Instances of this ecoregion rise-up as “islands” or large plateaus. These are defined by deep furrowed hills punctuated by rugged peaks. There are few trees here, but ample grasses and shrubs. From space, the landscape has a pruned appearance. Elevations are between 500 meters in the troughs, and upwards of 1,500 meters where there are peaks. These altitude differences across the region are linked by slopes of landscape between 5° and 15° degrees. These increase towards the center of the region. Exposed bedrock along the mountainside is another distinguishing characteristic of this region, compared to surrounding interior forested lowlands and uplands. Vegetation here varies greatly according to elevation and slope position. The highest reaches of this region are lone rock outcroppings. On surface-faces exposed to wind, dwarf scrub species are fount, such as avens, ericads, and willow. Lower down there is greater shelter from the elements in the valleys and trenches. Here pine trees and other forest species are common. White and black spruce are common, as is willow, Bearberry, cranberry and blueberry are frequent. Prickly rose is another common sight. Moses and lichens find a home at the bottom of the eco-system (A Gallant et al., 1995: 21).

Sub-Cases

While the individual ecoregion is the specific case set, there are three variables this study considers for each; albedo, vegetation index, surface temperature. In the context of this study, these serve as the sub-cases—the subjects of focus of the research lens. By taking one case (a.k.a

ecoregion) and putting it through a prism which separates these variables, inferences about the landscape and its response to environmental change through time.

Type of Case Study

This is an exploratory case study in which a "typical" case is chosen as an average representative of a larger group. From its study (through space and time), conclusions about the "typical" cases' behavior (expected vs observed) are made. The ecoregion is the "specific" case when talking in terms of scale. It is "typical" in that the entire arctic region--encompassing Alaska, Canada, Greenland, Norway, Sweden, Finland, and Russia—is documented to be experiencing significant environmental change because of the warming there occurring at above average rates. The five regions chosen in Alaska serve as a microcosm of the different surface conditions in the Arctic and how they are each individually responding to global warming. By assessing their baseline trends in the three variables of study (albedo, vegetation, surface-temperature), inferences can be made about the arctic as a whole.

Relationship between Cases and Variables

This relationship is one based on intrinsic properties and conditions occurring within the spatial bounds of each specific ecoregion. Albedo and NDVI surface temperature are measurements of physical properties. They are directly linked. They also theoretically exist at any scale. In practice, the scale of measurement is dependent on the instrument used to gather the information. This scale is specific to each of the three variables.

Units of Observation vs. Units of Analysis

The question of scale lies of the heart of the comparison of units of observation vs analysis. In this case, the units of observation exist at two scales in this research. At the first scale, these are the three variables: albedo, vegetation index, surface temperatures. Each of these is recorded by a separate satellite instrument recording its data at a set scale. These define the minimum pixel size of the image which is processed through the Earth Engine software. For albedo this is 500 meter squared. This is the same dimension of the vegetation index pixel. The surface temperature data is at 1 km squared resolution. Yet "observations" are not possible from a spatial dimension alone. They require a context with a data structure. In this study, these structures are the x and y dimensional axis of the variables. Not spatially, but through time (x) and by value (y)—bsa, ndvi, surface temperature. From these, an analysis is made regarding each unit of analysis; equivalent to the individual cases/ecoregions.

Inferences and Predictions

There are several predictions that can reasonably be made at the outset of this study. Firstly, regarding the trend of albedo-snow loss across all five regions, a more drawn out thaw period is expected in boreal forested regions because of the conditions which prolong the presence of wet snow (the mixture of snow and plants and crossing the thawing mark on multiple occasions. (Kim, 2018: 4-5). If there is observed lengthening of this period in tundra regions, this can be interpreted as conditions indicative of melting of permafrost underneath the snow, further propagating conditions for wet snow and a prolonged melt. In terms of temperature, it has been well documented that the arctic is experiencing dramatically increased temperatures.

This was confirmed as recently as June 22, 2020 (BBC.com) which saw this year's temperatures the highest ever recorded. This increasing thermal trend is expected to appear in the data. In response to this, it can be inferred that NDVI and BSA will respond to this change. For NDVI, this should result in a visible "greening" trend in the data as we forward through time, as warmer temperatures engender more vegetation growth per spatial unit, and renders formerly unhospitable climates in the far north survivable to greater types of vegetation. In this way, greening has two dimensions: earlier (spring growth period earlier in a calendar year), and faster (the rate of vegetation growth as measured through a line chart). For albedo, the expected trend is one of loss. There should be a visible decrease in surface reflectivity as we move forward through time. This is caused by habitual snow loss on the one hand and increases in vegetation cover on the other. Again, this can be measured from two dimensions. Earlier (corresponding to earlier snowmelt in a calendar year), and faster (the rate of snowmelt observed as measured through a line chart).

4. Operationalization: Data Selection and Visualization Methods

Data (selection and accessibility)

The magnitude of data required for this study was a challenge to overcome. To study a geographic area of this size through the assessment of any single image would be a challenge. However, this is further complicated because this is a time-series study, in which images are needed over multiple years. Add to this the fine grain resolution (500m to 1km) of the images used and the scale of the data becomes apparent. In fact, traditional remote-sensing applications, such as ENVI, are insufficient because they can only process one image at a time, and these must reside on the home computer. The only plausible means of completing this work was to find a cloud server storing an entire image collection, that can be queried by a user through an application program interface (API). Fortunately, the Google Earth Engine (GEE) Code Editor is precisely this. An online application interface that allows for researchers to query and process hundreds of the largest satellite collections today, from both governmental and private research missions.

Black Sky Albedo

The albedo data (hosted by GEE) comes from the NASA Earth Data collection available at the Land Process Distributed Active Archive Center. Specifically, the data is collected by the MODIS-terra satellite mission. The Moderate Resolution Imaging Spectroradiometer (MODIS) is low-orbit satellite following a north-south polar orbit at 705 kilometer altitude (438 miles), active since the year 2000. At this distance from the earth, each individual image "swath" taken is a

2,330-km by 10-km (1447.795 by 6.2 mile) rectangle. The resolution of an individual pixel from within this image is 500 meters (1640.42 ft). This is a passive system, in that the aperture of the satellite camera is simply opened and incoming electro-magnetic radiation reflected by the earth is then recorded. The movement of the lens across the earth's surface is of the push-broom variety, in which the camera scans the 705 km area from right to left, then moves forward to the next adjacent position record again from right to left. At this combination of altitude and aperture, the entire earths' surface is recorded every two days, across thirty-six spectral bands. These are bands are grouped according to scientific usefulness. For the full list of 36, see modis.gsfc.nasa.gov/about/specifications.php. For this research "Albedo_BSA_Band1" at 620-670nm frequency was chosen, measured from 0 to 32766, with a scaling factor of 0.001. This is at the red side of the visible light range. As this is an evaluation of visible reflectance and has a vegetation component (vegetation is best discernable in infra-red frequencies) this choice was deemed a viable compromise for the intersection of peak snow and vegetation spectral values. However there is an argument for using full-spectrum albedo. Ultimately this fell outside viable workability for this project, but can be considered for future addition.

NDVI

The normalized difference vegetation index (NDVI) data is also a MODIS-terra product. Index values are coded into each pixel, which are each 500 meters squared. The NDVI band used is understood as extension of the retired NDVI scale used by the National Oceanic Atmospheric Administration-Advanced Very High Resolution Radiometer (NOAA-AVHRR). This current MODIS data collection spans in 2000-02-18 to the present. In all, there are twelve bands to choose from, each comprised of a data grid of 2400 by 2400 rows. The NDVI band is measured on a range of -

2000 to 10000. The scale factor is 0.0001. The images produced are composites. Each pixel's data is a 16-day composite of information centered around the date of image capture. This 16 day period is itself a composite of two 8-day periods either side of the date in question. This assures two things. It reduces the interference of cloud formations on the image, as they are blended out in the average. It also brings out the maximum vegetation value for a season, as full bloom can be accurately evaluated from the scale of three weeks (circa 16 days). The equation used to calculate NDVI is a standard one used in remote sensing. It is NDVI = (Near Infra-red – Red) / (Near Infra-red + Red). Translated to MODIS, this is

NDVI = (Band 1 - Band 2) / (Band 1 + Band 2).

Temperature

The surface temperature data is likewise a MODIS product. However, unlike the other two datasets, this comes in at 1 kilometer pixel resolution. The grid of pixels itself in each single capture is 1,200 by 1,200 km2. The data is standardized by an 8-day averaging period. This duration is equal to half the time it takes for the camera to move across a single image capture. This scalable relationship enables two measurements taken for a single pixel from a single capture. These can be averaged in turn, giving a higher level of accuracy. Twelve bands of information are recorded. Most of these are auxiliary data such as time of day observation, view zenith angle, day clear-sky coverage (to name a few). The operative band in this case is band 1: Daytime Land Surface Temperature. This is measured in degrees Kelvin, for which the conversion calculation into Fahrenheit is: (0**K** − 273.15) × 9/5 + 32 = -459.7**°F.** The minimum recordable value is 7500 while the maximum is 65535. Crucially, there a scaling factor of 0.02 is used. Therefore, to relate these values back to Fahrenheit (enabling real-world comparison), a scale factor of 0.02

must be applied before the conversion. In this way, 13650° Kelvin x 0.002 is 273°, which converted to Fahrenheit is 31.73, the approximate freezing/thawing mark. 13650 is therefore a crucial evaluation mark in the temperature charts produced.

Coding

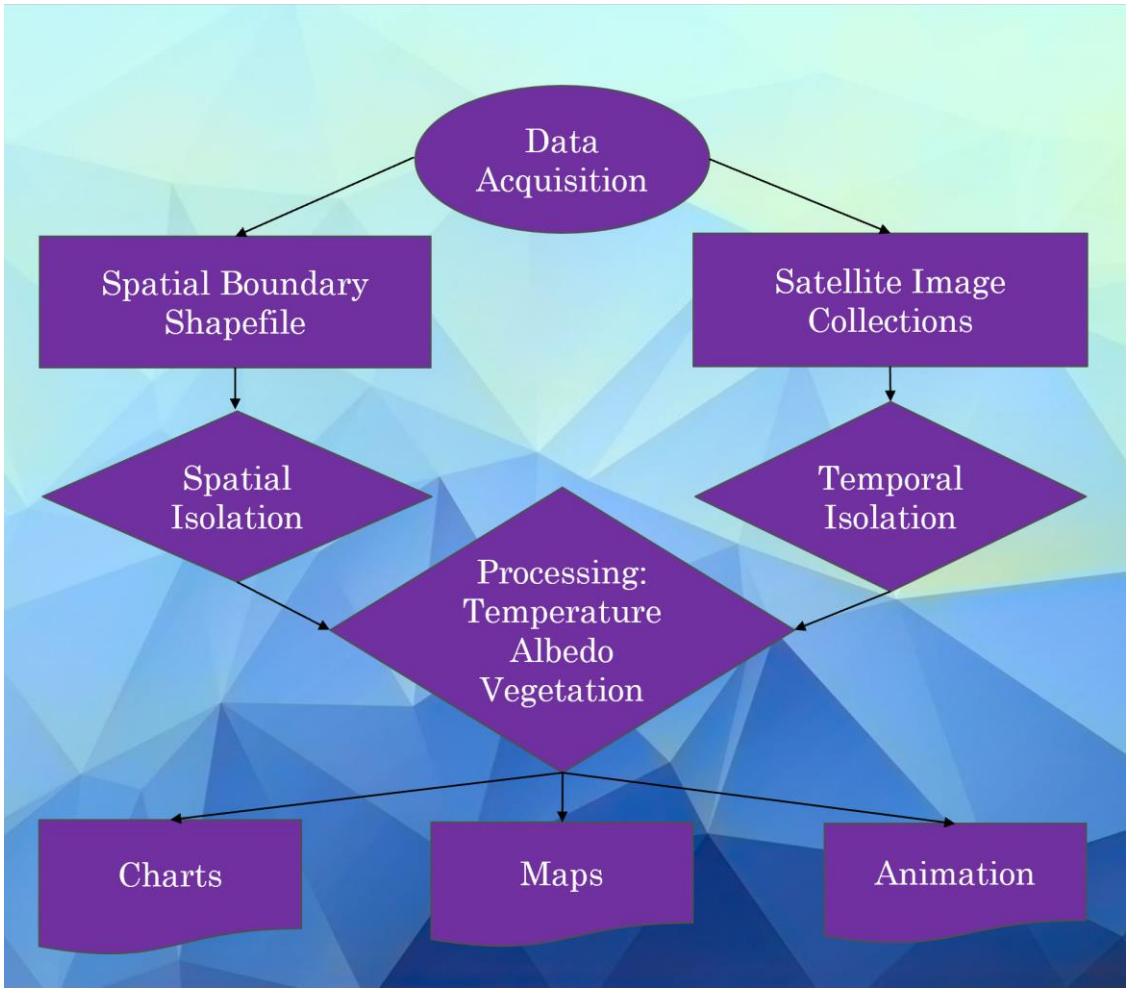

Figure 7: Coding Flowchart

Isolation

The isolation of the data has two components, space and time. These parameters relate to a specific source. Space—the geographic bounds of the ecoregions—are obtained from a *shapefile* for use with geographic information systems (GIS) software. This is made public by the by the US Environmental Protection Agency (EPA) from their archive. The specific data used for Alaska is the Level III version (https://www.epa.gov/eco-research/ecoregion-download-files-state-region-10). The mapping effort itself was led by the USGS under the work of Gallant, A. et al. 1995. Ecoregions of Alaska. This includes the boundaries for all twenty Alaskan ecoregions. In tandem, attribute information augments the spatial projection. This includes various identification codes and sub-divisions determined by the USGS. By using these, it is possible to filter the Alaska-wide shapefile down to specific regions. Picking up the process in the Google Earth Engine Code Editor, the shapefile is imported. From here, two methods are used to separate the ecoregions out. In the NDVI dataset, the for the processing of charts, the shapefile can be defined as a variable, and then used as input:

```
var eco_merge: Table users/reckhauslucas/ak_eco_101_to_105_merged
```

Figure 8: Shapefile Import Code to GEE

In the case of the map visualizations, the complexity of the task requires a slightly different structure to the spatial data. The shapefile is separated into a different variable for each eco region, and then merged back together into a new file. This allows for the software to process all the spatial extents at once, without diluting all their data into one single region.

```
var eco_101 = ee.FeatureCollection(ak_101_105.filter(ee.Filter.eq('US_L3CODE', '101')))
var eco_102 = ee.FeatureCollection(ak_101_105.filter(ee.Filter.eq('US_L3CODE', '102')))
var eco_103 = ee.FeatureCollection(ak_101_105.filter(ee.Filter.eq('US_L3CODE', '103')))
var eco_104 = ee.FeatureCollection(ak_101_105.filter(ee.Filter.eq('US_L3CODE', '104')))
var eco_105 = ee.FeatureCollection(ak_101_105.filter(ee.Filter.eq('US_L3CODE', '105')))

var combined_eco = eco_101.merge(eco_102).merge(eco_103).merge(eco_104).merge(eco_105)
```

Figure 9: Shapefile Processing Code

The "combined-eco" method is sufficient for the entirety of the BSA calculations. In the case of the surface temperature data, the unaltered shapefile can be used, and the regions differentiated in the chart from the attribute data. Why the three datasets have different coding format requirements relates to the very structure of the data, stemming from its physics, and the instrument used for its capture on the satellite.

The time variable is isolated for in a different way. The data provided by the MODIS has a time stamp encoded (in fact numerous different types for different bands of data). This attribute information must be activated during processing by a date variable which picks out the right MODIS image. In the example below, two variables are created for start and end the 2018 research period:

```
var startDate2018 = '2018-03-01';
var endDate2018   = '2018-07-30';
```

Figure 10: Start Date & End Date Code

These are then used as input into a secondary variable which trims the MODIS data according to these dates. Examples of this variable for each of the three physical processes observed (temp, albedo, vegetation) is shown below:

```
temp_2020 = temp8d
   .filterDate(startDate2020, endDate2020)

var BSA_collection2020 = ee.ImageCollection('MODIS/006/MCD43A3')
   .filterDate(startDate2020, endDate2020)

var m_veg_2010 = m_veg.filter(ee.Filter.date('2010-03-01', '2010-07-30'));
```

Figure 11: Variable & Date Code

Mapping

With the spatial and temporal boundaries of the study built into the code, the processing of the data can be run. There are three different output in this study, each providing a different lens through which to deconstruct findings. The first and most straightforward are the sets of line graphs which show the respective ecoregions values for temperature, albedo and NDVI through time. This is the foundation of this paper's data analysis, as it allows the most procedural method to review and analyze the findings. However, while simple conceptually, these charts proved to be incredibly cumbersome to construct—and altogether impossible within the framework of Google Earth Engine. This is because the need was to produce a chart that shows a single regions' values over a series of years. However, the only output possible showed all five regions together in one chart for a given year. As the primary analysis is of a region through time, the latter option was insufficient. To circumvent this, first a graph in this limited matter was produced for each year of study (example albedo 2016 below):

```
var EcoRegion_Albedo_Histogram_2016 = ui.Chart.image.seriesByRegion(
BSA_collection2016, combined_eco, ee.Reducer.mean(), 'Albedo_BSA_Band1', 200, 'system:time_start',
'US_L3CODE')
.setChartType('ScatterChart')
.setOptions({
title: 'Alaskan Ecoregion Black-sky Albedo 2016',
vAxis: {title: 'Black-sky Albedo'},
lineWidth: 1,
pointSize: 4,
//labelSize: 20,
series: {
0: {color: 'FF0000'}, // 1
1: {color: '00FF00'}, // 2
// 2: {color: '0000FF'}  NOTE: Additional colors automatically generated for extra regions
}});

// Display.
print(EcoRegion_Albedo_Histogram_2016);
```

Figure 12: Line Graph Code

In addition to the tabular output, the earth engine API offers a .CSV table of the data values for download. This proved to be key, as it allowed for further post-processing in Microsoft Excel. Here using standard Excel graphic functionality, the desired chart of individual region over several years can be constructed, from which the data analysis section draws. These provide the most accurate picture of change at a moment's glance. However, to inspect a specific area at the sub-region level, a map visualization is required.

Map Visualization

The map visualizations made herein are used to aid in the interpretation of results. They show average pixel values (as discussed earlier in the "data" section) across a color range. By comparing the maps of different years for the same region, contrasts in dark and light areas

indicate changes in the data composition. These can be localized by visually auditing the terrain through real-world satellite imagery and the general identification of major landmass features. In this way trends at a scale beneath the ecoregion can be identified. The code below shows how such a “map viz” is generated for albedo and NDVI in the year 2012.

```
var collection2012 = ee.ImageCollection('MODIS/006/MCD43A3')
.filter(ee.Filter.date('2012-04-01', '2012-07-30'))

var blackSkyAlbedo2012 = collection2012.select('Albedo_BSA_Band1');
var blackSkyAlbedoVis = {
min: 0.0,
max: 1000.0, //
};

var clipped2012 = blackSkyAlbedo2012.mean().clip(combined_eco)

Map.addLayer(clipped2012, blackSkyAlbedoVis, 'BSA 2012');
```

Figure 13: Albedo Map Code

```
var dataset2012 = ee.ImageCollection('MODIS/006/MOD13A1')
                .filter(ee.Filter.date('2012-04-01', '2012-07-30')); // Data past 2016 is not available.

var ndvi = dataset2012.select('NDVI');

var ndviVis_v1 = {
  min: -2000.0,
  max: 10000.0,
  palette: [
    'FFFFFF', 'CE7E45', 'DF923D', 'F1B555', 'FCD163', '99B718', '74A901',
    '66A000', '529400', '3E8601', '207401', '056201', '004C00', '023B01',
    '012E01', '011D01', '011301'
  ],
};

var clipped0 = ndvi.mean().clip(combined_eco)

Map.addLayer(clipped0, ndviVis_v1, 'NDVI 2012');
```

Figure 14: NDVI Map Code

Measurement

Broadly speaking measurement can be broken down into two categories, lateral and vertical. The former representing a change in time, the latter representing a change in value. Through this lens the charts are reviewed forming backbone of the data analysis. From this broad understanding, a few more conceptual metrics are derived. For lateral measurement: the starting and ending date of the spring transition period. From this, measure is the duration of the transition. This can be applied to the individual year of a region, a single region over many years, or all the regions viewed together. The most important of these is the duration established from one region's data over all the years of study. The same principles of measurement are applied to the vertical scale. Here the resting winter value (high in the case of albedo, low in the case of vegetation and temperature) is measured, and then the resting summer value (the respective inverse of the winter trend). This duration is noted, and can be viewed at different scales, the most pertinent of which is single region-multiple years. In conjunction to this, the shape of the data-line is also observed, as it conveys not only duration, trend, and high-low values, but also the occurrence of significant weather phenomenon that may express themselves in the data.

Aside from the charts, the map visualizations provide a way to spatially place observed changes within the spatial bounds of an ecoregion. While the numeric values used to calculate albedo and vegetation for these is the same is in the graphs, there is another element required to symbolize this data over space. That is the ingredient of color coding, which allows for the differentiation of value between pixels immediately (rather than a numeric comparison). The use of a light to dark color scale to indicate an increase from low to high values is a standard in data visualization theory stemming from the *Gestalt Principles*, founded by the German psychologists

Max Wertheimer, Kurt Koffka, and Wolfgang Kohler in the 1920's (Koffka, w., Kohler, W., Wertheimer, M. et al., 1923).

5. Data Analysis & Results

Region 101– Arctic Coastal Plain

Temperature Graph

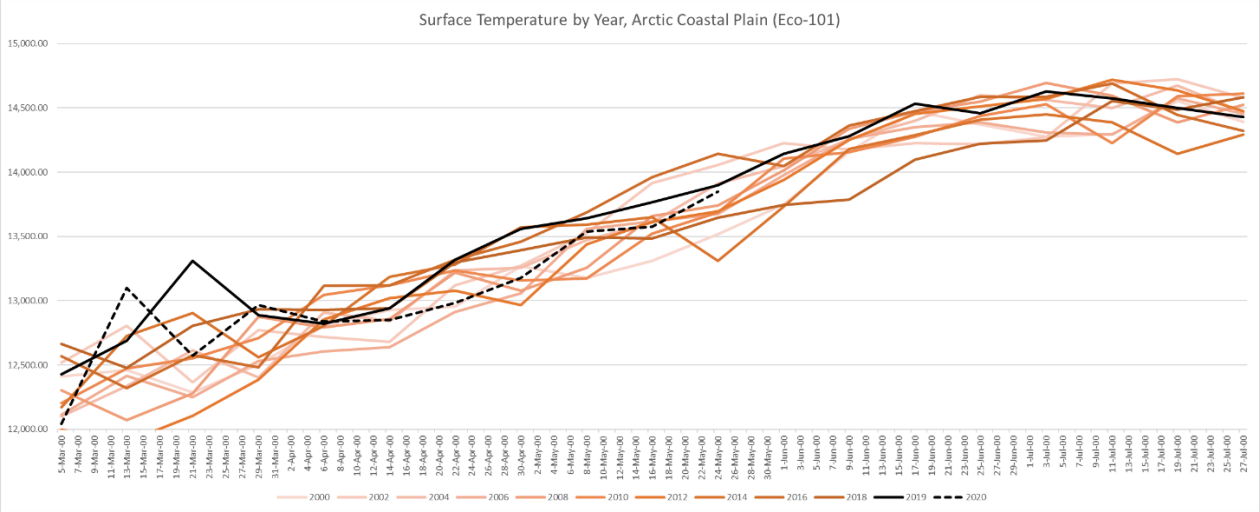

Figure 15: Surface Temperature Graph, Arctic Coastal Plain (Eco-101)

Surface temperatures in the Arctic Coastal Plain (Eco-101) are of special significance because this is a permafrost region. Surface temperatures therefore give one of the best indications as to the occurrence of permafrost melt. The permafrost lies underneath the "active" layer of topsoil. This thaws in the summer and freezes in the winter. However, when temperatures linger for several weeks around the thawing mark conditions present in which the permafrost underneath begins to decompose. The broader effects of this have already been discussed at length. With this in mind, we look for indications of potential permafrost melt when surface temperatures hover around the thawing/freezing mark of 13,650 Kelvin. The minimum and maximum value ranges along the x and y axis are considered as the markers of the spring

transition period. Individual years which exhibit slopes that deviate from the average are explored in more detail.

Beginning then by looking for indications of wet snow conditions, these are evident in the most recent year of the study (2020) in which the line goes horizontal at this thawing mark from roughly the 8th to 16th of May. In the chart, light lines represent early years, dark more recent. With this visualization aid, there is an observable trend of more recent years spending circa two weeks around the thawing mark, while in early years of the study, the slope spends no time around the thawing period, instead transitioning decisively from winter temperatures to summer. While temperatures begin to rise in March, it is not until the end of April that temperatures in the earliest cases cross the thawing mark. This is so for 2019, as well as 2014, a first indication of earlier temperature onset in recent years. The latest the thermal transition mark is crossed is in late May. Here the year 2000 and 2014 cross the mark. This is significant for two reason. First, it shows the first year of study with a late thermal transition. Second this is a sign of strange behavior in 2014, as temperatures hovered around the thermal mark for from April 30th to May 16th, only to fall again and not pass the mark for good until May 30th. Overall, it seems the early years have less of a spread (both horizontal and vertical) and that this has become exacerbated through time. From this data, with BSA and NDVI in mind, the month period from April 28th to May 28th is to be studied further. The years 2020, 2019 and 2014 stand out as exhibiting some thermal anomalies. 2020 and 2019 both show early warming events that precede the expected date by two months. At the expected time in early May, both years then present wet snow conditions. 2014 also shows wet snow conditions, but then experiences an unexpected cold snap at the end of the expected thawing period.

Albedo Graph

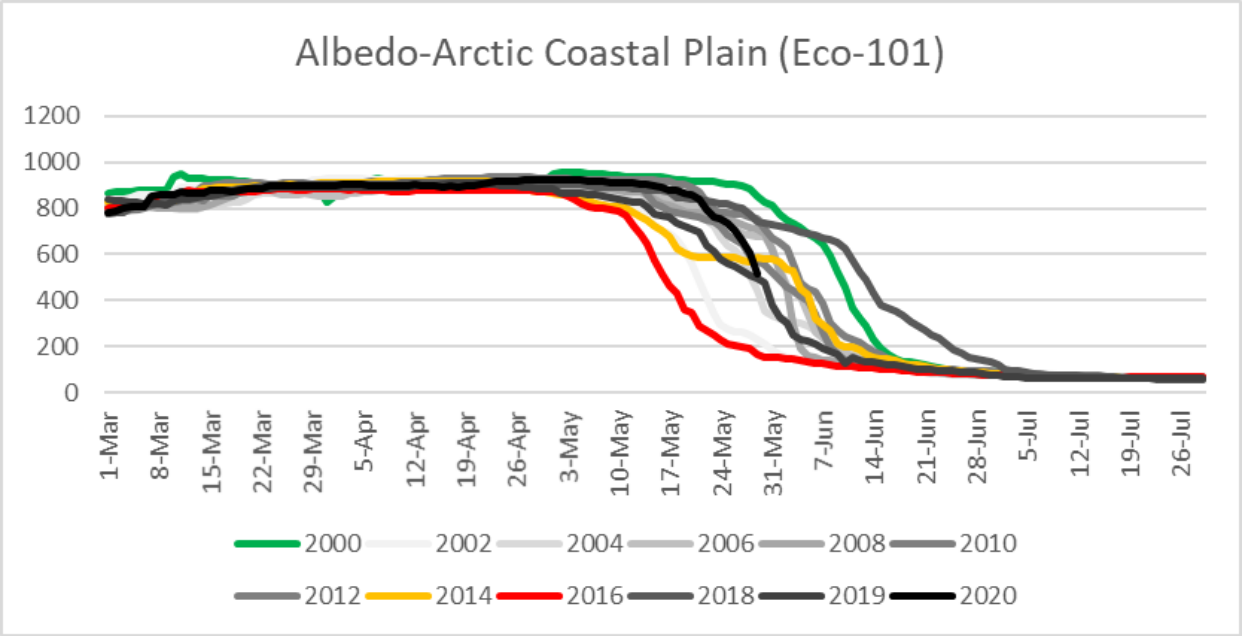

Figure 16: Albedo Graph, Arctic Coastal Plain (Eco-101)

The April 28th to May 28th period represents the time during which thermal transition was observed. During this period, Albedo values also transition from maximum winter reflectivity from snow covered conditions lasting until late April early May, which then in most cases fall drastically by mid-May. Evaluating the first and last date by which albedo loss is observed, these are roughly May 17th (earliest) to June 14th (latest). Interestingly, these two min and max values are both from recent years; 2016 and 2018. However, the years 2019 and 2020 have very average slopes. Taken as a set of three, this suggests that albedo values are increasing in annual variance. This correlates strongly with the documented warmest years on record in the arctic occurring within the last five years. In terms of maximum albedo values, there is little to distinguish the region in the winter across its years with BSA consistently at around 800 - 900. Similarly, there is little to differentiate in albedo once full-snowmelt has occurred (<100). The most interesting "event" to be seen in the data is in fact in 2014, one of the years identified by the temperature

study as exhibiting anomalous temperature patterns. These showed wet snow conditions for two weeks from April to May and were directly followed by a cold snap. In the BSA for this year, there is a prominent plateau which interrupts the normal descent of BSA values. This begins on about May 17th and lasts to the beginning of June. Comparing the dates of these two sequences of different data sources, the BSA plateau follows the completion of the wet snow period and then aligns with the cold-snap of temperatures. This shows that in this year, there was likely to a re-freeze of the surface cover and new top-snow to stabilize albedo values in this way. How this affected the vegetation growth that occurred up to that point is a logical comparison to draw in the next chart.

Albedo Map Visualization

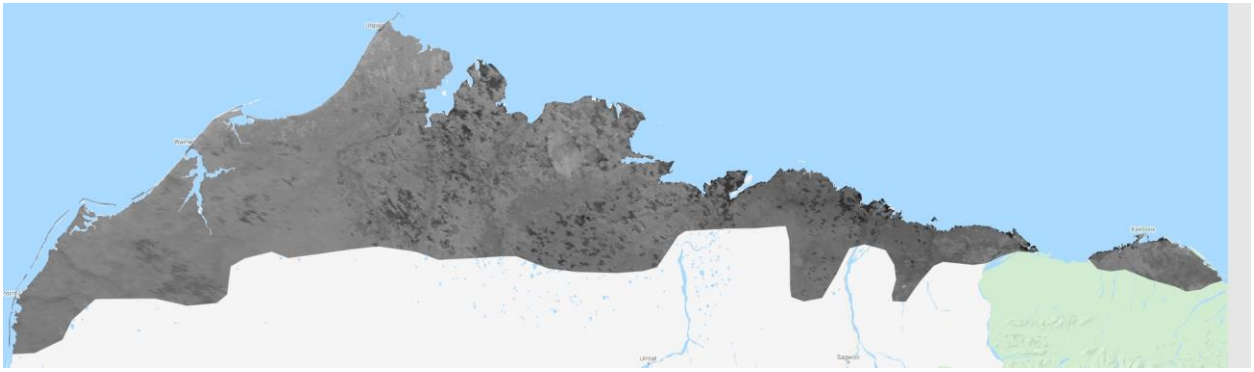

Figure 17: Eco-101, Average Black-sky Albedo in 2000 (April – July) (Latest Melt Year)

Figure 18: Eco-101, Average Black-sky Albedo in 2014 (April – July) (Average Melt Year)

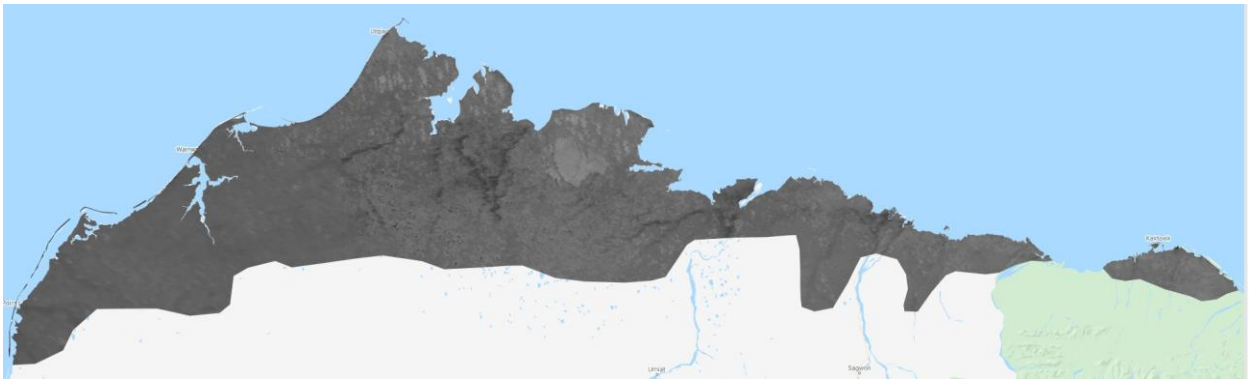

Figure 19: Eco-101, Average Black-sky Albedo in 2016 (April – July) (Earliest Melt)

From the albedo charts, the three years presented in figures 16 -18 (2000, 2014, 2016) represent the latest, average, and earliest melt years of the study. Several differences between the years can be observed. In 2000, the darkest pixels are scattered like pockmarks across the landscape, concentrated in the center—these are melt ponds, where thaw has occurred. Rivers are recognizable only by the faintest trace of their path. Overall, the surface texture is of a light-grey hue, indicating high levels of frozen content in the ground. 2014 was a year that showed wet snow conditions, followed by a re-freezing event in May. Albedo loss plateaued in response. In the map view, this is reflected in the absence of the pock-mark effect of thaw-pools observed in 2000, as these re-froze in this year and have higher albedo as a result. However, viewed in its entirety, in 2014 the arctic coastal plain appears darker. Riverbeds are now clearly visible as dark contour lines snaking to the coast. In the western region—a large permafrost area—significant shading has occurred. There is further transition to the year 2016, in which again overall pigmentation has darkened. Riverbeds are now clearly identifiable as the features with the lowest albedo value. In riverbeds, a significant layer of silt and earthen deposits sit on top of the permafrost. A darkening of this intensity likely reflects the thawing of the river's water and this mixture underneath. In the western portion of the region, where an overall darkening has advanced, this is the onset of thawing of permafrost beneath a shallow layer of topsoil. Interesting is that the melt-pools appear largely frozen in this year, especially along the coast. This could relate to marine temperatures, whose differing temperature fluctuations are not captured by the charts used.

NDVI Graph

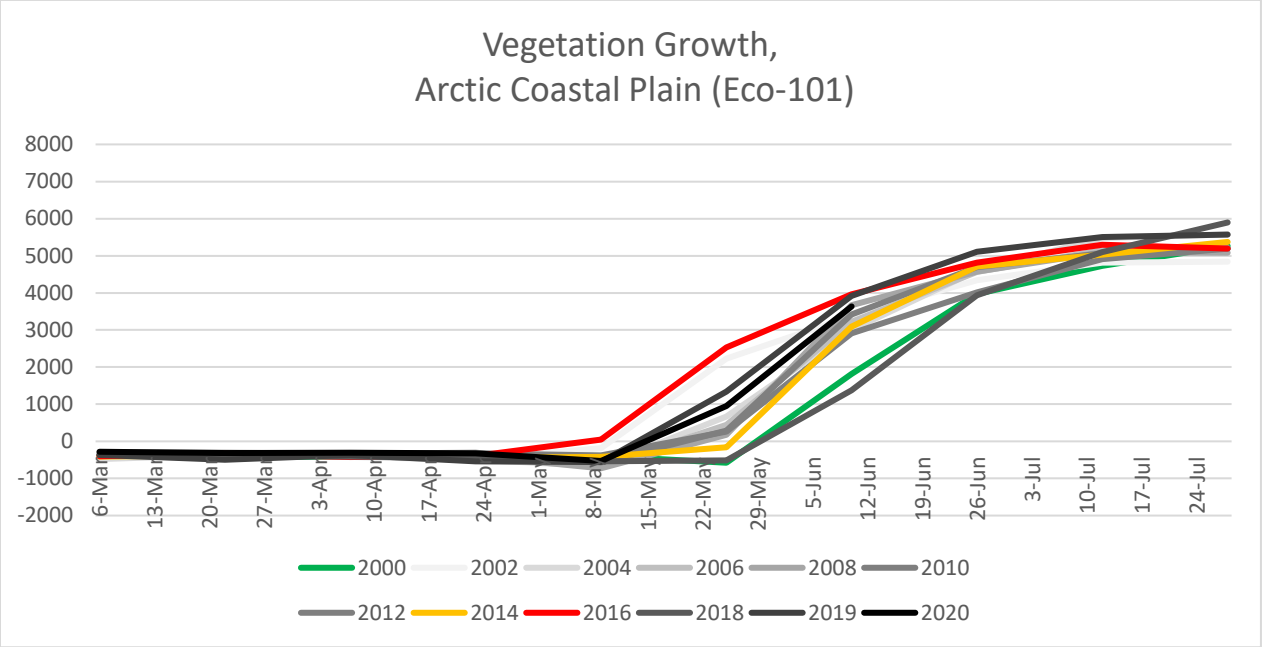

Figure 20: NDVI Graph, Arctic Coastal Plain (Eco-101)

In this region, the farthest north in the US, there appear to be two significant vegetative growth dates that mark the onset of spring. The earlier of these is roughly May 9th, during which in several years the region shows the first signs of vegetative activity. In years where this is not the case, the date is some two weeks later close to the 25th of May. In all years by this date, spring vegetation growth is fully underway. In this region, vegetation is extremely sparse and limited to grasses and shrubs residing on the topsoil above the permafrost. In the year 2014 a cold snap was observed from the 14th of May to the 30th, with a corresponding stagnation of albedo loss. Comparing with the NDVI data two things stand out. This first is that vegetation does not show any sign of growth before the late-cold snap. This is unexpected as the vegetation was presumed to be in growth during the wet snow conditions of thawing temperature which preceded this cold snap. Instead, the NDVI shows the region did not significantly develop any vegetation in that year

until after the cold snap ended in late May. Overall, the shape of the NDVI data in this year does not reflect the unique slop of that of BSA for the same year. This merits further consideration. In other regards, the data does mirror those of BSA and temperature, as this graph too tells the story of a region with increasing variance of vegetated growth periods as we move towards the present day.

NDVI Map Visualization

Figure 21: Eco-101, Average Vegetation Growth (NDVI) in 2000 (April – July) (Latest Growth)

Figure 22: Eco-101, Average Vegetation Growth (NDVI) in 2014 (April – July) (Average Growth)

Figure 23: Eco-101, Average Vegetation Growth (NDVI) in 2016 (April – July) (Earliest Growth)

From the vegetation index map visualization, the “greening” trend observed in the charts is clear. While in 2000, the region is a covered in a fine speckle of yellow and orange (strongest over Teshekpuk Lake), from 2014 to 2016 this color is lost to green. By 2016, the orange color is restricted to clearly delineated patches—correlating with the largest of the melt ponds and rivers. This then is a picture vegetation gains across all intermediate areas in this region. Where in years past the land between melt ponds was locked in ice with no active vegetation, the warming of this ground cover has enabled the rise of light vegetation. In the south western region, there is evidence of second stage vegetation with its darker green pigmentation. This indicates a transition from grasslands to low shrubs. For a region dominated by permafrost reaching depths of 300 meters, the greening observed here has been significant, indicative of wholesale changes to surface conditions to engender such a transition.

Region 102 – Arctic Foothills

The arctic foothills are an evolution of the arctic coastal plain, as land shaped by the harsh co-existence with the arctic sea’s constant push and pull of wind and tide, saturate the land and flatten everything for hundreds of miles. The arctic foothills then represent the first surface cover and geology whose primary influence has not been the climatology of the ocean, but that of inland configuration. However, this is still a permafrost area with no tree cover. Therefore, temperatures here are expected to be closely reflective of region 101, and any indication of wet snow persistence an important marker for permafrost melt evaluation.

Temperature Graph

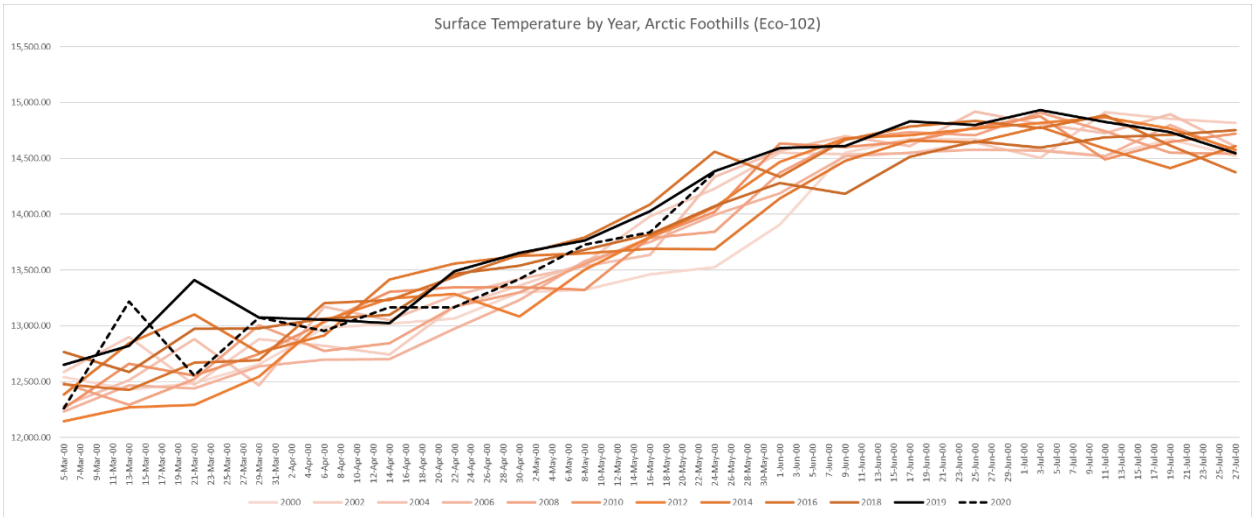

Figure 24: Surface Temperature Graph, Arctic Foothills (Eco-102)

Beginning with the earliest and latest dates of transition past the thawing mark (13650 Kelvin), these are April 30th (2019, 2014) and to May 26th (2000). Again, as in with region 101, the year 2014 stands out. However, in this year, in this region, there is no observed late cold snap as in the arctic coastal plain (Eco-101). Instead, there are other noteworthy observations. The first is that 2014 is one of the last years to reach the thawing point, but then presents wet snow conditions for another three weeks languishing at the thaw/freeze mark. When temperatures that year do finally cross the mark for good in late May, it is one of the last years to do so, only exceeded by the first year of the study, 2000. Other noteworthy years are 2019 and 2020. These show early-onset warming events in May, followed by some of the overall highest temperatures recorded. Overall, the horizontal x-axis trend is one to the left indicative of earlier warming dates. The trend along the y-axis is upward, indicating higher overall temperatures. The variance of data here is not as pronounced as in ecoregion 101. This suggests that the regions' surface

composition changes in a uniform way. As this is a permafrost region, this is an important observation.

Albedo Graph

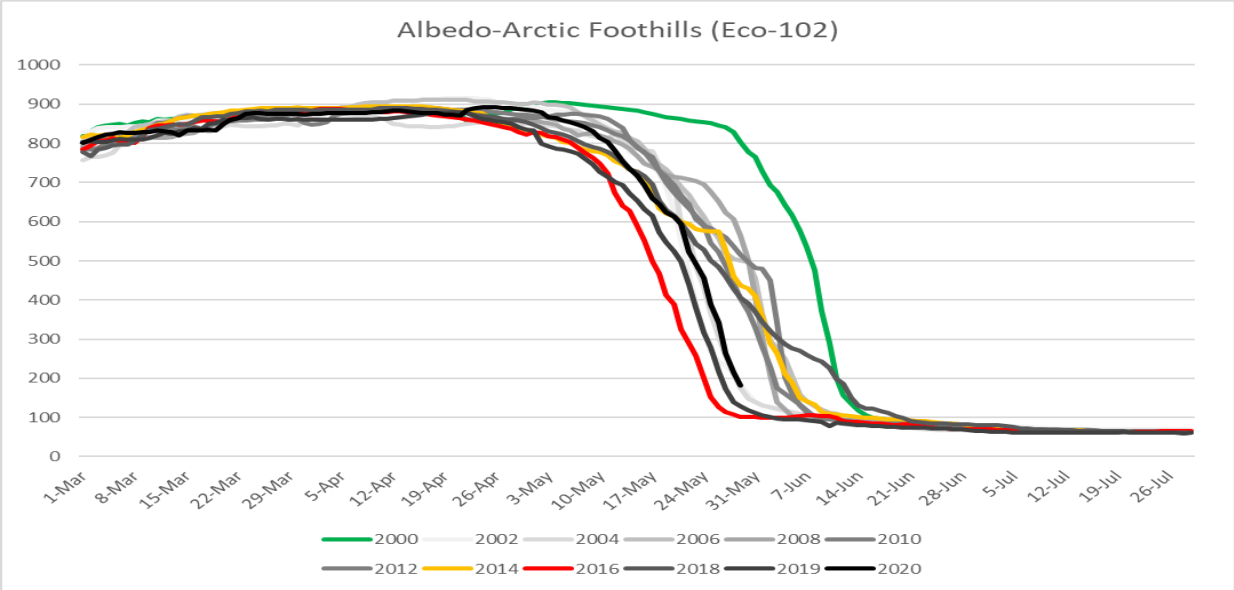

Figure 25: Albedo Graph, Arctic Foothills (Eco-102)

The overall albedo trend for the Arctic Foothills is one from right to left. That is to say, the date by which the winter high values fall off is happening earlier. In the first year of study 2000, the data shows what could be interpreted as an ideal representation of expected albedo behavior. Levels from the winter stay between 800 – 900 until the last day of May, after which they plummet to less than 100 BSA in two weeks. No year since has displayed the same combination of late date of decline; total BSA loss over two weeks; and an uninterrupted linear slope. The move left from 2000 to all other years is by a full two weeks. Winter values before the spring melt are stable across all years. Noteworthy is that the BSA values seem to increase from 800 – 900 from March to May before then receding. Why this late in the winter season the albedo

increases further still is something to consider. Evaluating the thaw range from the temperature chart (April 30th to May 26th) this corresponds to the loss of BSA over the same period, and another two weeks further in the case of some years. The year 2014 was again identified in the temperature chart as of unusual thermal composition, crossing the thermal mark early, experiencing an elongated wet snow period, and then transitioning to spring values on May 24th. For the albedo of the same year, there are two movements in the data corresponding to this. Firstly, looking at the trend leading up to the 24th, the data plateaus to a near horizontal slope. Secondly, the slope then suddenly drops on the 24th, resuming a more expected linear downward slope. There is one more similar movement on May 31st, but the trend from the first event thereafter is more consistent with expected behavior. Here then we see the relationship between surface temperature and albedo expressed across two charts. This is a point for further analysis. 2010 is another year that shows a similar behavior in which the slope of the line changes direction on May 31st, significantly increasing its downward trajectory.

Albedo Map Visualization

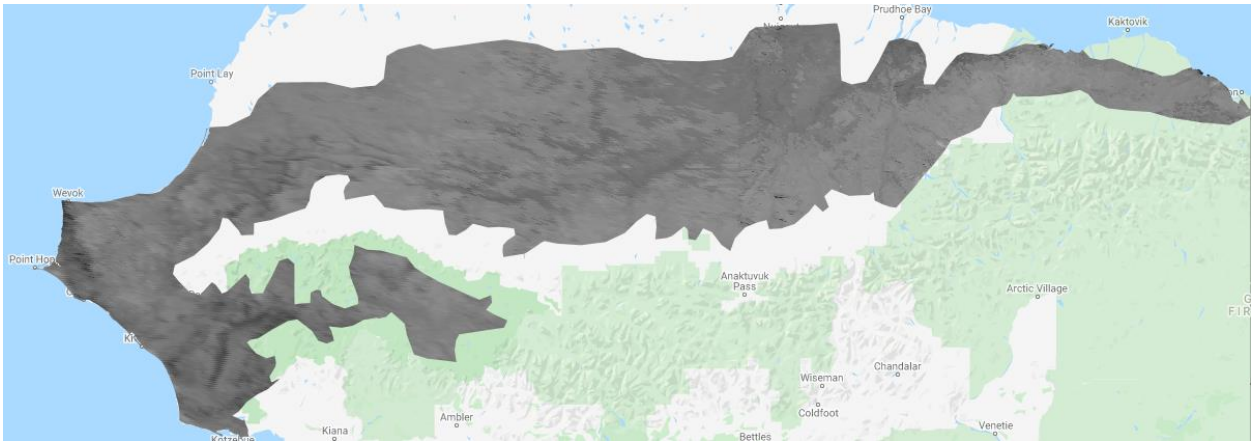

Figure 26: Eco-102, Average Black-sky Albedo in 2000 (April – July) (Latest Melt)

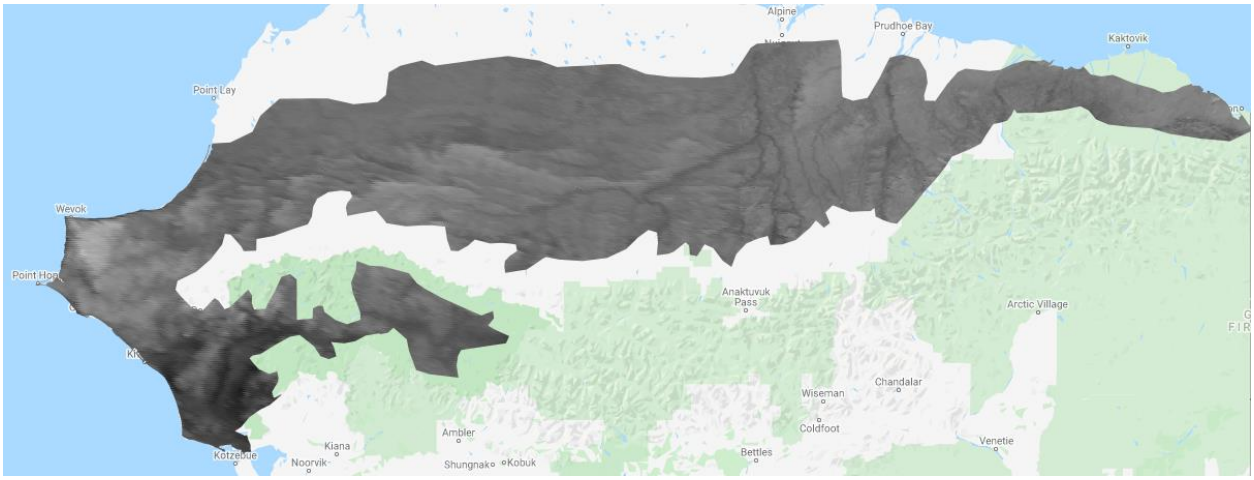

Figure 27: Eco-102, Average Black-sky Albedo in 2014 (April – July) (Average Melt)

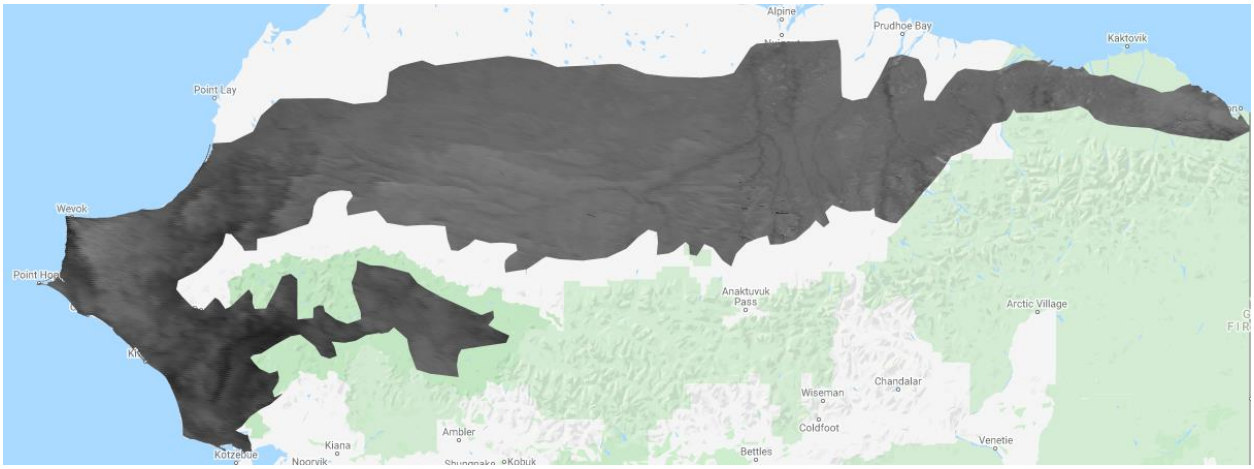

Figure 28: Eco-102, Average Black-sky Albedo in 2016 (April – July) (Earliest Melt)

A look at the spatial dispersion of albedo values in the arctic foothills shows significant change. As in the Arctic Coastal Plain (Eco-101), the years' most indicative of early, average, and late onset albedo loss were 2000, 2014, and 2016. Viewed in sequence, the map from 2000 shows the extent of permafrost in the region as the lightest coloration area, covering most of the region. It subsides only along the faint outlines of rivers and the in a few atypical areas.

In 2016, significant darkening has begun. This is most prevalent in the south-west of the region, where near black pigmentation is visible. Riverbeds are now clearly defined throughout, and the overall light hue of the permafrost pixels has decreased. By 2016, further near black pixelation is observable on the western coastal portion. Inland, the permaforst of such a light grey in the year 2000 has significantly darkened. The change from 2014 to 2016 is primarily one of contrast, where the latter has less contrast then the former. This suggests that overall values have shifted to a lower mean albedo, with more dark anomouls regions than light.

NDVI

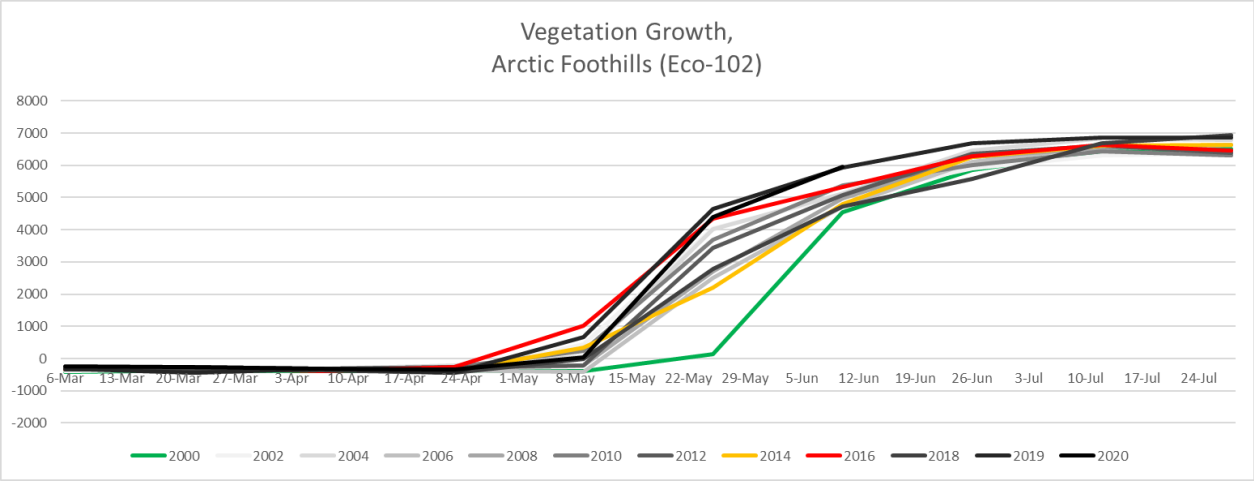

Figure 29: NDVI Graph, Arctic Foothills (Eco-102)

Starting the review of NDVI with the thaw time-period April 30th to May 26th a closer view shows this aligns with the earliest stages of vegetation growth to the last. Again there is a direct correlation between the May 26th date of the end of the wet snow period, the change of slope in the BSA data at this date, and here in the NDVI the first signs of vegetative growth for the region on the same date in that year. Overall, the trend is one of growth occurring earlier. The year 2000 stands out for how late the vegetation growth occurs, and how quickly when it does. This time difference is roughly two weeks. Interesting is this same date (May 26th) is observable in the other years as a levelling of the data. This suggests the date could correspond to a specific stage of vegetation growth occurring. There are in any case—even in the most rapid years of vegetation growth—stages to vegetation growth. These appear as an initial growth up to 1000 NDVI in May. After this, the main growth stage occurs, in which values rise drastically for circa two weeks arriving at about three-quarters of their eventual summer value. The last quarter of growth lasts from mid-June to July. Overall, this growth is increasing in strength, as the most recent years 2019 and 2020 show many of the highest values, and end the chart resting at circa 7000 NDVI, some 900 points higher than in other years. This trend, in a permafrost region barren of any larger vegetation types, is significant. What is making up for this increase could likely be related to carbon release from underlying permafrost.

NDVI Map Visualization

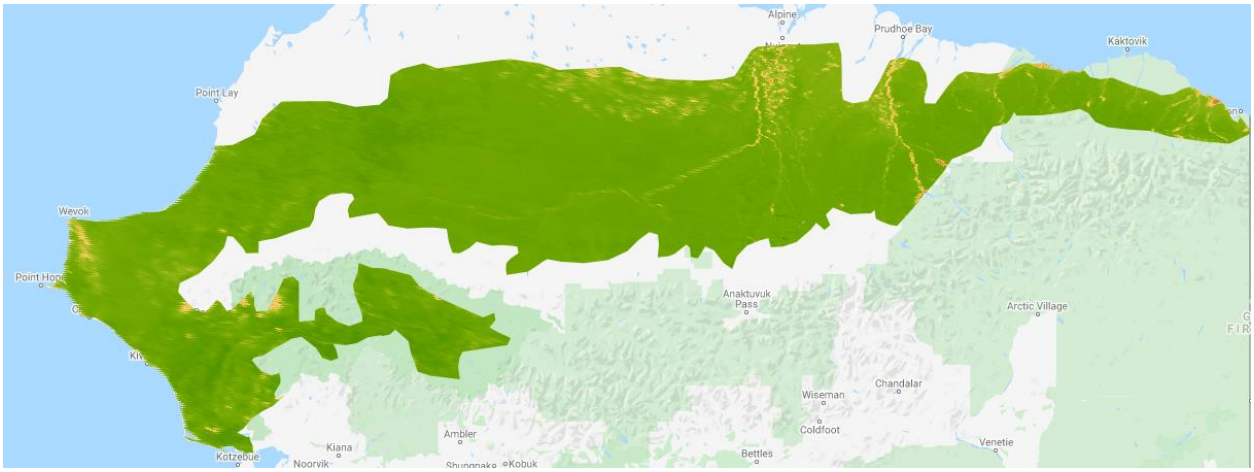

Figure 30: Eco-102, Average Vegetation (NDVI) in 2000 (April – July) (Latest Melt)

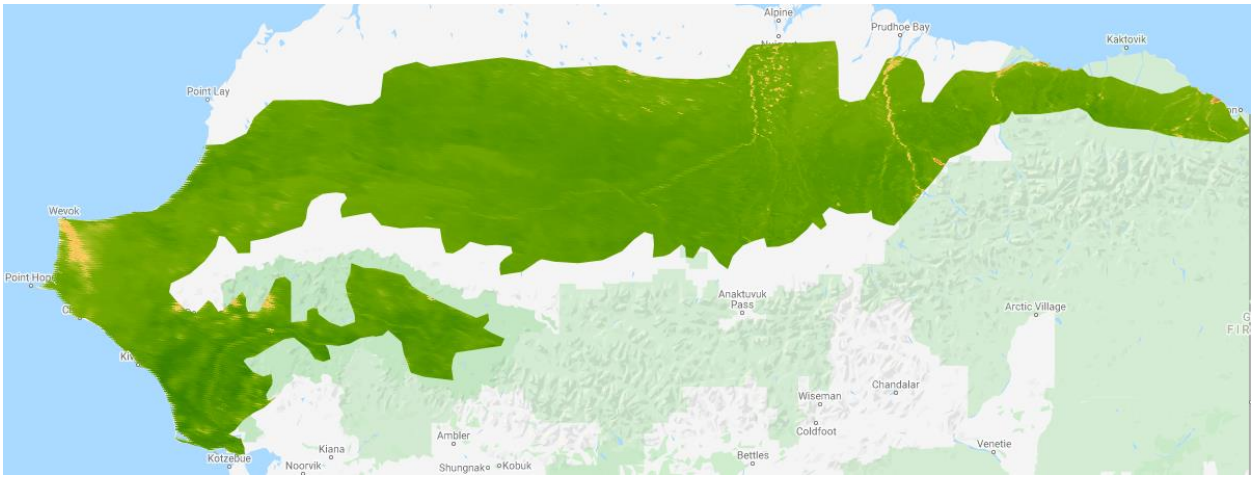

Figure 31: Eco-102, Average Vegetation (NDVI) in 2014 (April – July) (Average Melt)

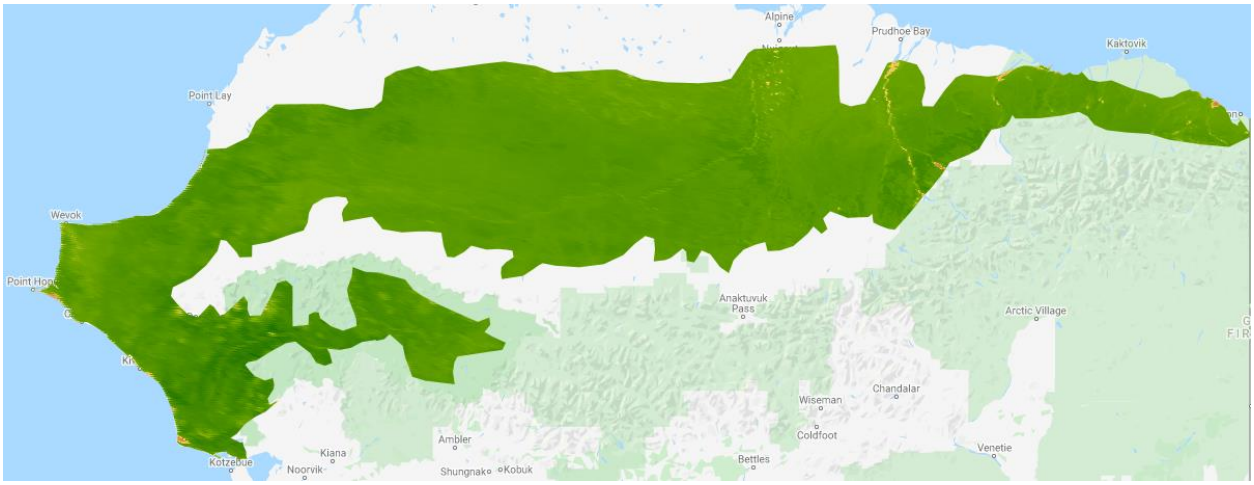

Figure 32: Eco-102, Average Vegetation (NDVI) in 2016 (April – July) (Earliest Melt)

The picture to emerge from the vegetation maps is that of encroachment into previously untenable geographies as climate conditions have shifted. For example, this is reflected on the Wevok Peninsula. This windswept outcrop into the Chukchi Sea is colored yellow in 2000 and 2014—an area of frozen dunes, ice formations, and emergent permafrost. However, by 2016 it has become solid green. This reflects that a combination of weather and surface conditions have changed enough to allow the formation of grasses, mosses and other basic vegetation. In fact, by 2016, all but the largest riverbeds appear to have been permeated by vegetation. This encompasses all the tundra region at the heart of the arctic foothills, beneath which is permafrost. Greening to this degree is only possible in this baren landscape with the decomposition of previously frozen organic material to feed the metabolic cycle of plant life.

Region 103 –Brooks Range

Temperature Graph

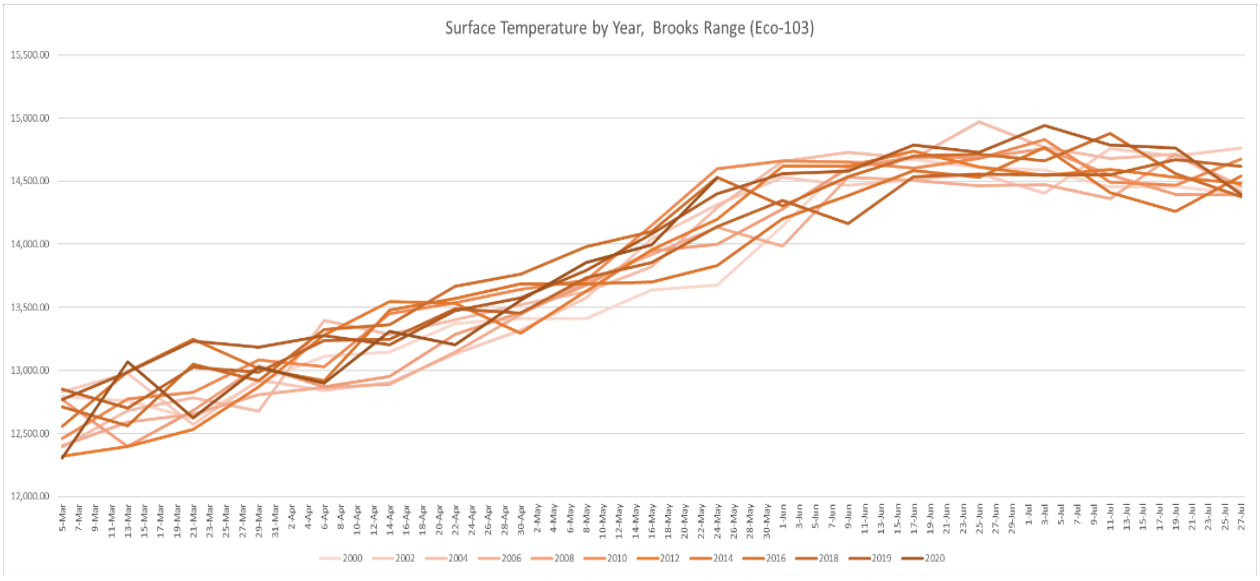

Figure 33: Surface Temperature Graph, Brooks Range (Eco-103)

In topographic terms, the Brooks Range is more varied than the Arctic Coastal Plain and the Arctic Foothills. It contains high altitude zones, boreal forests, inland plains with permafrost. Therefore, the temperature distribution here is expected to be more varied than the first two ecoregions studied. Look closely, and this can be seen. In this region values peak at nearly 15,000 K (80.33 degrees Fahrenheit) higher than 101 and 102, yet in some years temperatures in late July are below 14500 (62.33 degrees Fahrenheit), lower than in either 101 and 102, suggestive of the high elevation areas that stay snow covered year-round. Evaluating years with suggestive wet snow conditions, these appear to be 2014 (consistent with regions 101 and 102) from April 30th to the 16th of May, and the year 2000 from May 16th to 24th. Overall, the trend is again of movement to the left along the y-axis. 2000, the first year of study, experiences the latest rise in temperatures. All other years rise earlier to the left, with 2019 and 2020 showing some of the highest temperatures recorded at the earliest times. 2019 is also shows borderline wet snow conditions from 20th April to 30th April. The five-week period from this April 20th date to the May 24th date (from 2000) is the timespan during which the Brooks Range crosses the thawing mark into the spring/summer season.

Albedo Graph

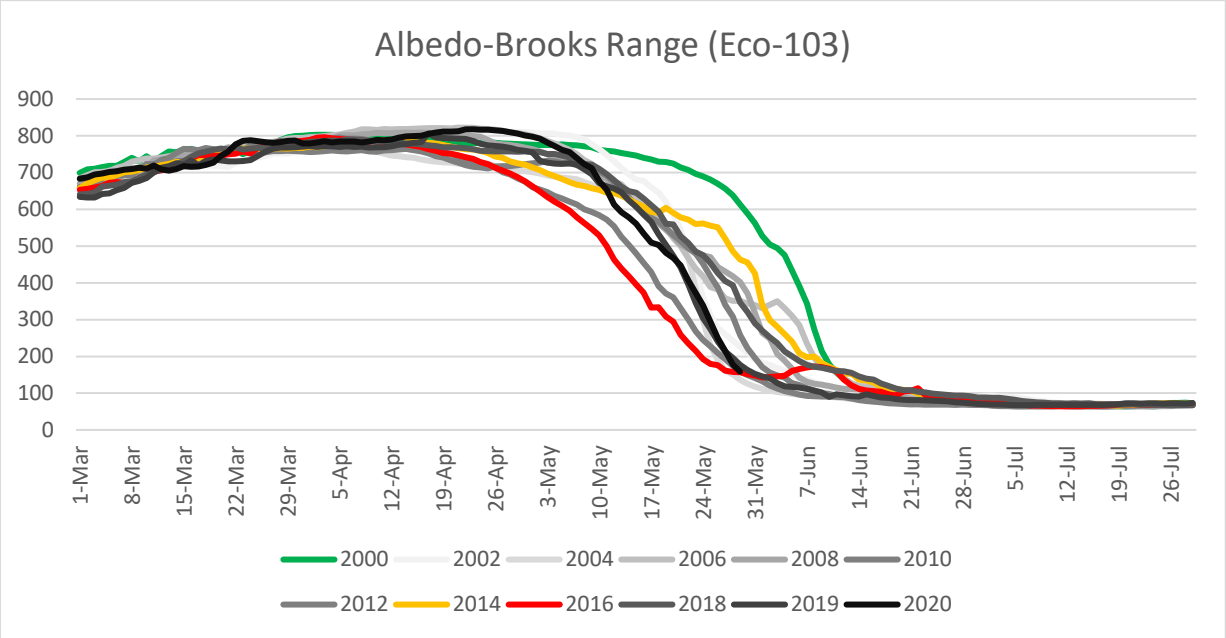

Figure 34: Albedo Graph, Brooks Range (Eco-103)

Beginning with the thaw period identified from the temperature graph as April 20th date to the May 24th, this corresponds to the start of the albedo-loss period. The delay between the time it takes for snow to fully melt and temperatures rising above freezing shows this is a physical process which is subject to significant variation, much of it dependent on surface conditions such as contour of the surface, underlying vegetation, and exposure to sunlight. The trend here is one of albedo loss occurring earlier over the years. 2000 stands out here as it has in other charts for its combination of late date of decline; steep loss of BSA over two weeks; and an uninterrupted linear slope. If this is taken to represent a baseline value, all other years measured in every dimension are a deviation from this trend. 2006 shows an interesting plateau phenomenon from May 24th to June 7th in which albedo stabilizes and even increases for briefly, before returning to its downward trending slope. This suggests a late season cold-weather phenomenon which upon

review is also observed in the temperature data. Even though this thermal dip did not go beneath freezing on the chart, it would appear the affect was enough (perhaps at high-altitude) to create frozen/semi-frozen conditions that would stabilize black-sky albedo in this way. Notably lackluster "performance" is observed in 2016 and 2010 in which albedo loss began around April 19th, and then decreased at a more gentle than average slope until roughly June 7th. Overall, the difference in data trends from year-to-year basis are significant in this region. This high degree of variance likely reflects two aspects of the data: the region is undergoing significant climatological shifts; the region is varied in elevation leading to a higher degree of variance in surface temperature values.

Albedo Map Visualization

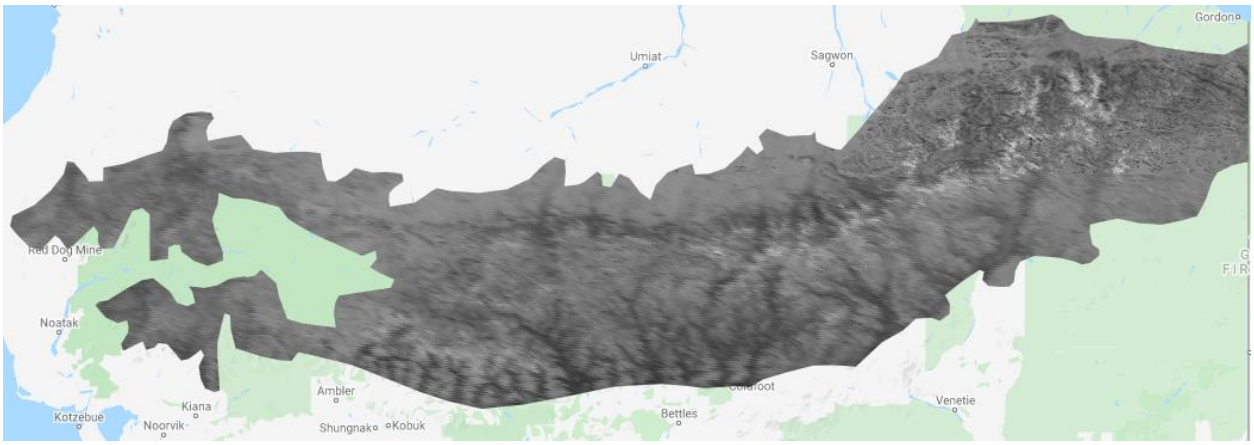

Figure 35: Eco-103, Average Black-sky Albedo in 2000 (April – July) (Earliest Melt)

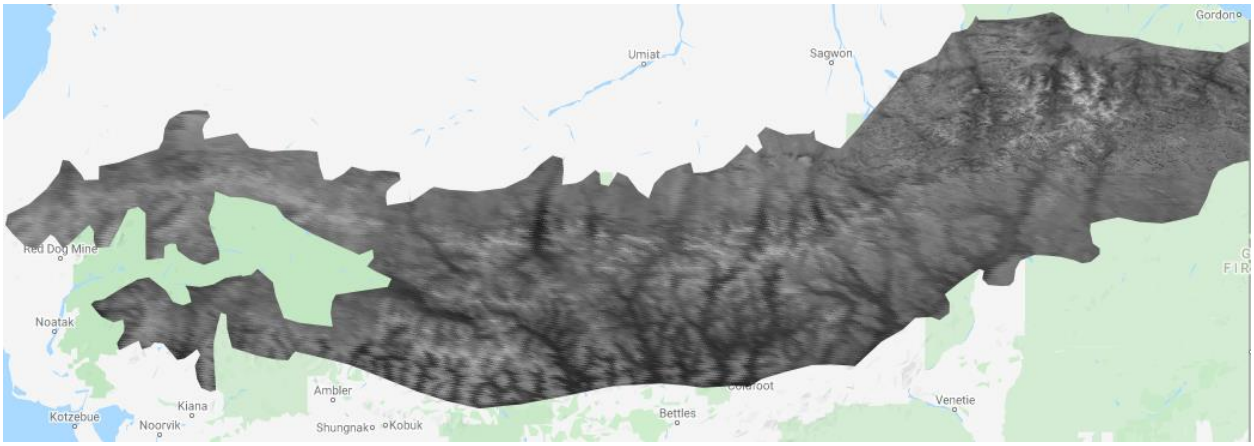

Figure 36: Eco-103, Average Black-sky Albedo in 2014 (April – July) (Average Melt)

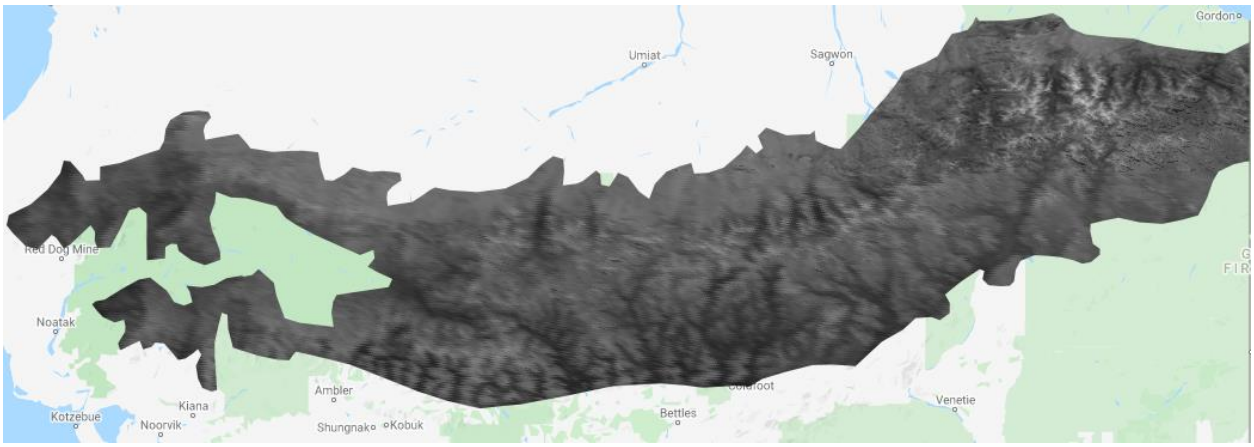

Figure 37: Eco-103, Average Black-sky Albedo in 2016 (April – July) (Latest Melt)

The Brooks Range has a truly varied topography, predominantly comprised of mountains and valleys. This aids the analysis of albedo over the same area. In the map, the mountain ridges and peaks are clearly identifiable by their lighter complexion. Dark valleys reach out like tentacles into these ranges. In the year 2000, there is near white pixilation over much of the mountains' ridgelines. Dark albedo values are most pronounced along the valleys of the southern slopes. In 2014 the intensity of these valleys on the north slope increases significantly, while in 2016 this has been accompanied by an overall darkening shift across the entire region. As the Brooks Range acts as the natural boundary between the artic climate to its north and the sub-arctic boreal climate to its south, these homogenizing albedo changes indicate that surface conditions at lower elevations are trending towards the latter.

NDVI Graph

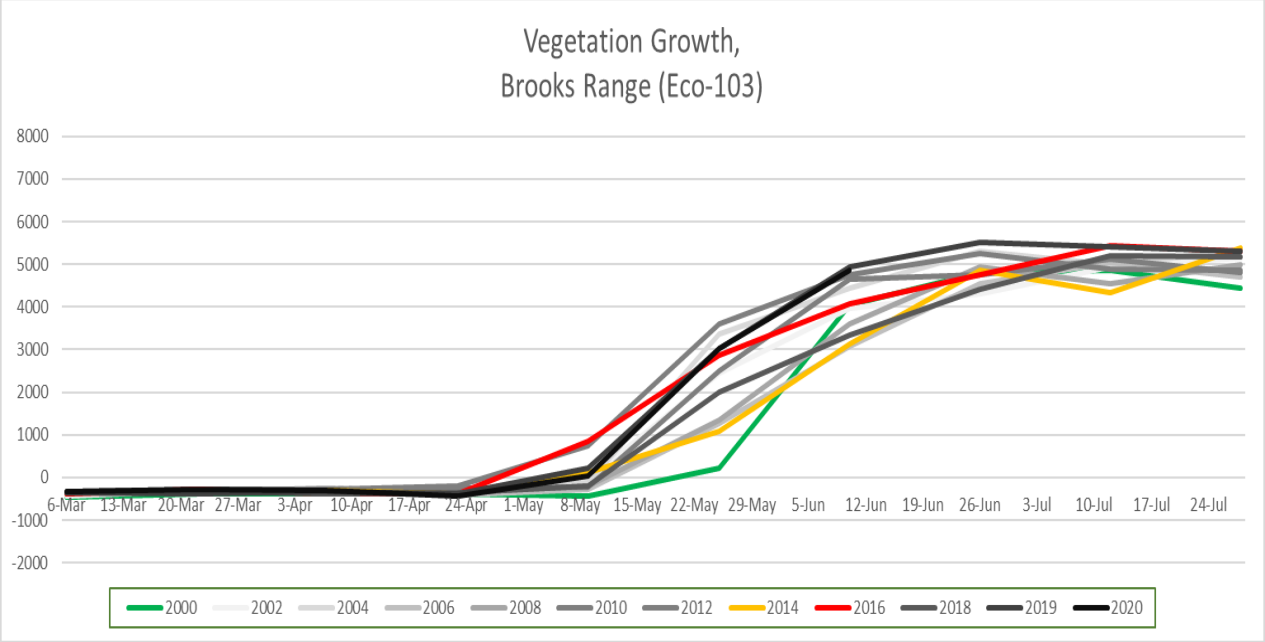

Figure 38: NDVI Graph, Brooks Range (Eco-103)

During the identified wet snow min-max date range (April 20th date to the May 24th) the first traces of vegetation growth can observed up to the end of the first angular slope of the line (across all years). The year 2000 stands out as showing up late, then "greening" very rapidly, and until June 8th, and then peaking in NDVI value just under 5,000. In the years elapsed since, this peak vegetation value at the end of July has on average increased past the 5,000 mark up to circa 5500. This top-end increase in NDVI value indicates that more vegetation is present. In a region defined by mountains and valleys, this potentially shows regions previously devoid of vegetation at high altitude zones are transitioning in surface composition as the temperatures increase and permanent snow cover recedes. These effects are likely to be profound for the eco-systems of these mountains. The year 2014 also shows an interesting event in the data, with NDVI levels experiencing a drop in values late in the study period from June 26th to July 12th, where after levels increase once more ending at the highest value of all years on the last day of the study. That such a lull occurs so late in the season, when vegetation is already near peak, is peculiar. Indeed, there is a temperature lull in this period. This suggests that even as late as July, there is still growth potential in the overall landscape, which can be affected by changes to expected climate conditions. Considering the BSA for this same time, the trend of the data becomes jagged, altering the slope of the line unto that point and rendering it slightly bulbus with elevated values than would have been expected to occur. Herein are the traces of the nuanced interaction between vegetation at its different stages and different types and albedo.

NDVI Map Visualization

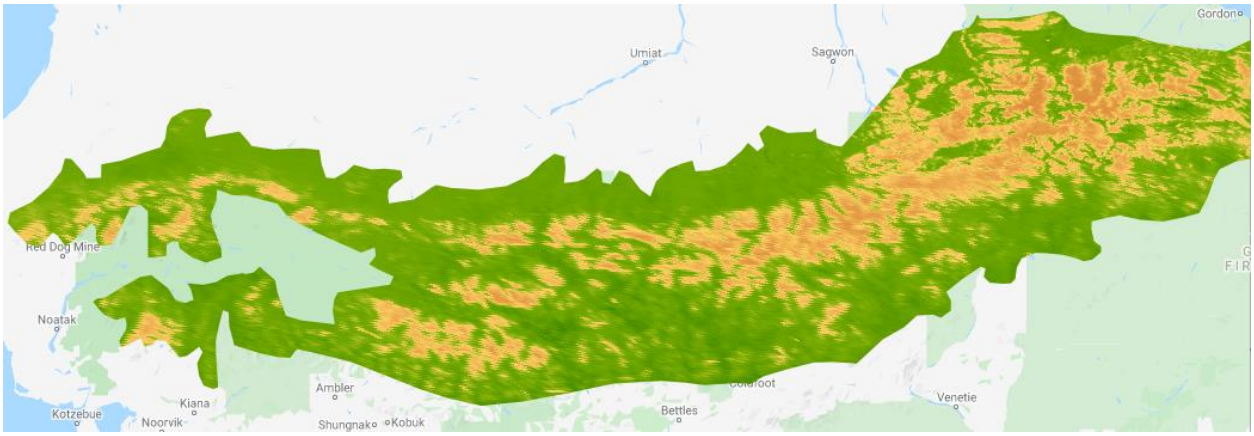

Figure 39: Eco-103, Average Vegetation (NDVI) in 2000 (April – July) (Earliest Melt)

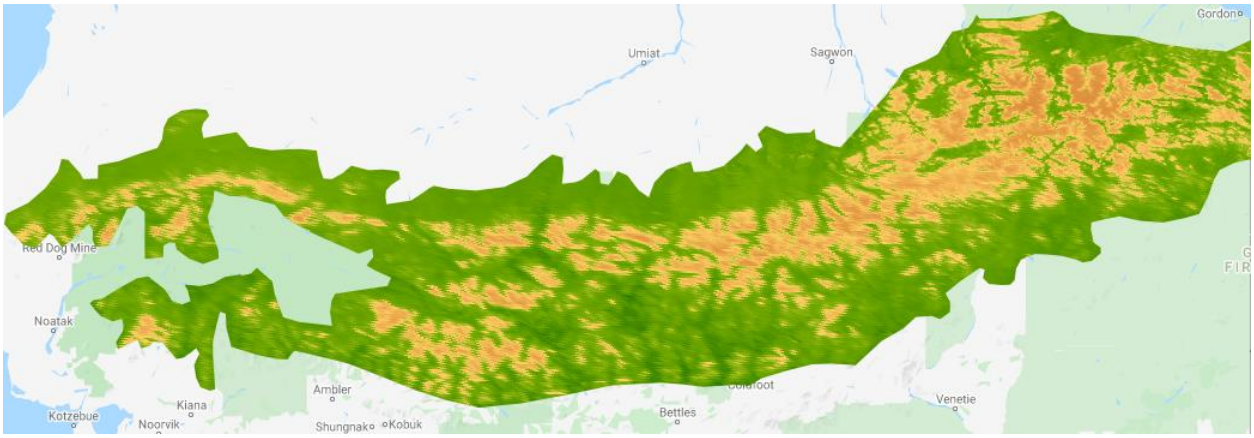

Figure 40: Eco-103, Average Vegetation (NDVI) in 2014 (April – July) (Average Melt)

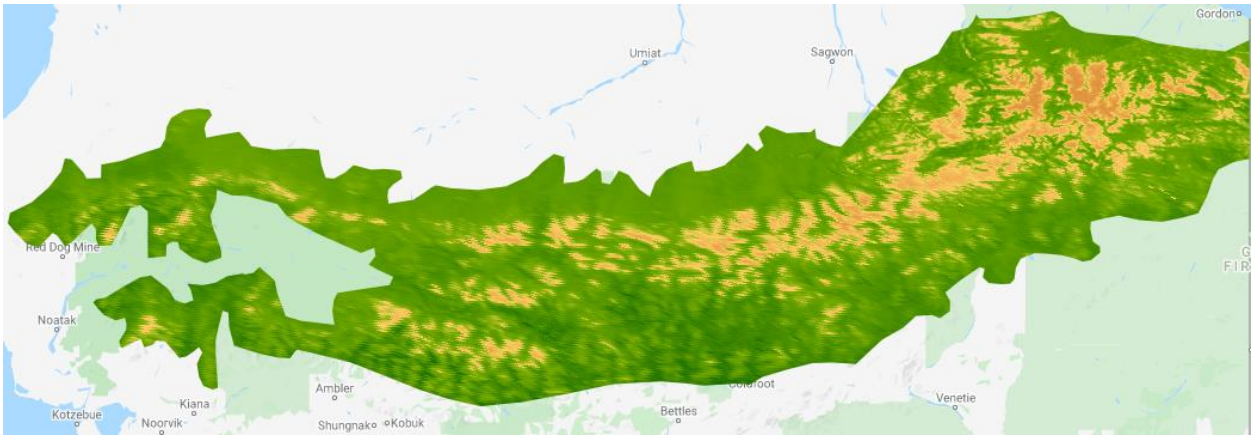

Figure 41: Eco-103, Average Vegetation (NDVI) in 2016 (April – July) (Latest Melt)

The spatial correlation between low-albedo and vegetation is easily spotted. Over the course of these three intervals, dark green begins to creep into the mountainous topography from the south. In 2014 some of this coloration is present on the northern slope, and in 2016 there are green chasms running north south across the entire region. Meanwhile, the dark orange values representing barren mountain peaks have receded in every corner of the region. In the eastern portion of the range, green splotches appear deep within the recesses of the highest peaks. In the far west, nearly all traces of low-yield orange surface cover are left, replaced by varying shades of green.

Region 104 – Interior Forested Lowlands and Uplands

Temperature Graph

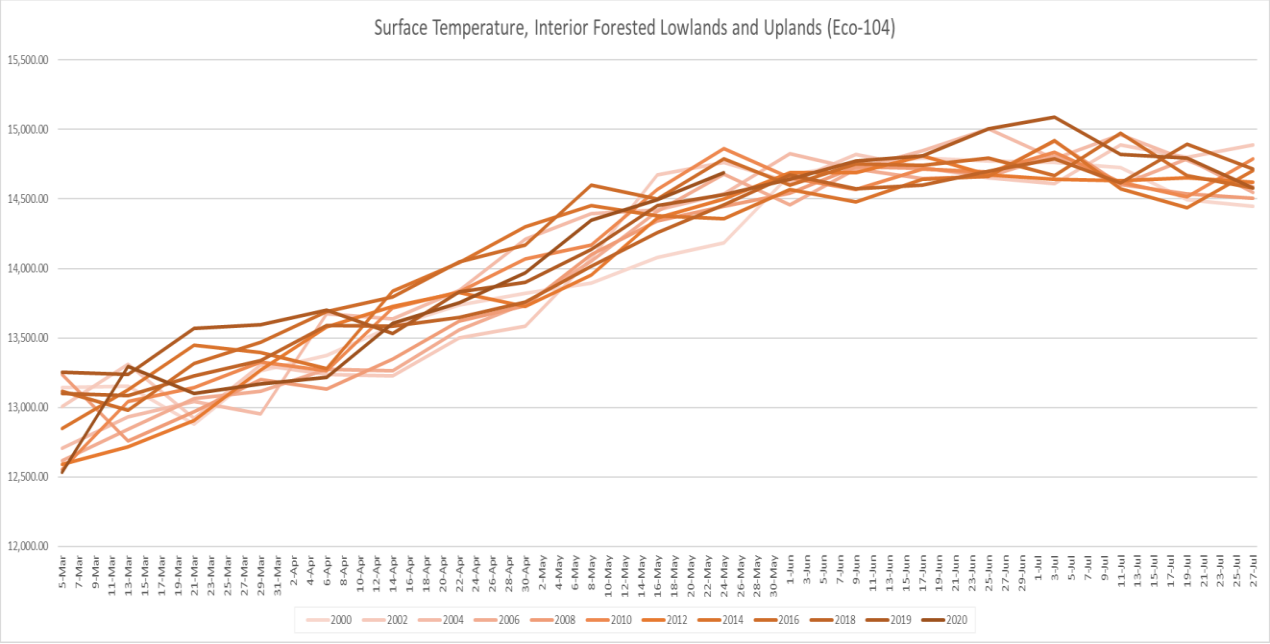

Figure 42: Surface Temperature Graph, Interior Forested Lowlands and Uplands (Eco-104)

The Interior Forested Lowlands and Uplands are a naturally diverse ecoregion as the name suggests. In fact, this is the largest region studied. No longer in the exclusive domain of permafrost on the north side of the Brooks Range, this ecoregion is dominated by coniferous forests, waterways, sloped hillsides, and a frequency of lighting fires. These ingredients should result in varied surface temperatures, and a prolonged thawing period due to the abundance of vegetation and its many-layered physical interaction with snow. Upon inspection, there is a reflection of this in the data. In no year does the linear temperature trend display a continuous trajectory. Temperatures rise and fall throughout the spring season. In Early March, there are significant temperatures spikes and falls across all years before the thawing point (13650) is reached. As temperatures rise this continues, right until the charts data ends in July, where there is again significant variance from as low as <14500 in 2014 (emerging as a significant year across all regions) to >15000 in 2019. In terms of wet snow conditions, there are three years to note. 2019, 2018, 2004. Overall, the maximum range of the thermal-transition period for this ecoregion is April 6th to April 30th. This is now a full month earlier than the determined transition period for regions 103, 102, and 101. This is undoubtedly an expression of the more southerly latitudes this region reaches. It is also likely related to the more multi-faceted vegetation which inhabits this area, which through its own growth contributes higher surface temperatures and affects snowmelt. This is something to observe in the subsequent two charts.

Albedo Graph

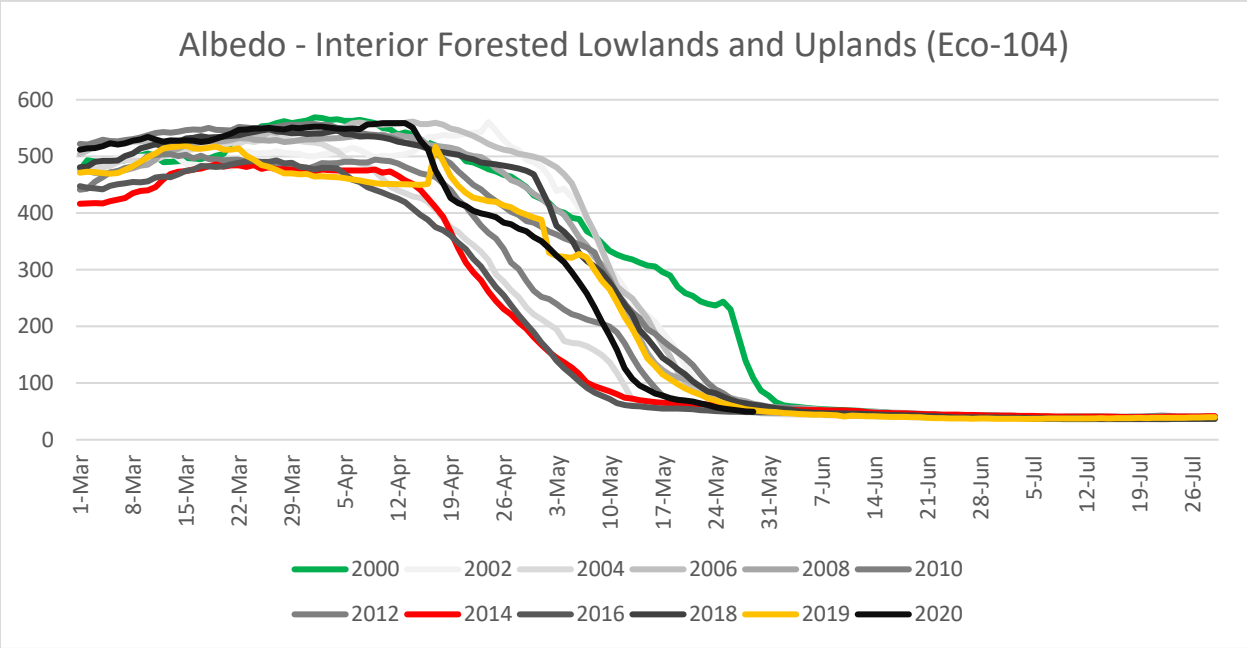

Figure 43: Albedo Graph, Interior Forested Lowlands and Uplands (Eco-104)

The albedo data for this region is one of the most unique of the entire set studied. It shows the most variance in terms of slope, with several notable peaks and troughs that are indicative of specific events in the snow-albedo feedback process. Most recently, 2020 and 2019 show peculiar trajectories. In 2020 albedo values drop precipitously from April 12th to 19th, and then resume nearly plateau before giving way to a more gentle than expected slope. In 2019, the form of this gentle curvature is broken up by two highly contrasting events: a jagged spike in high values of albedo around April 19th; and a drop-and-plateau movement from May 3rd to 10th. Also, for this year early values in March experience a plateau from 15th to the 22nd. As albedo is most indicative of snow cover, the first presumption is these are the expressions of weather events. The spike April suggests a sudden snowfall event of significant size. The region's large and discontinuous area makes it difficult to infer from this data alone where this might have occurred.

Because it happened so late in the season, the resultant snowfall did not last long. The opposite is true of the drop observed between May 3rd and May 10th. Something has led to a sudden decline. A rise in temperatures is an obvious possibility. However, a view of the same period in the temperature chart reveals only a marginal decrease. This is then an intriguing finding, as there appears another variable to account for this observation. Viewed from the beginning of the study period in 2000, and all the other years since have trends significantly earlier in the calendar year, with more rapid rate of albedo loss, and at lower peak winter levels in March. This is trend is increasing in frequency in more recent years. Overall compared to the first three regions studied, the Interior Forested Lowlands and Uplands experience albedo loss significantly earlier, at more varied rates, and significant differences in peak winter albedo values across different years. This last point is arguably the most interesting, as it suggests that winter surface conditions in this ecoregion are subject to significant variation. This so far is unique to all the regions, of which the others show far greater homogeneity in their dormant winter-snow albedo states. This again suggests the explanatory role of vegetation, as the dense forests of this region create the most multi-faceted surface type studied, whose physiological process are therefore the most complex.

Albedo Map Visualization

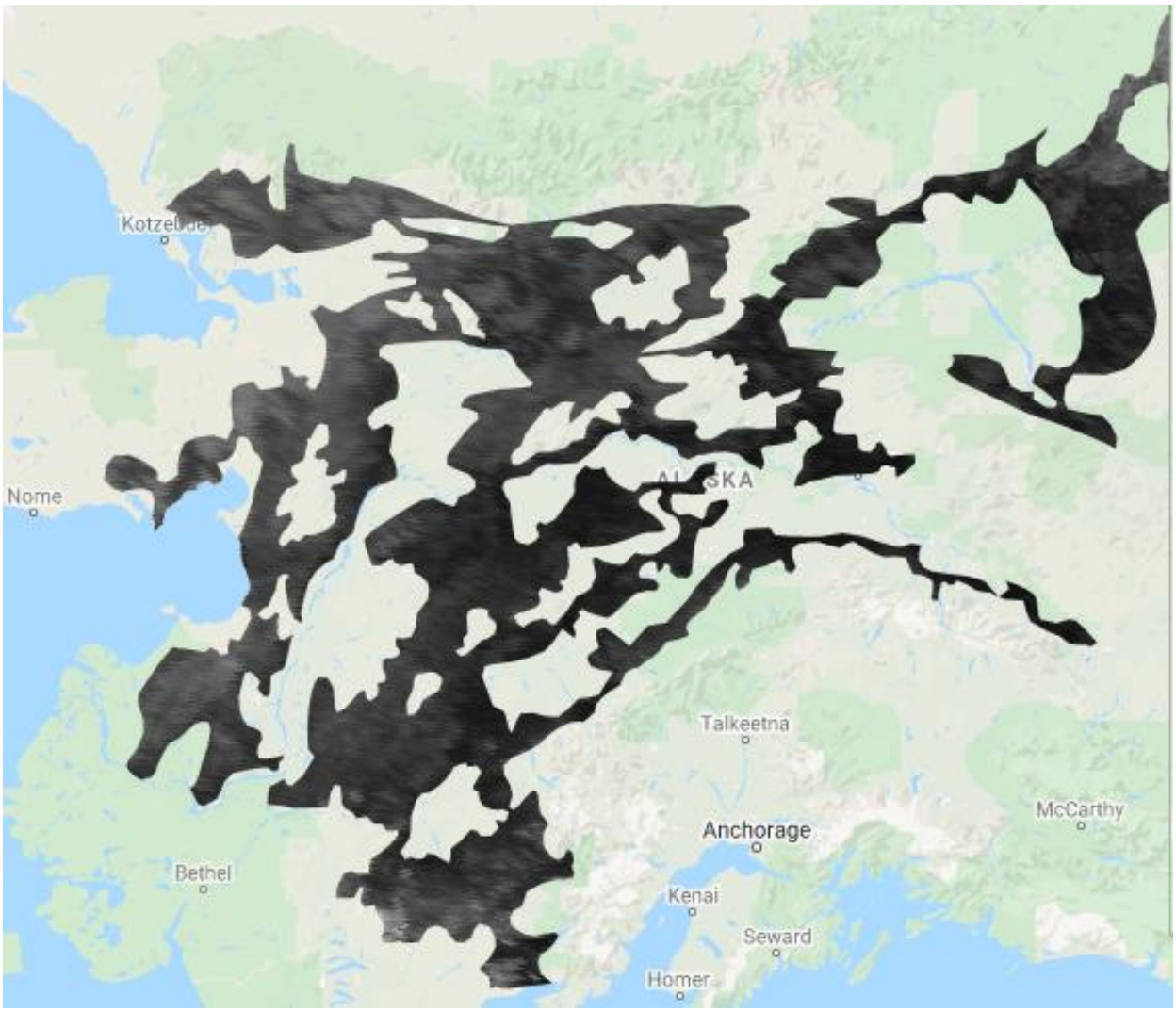

Figure 44: Eco-104, Average Black-sky Albedo in 2000 (April – July) (Latest Melt)

Figure 45: Eco-104, Average Black-sky Albedo in 2014 (April – July) (Average Melt)

Figure 46: Eco-104, Average Black-sky Albedo in 2019 (April – July) (Earliest Melt)

Albedo for the Interior Forested Lowlands and Uplands is expected to be significantly lower than any of the other regions studied. This region contains a true conifer forest with canopy, understory, and brush. Permafrost is present but not the dominant feature. Yet even in such a heavily vegetated area, in the year 2000 there are still large areas of grey coloration, particularly to the north west. In the subsequent two years of focus, these areas have transitioned to a much darker shade grey. Elsewhere as well, shading has increased. Across this region, little topographical variation is discernable from the albedo. Neither rivers nor lakes nor mountains appear as distinct features. This homogeneity of low albedo increased through the years.

NDVI Graph

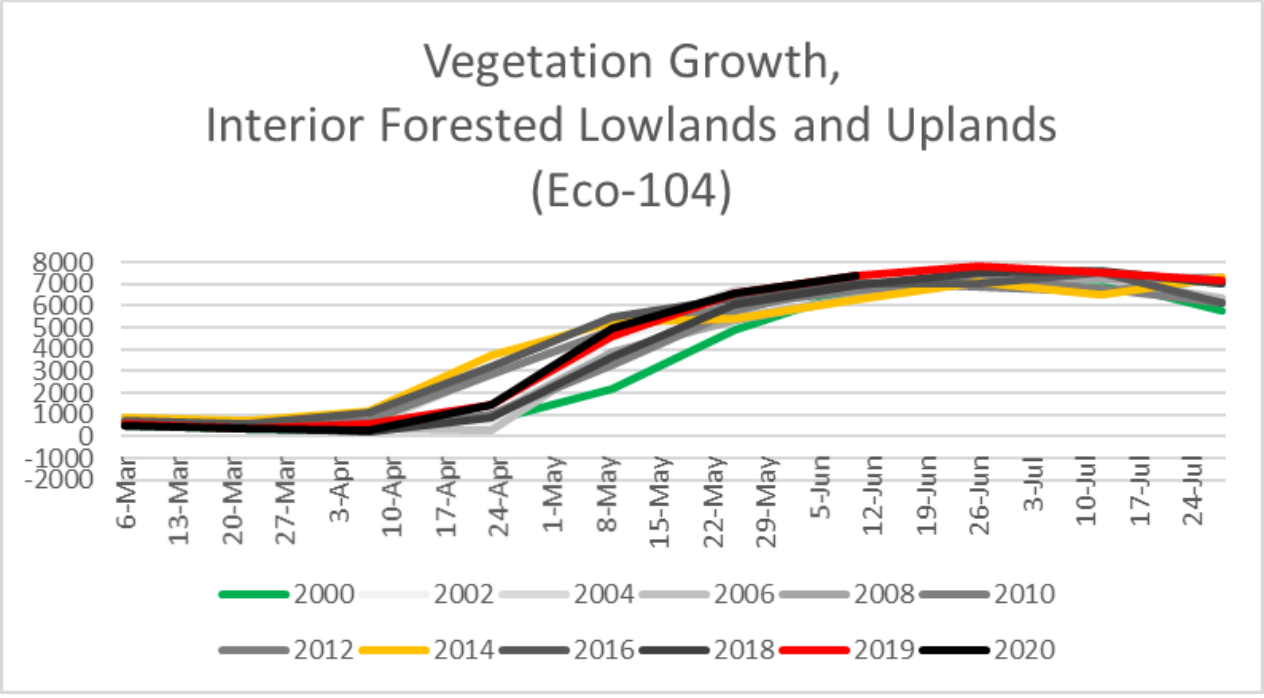

Figure 47: NDVI Graph, Interior Forested Lowlands and Uplands (Eco-104)

Beginning the analysis of NDVI by reviewing the thermal transition period for the region of April 6th to April 30th, this period precisely aligns with the earliest signs of vegetation growth on the 6th, and the last years to shows these signs on the 30th. It is the period directly following this until May 25th which then sees the most significant phase of plant growth. This strong growth is then complete by July at which point the values of recent years approach 7500, some two-hundred points higher than in region 103. Further evidence of the rich plant composition of this ecoregion. Indeed, these max values in Jul are increasing. The trend then again of earlier greening happening at faster rates leading to higher resting summer values. In an already heavily vegetated region, significant growth of this nature leads to the question of where this is coming from. It is worth investigating if this growth comes from native species, or from new species whose range has reached this area as climate conditions have improved to support their survival needs. If this is the case, the repercussions for the established forest eco-system are to be significant. Looking for evidence of an expression of the peculiar line-slope of BSA data in the year 2019 (peak on April 19th, plateau on May 3rd) there is no such obvious correlation to the NDVI data for these same dates. This is unexpected. It suggests that there is another explanation for the sudden rise and fall of albedo. While snowfall may explain the first spike, if vegetation does not appear because of warming temperatures causing the albedo plateau, then there is another variable at play. This is a topic if significance for further discussion.

NDVI Map Visualization

Figure 48: Eco-104, Average Vegetation (NDVI) in 2000 (April – July) (Latest Melt)

Figure 49: Eco-104, Average Vegetation (NDVI) in 2014 (April – July) (Average Melt)

Figure 50: Eco-104, Average Vegetation (NDVI) in 2019 (April – July) (Earliest Melt)

Reviewing the spatial distribution of the vegetation charted vegetation trends, again the overall increase is evident, especially when contrasting 2000 and 2019. As this is already a forested region, the question arises where these gains in vegetation are coming from. Is there more of the same growth, are new species making encroachments into this domain, are certain species thriving while others are receding? Interestingly, the year 2019 displayed average NDVI growth, falling squarely in the middle of the years studied. Yet, there is only a negligible distinction between it and the data in 2014, while 2000 stands in starker contrast to them both. This is somewhat unexpected, as contrast between 2014 and 2019 was expected to be stronger. Across all three years, there are no indications of snow cover or barren surfaces.

Region 105 – Interior Highlands

Temperature

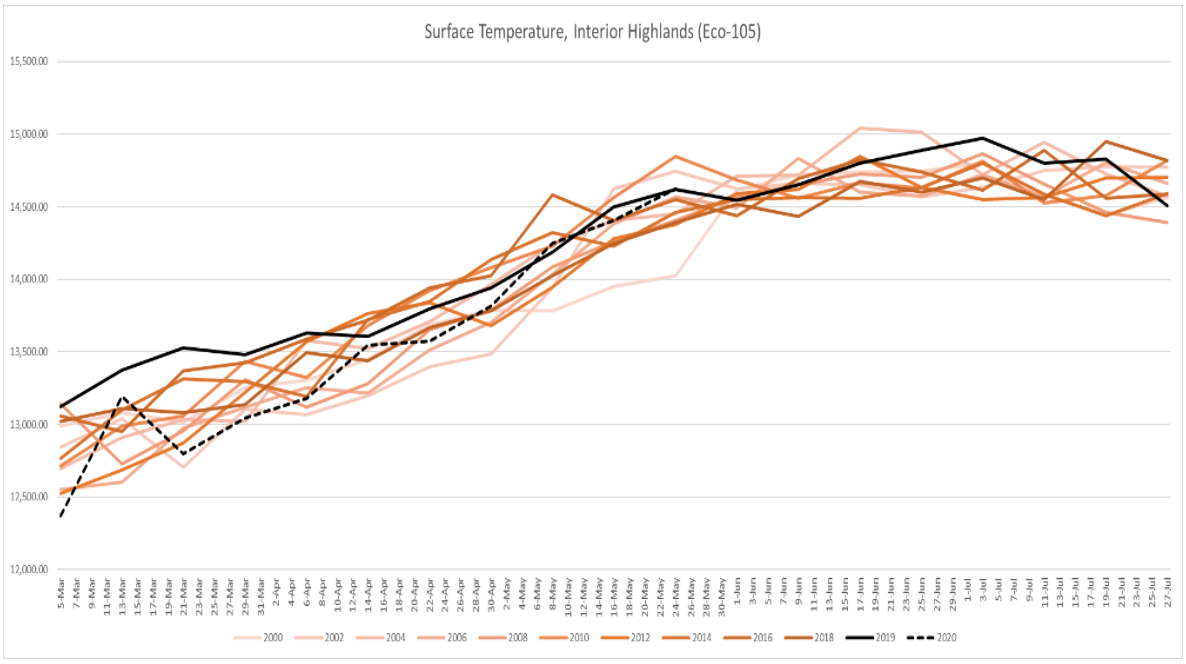

Figure 51: Surface Temperature Graph, Interior Highlands (Eco-105)

The interior highlands are a collection of low-lying scrub vegetation and spruce stands covering a series of low-inland mountains. These conditions describe a region that is likely to have lower average temperatures than compared to the region 104 (Interior Forested Lowlands and Uplands) but warmer than the arctic regions and mountains (101, 102 and 103) in the far north of Alaska. Indeed, the maximum summer surface temperatures recorded are less than 104 (which exceed 15,000) but on average more than the others. Similar to the linear trend observed in the forested lowlands and uplands, the highlands display linear trends which rise and fall sharply throughout the study period. This lack of a smooth continuous linear trajectory across all years indicates uneven warming across the region. Though there is more homogeneity to this region than 104, there is clearly enough varying surface composition in 105 to result in disparate warming patterns through time. Looking for indications of wet snow conditions, these present within the date range of April 6th to May 1st. This is a roughly month-long window, In which the earliest year of study (2000) makes up the last observed date of thawing, while recent years like 2016, 2014 and 2012 make up the earliest observed thawing date. Specifically, the years 2004, 2019 and 2020 show wet snow conditions. 2004 and 2019 show these these from April 4th to 14th, while 2020 does so two weeks later from April 14th to the 24th. In terms of overall trends, it is more difficult to draw conclusions here than for the other regions, as both old and recent years display some of the highest and lowest respective values at any stage of the study. However comparing only the most recent two years with the first year, and there is clear movement upward to the left; (higher temperature values at earlier dates).

Albedo Graph

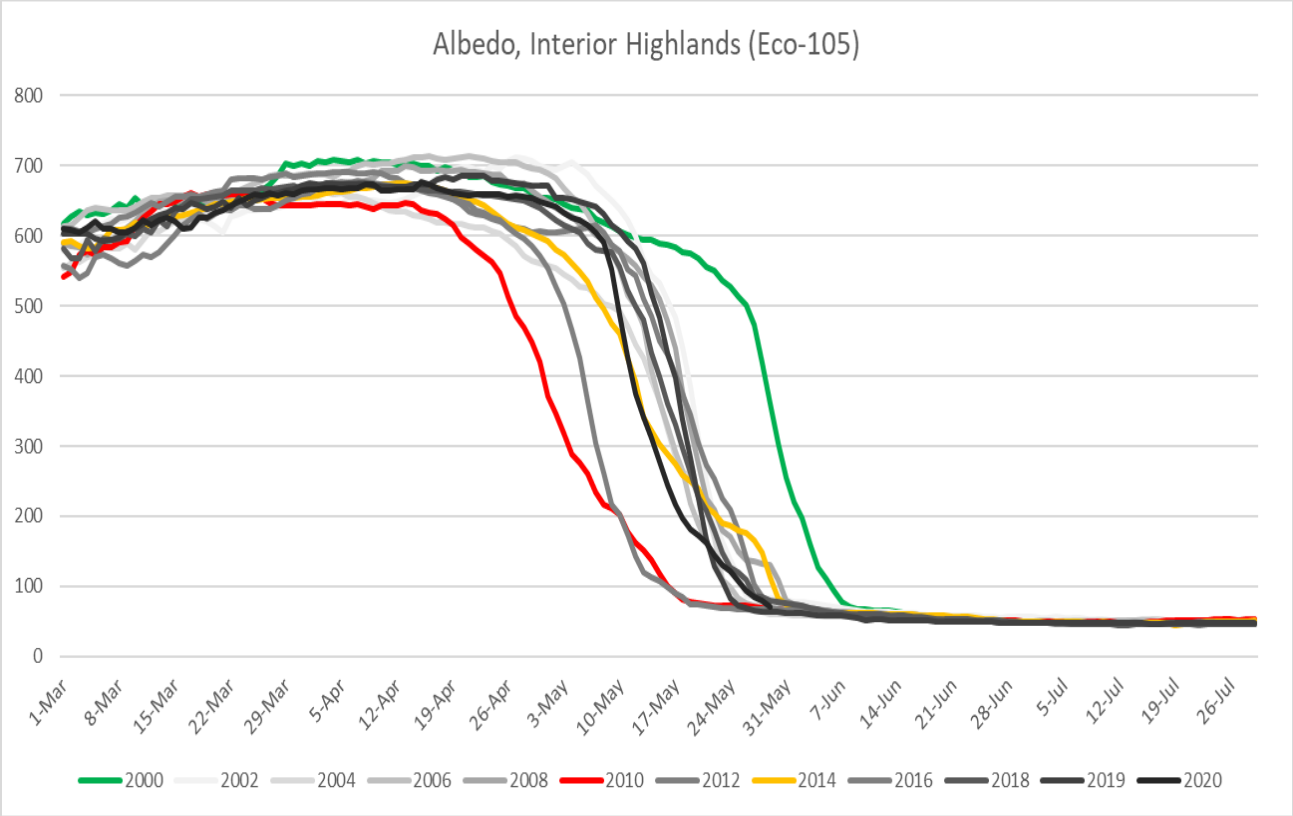

Figure 52: Albedo Graph, Interior Highlands (Eco-105)

Beginning with an assessment of the observed min-max wet snow period of April 6th to May 1st, it directly precedes the loss of albedo the following month. The year 2000 stands out for three reasons. It has the highest of any year in April, and the then the latest date of decline, and the most fluid linear trend. There is a two-week difference between the slope of this first year of study and the next (2002). In 2010, the difference from the first year is roughly a full month. Contrasting the peak values observed between these years, they fall roughly 60 points apart. Taken together, the trend is downward and to the left. This represents the earlier onset of snowmelt and the lower albedo values in peak snow-covered conditions. In terms to the shape of the data for this region, there are no abundance of peaks or plateaus to describe. Across all

years the slope of the lines is rounded and smooth and of similar proportion. The exception is 2012, in which there is a plateau-and-peak event observed on from around April 26th to May 10th. This in fact corresponds to a slight observed dip in temperatures over the same period. However, the change in the slope of the BSA is greater than expected from this. This likely indicates the influence of another variable.

Albedo Map Visualization

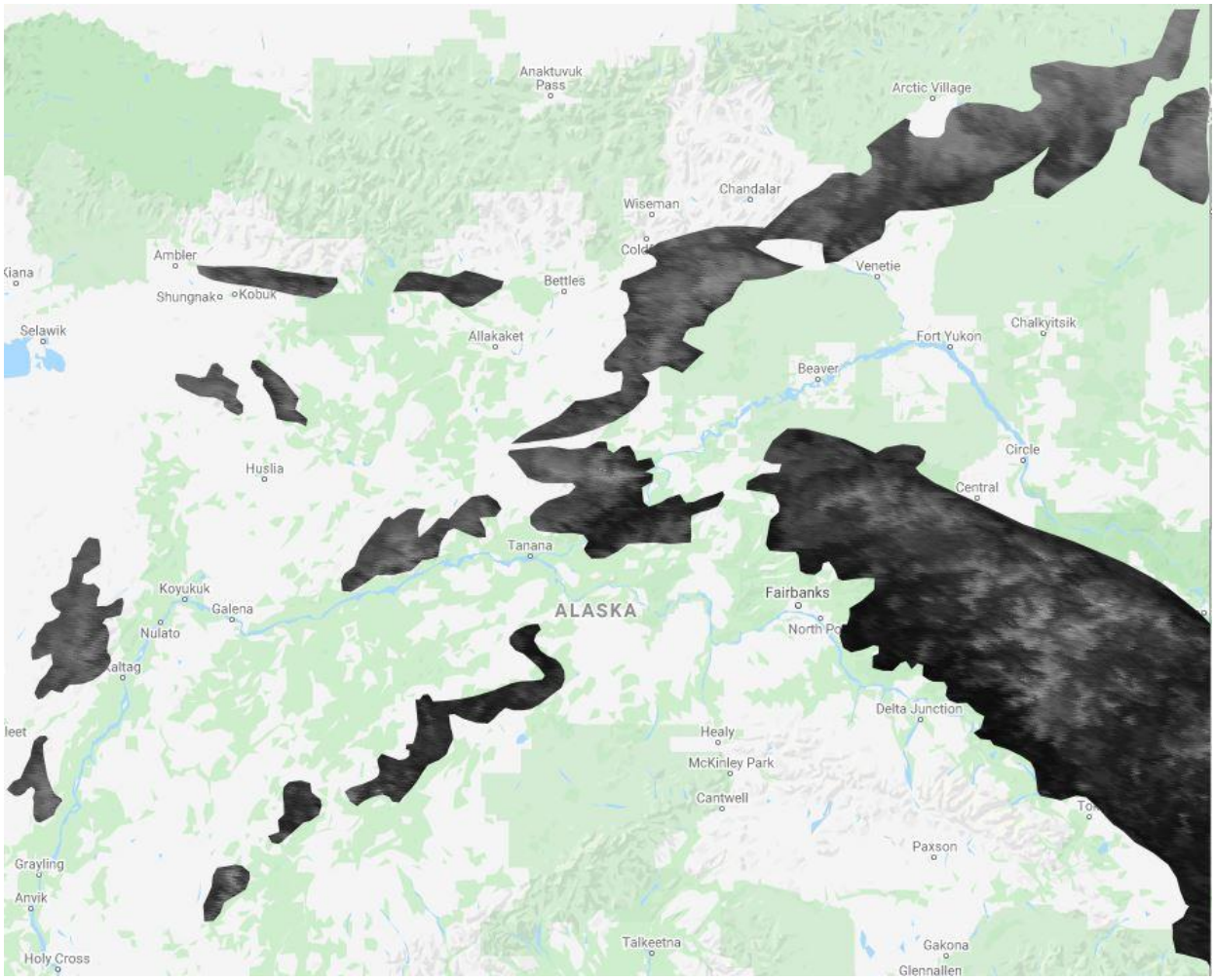

Figure 53: Eco-105: Average Black-sky Albedo in 2000 (April – July) (Latest Melt)

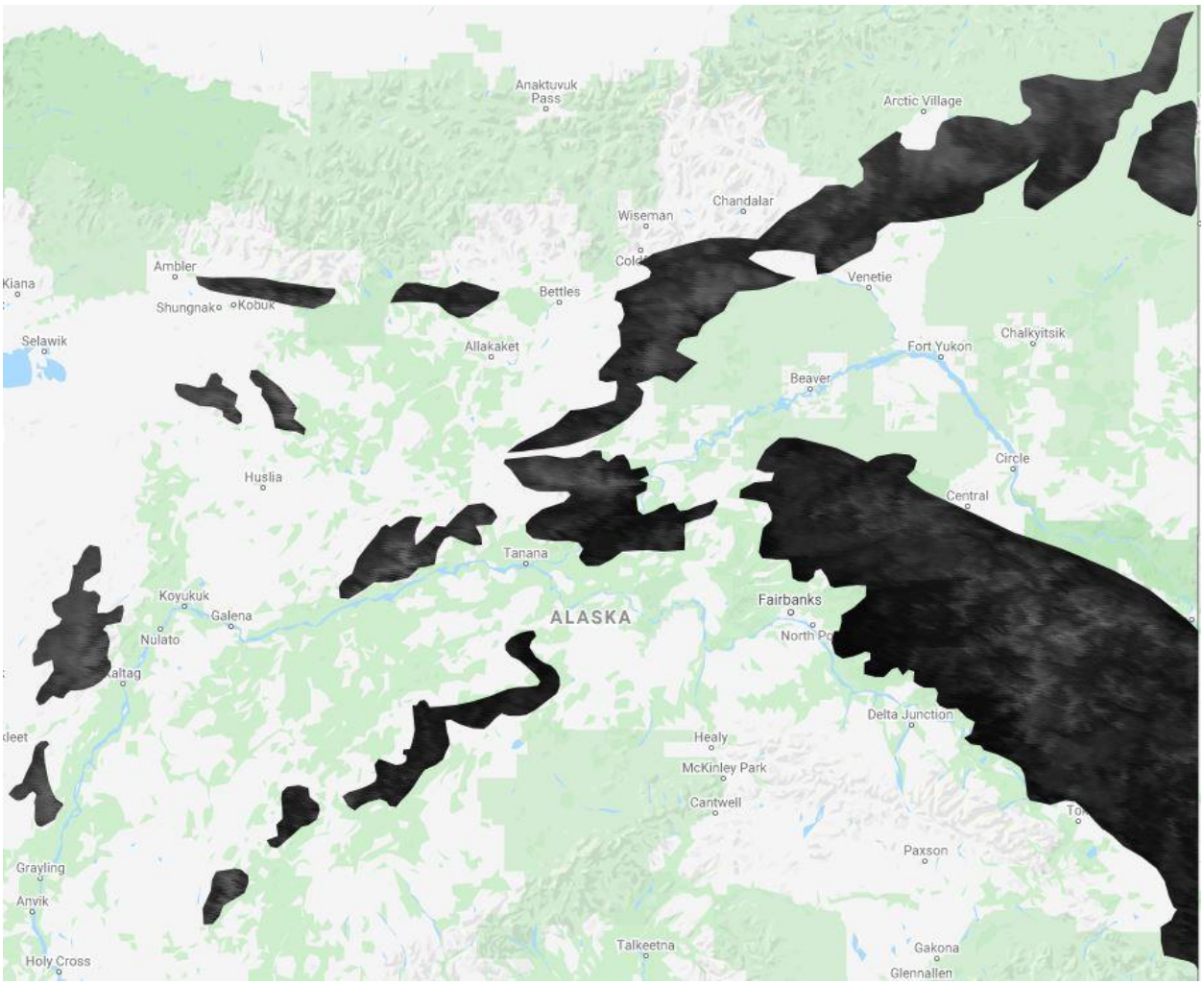

Figure 54: Eco-105: Average Black-sky Albedo in 2010 (April – July) (Average Melt)

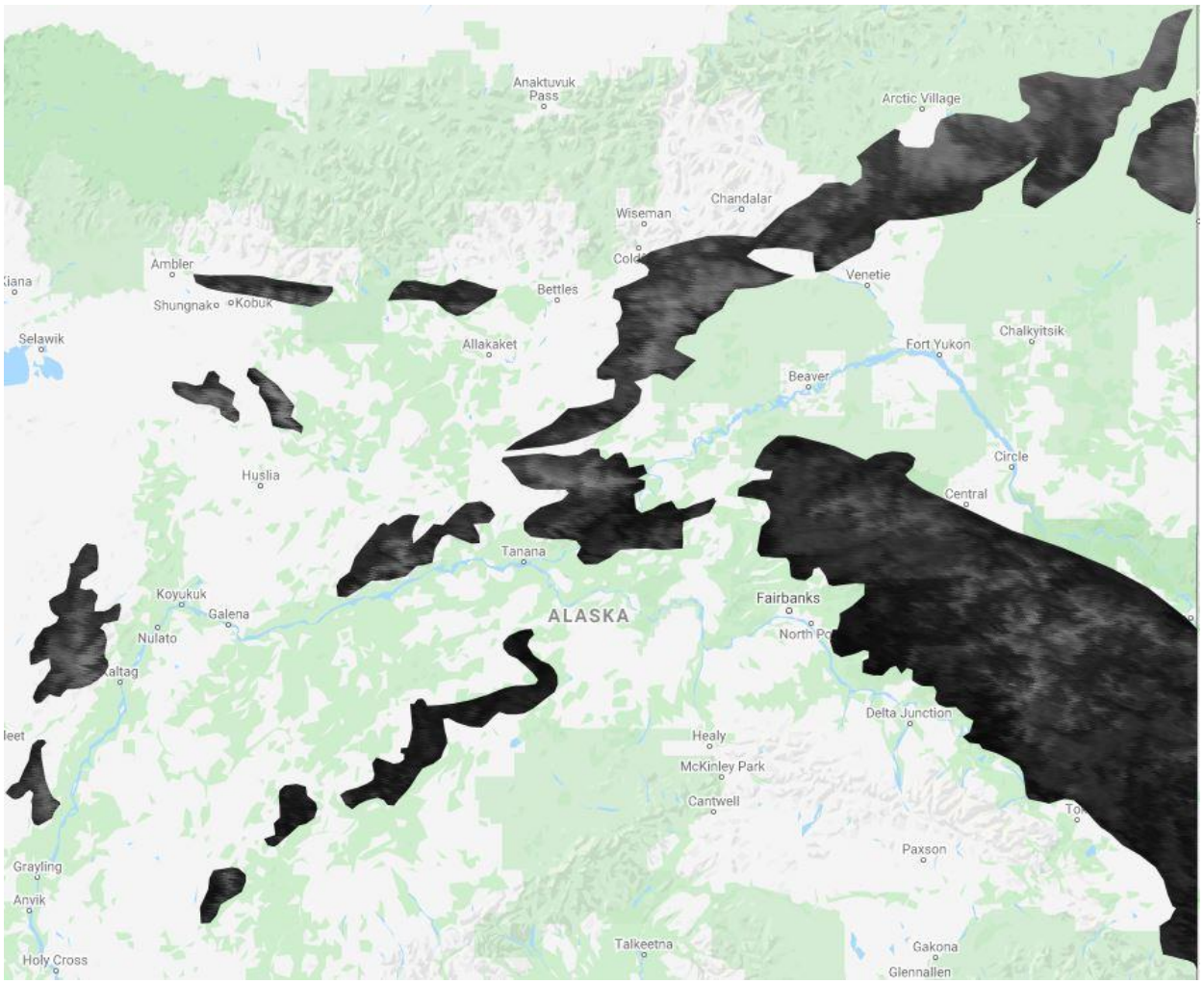

Figure 55: Eco-105: Average Black-sky Albedo in 2014 (April – July) (Earliest Melt)

The Interior highlands are topographically diverse, and this is evident from the albedo images. Light areas are those of the highest elevations, while the darkest regions are those bordering on the adjacent lowlands. In 2000, there are signs of significant snow and frozen surface cover, especially in the north and along the ridges of the east. At the same time, dark regions in close proximity highlight how quickly surface conditions can change. As a forested region, the multi-faceted surface cover plays a large role in the albedo affect. This likely changes along the slope of a single highland range. In 2014, the year representing the most average albedo trend, there is an overall darkening. This is most evident in the regions previously of light value in 2000 (the north and east). Here the contrast observed along the highlands has become less crisp. 2010 is an early onset albedo loss year. There is little to indicate their difference in spatial terms. However, it does appear to be darker overall than in 2014. This suggests the additional time for the vegetation to mature is palpable. This gain was made across the region.

NDVI Graph

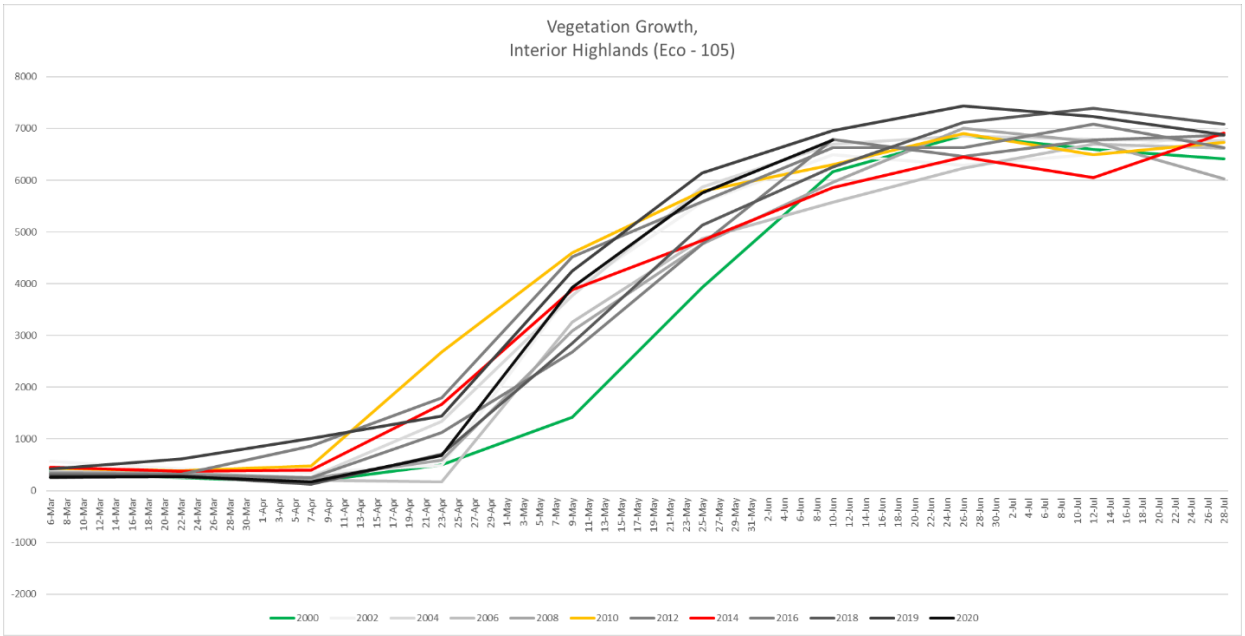

Figure 56: NDVI Graph, Interior Highlands (Eco-105)

Lastly, a review of the NDVI values for the Interior Forested Uplands reveals two dates from which to measure the start of the spring growth season April 7th and April 23rd. On either of these days, all of the year's data begins its upward trend. Checking the wet snow period from the temperature chart (April 6th to May 1st), these dates are nearly identical. In Interior highlands, there is little delay between the onset of thawing temperatures and the beginning of plant growth is the one of the least of all the regions studied. The trend is consistent with the data to this point, showing growth occurring earlier and reaching higher levels in July. The gap between the year 2000 and all other years is pronounced. Noteworthy is perhaps that in the year 2014, vegetation levels dropped in early July from 6443 to 6054, before recovering again. Such a late loss of NDVI values is not observed in any other year and is therefore a subject of potential further

inquiry. Peak NDVI values of 7431 in early July make this the second most vegetated region studied, following eco-104 (Interior Forested Lowlands and Uplands).

NDVI Map Visualization

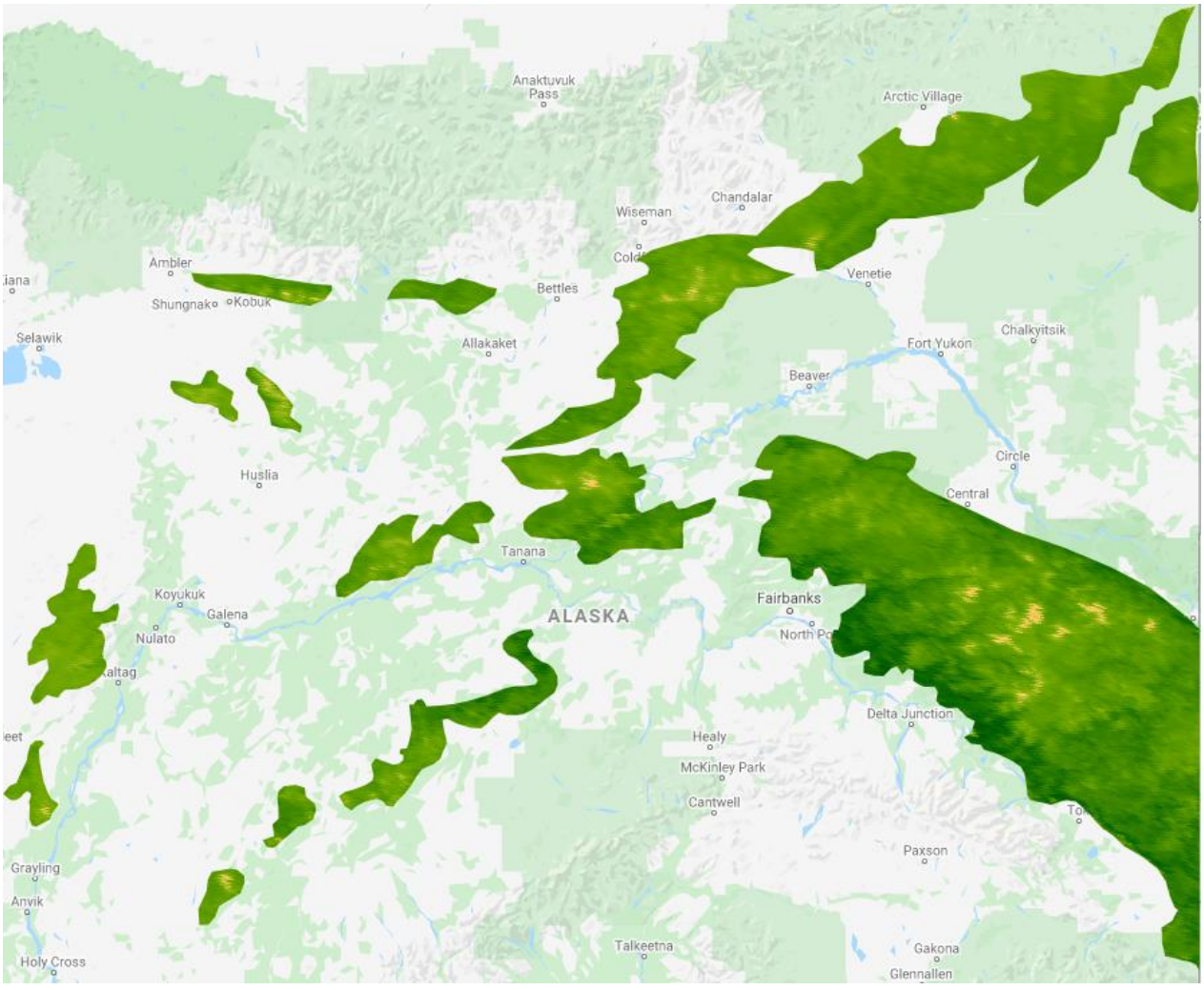

Figure 57: Eco-105, Average Vegetation (NDVI) in 2000 (April – July) (Latest Melt)

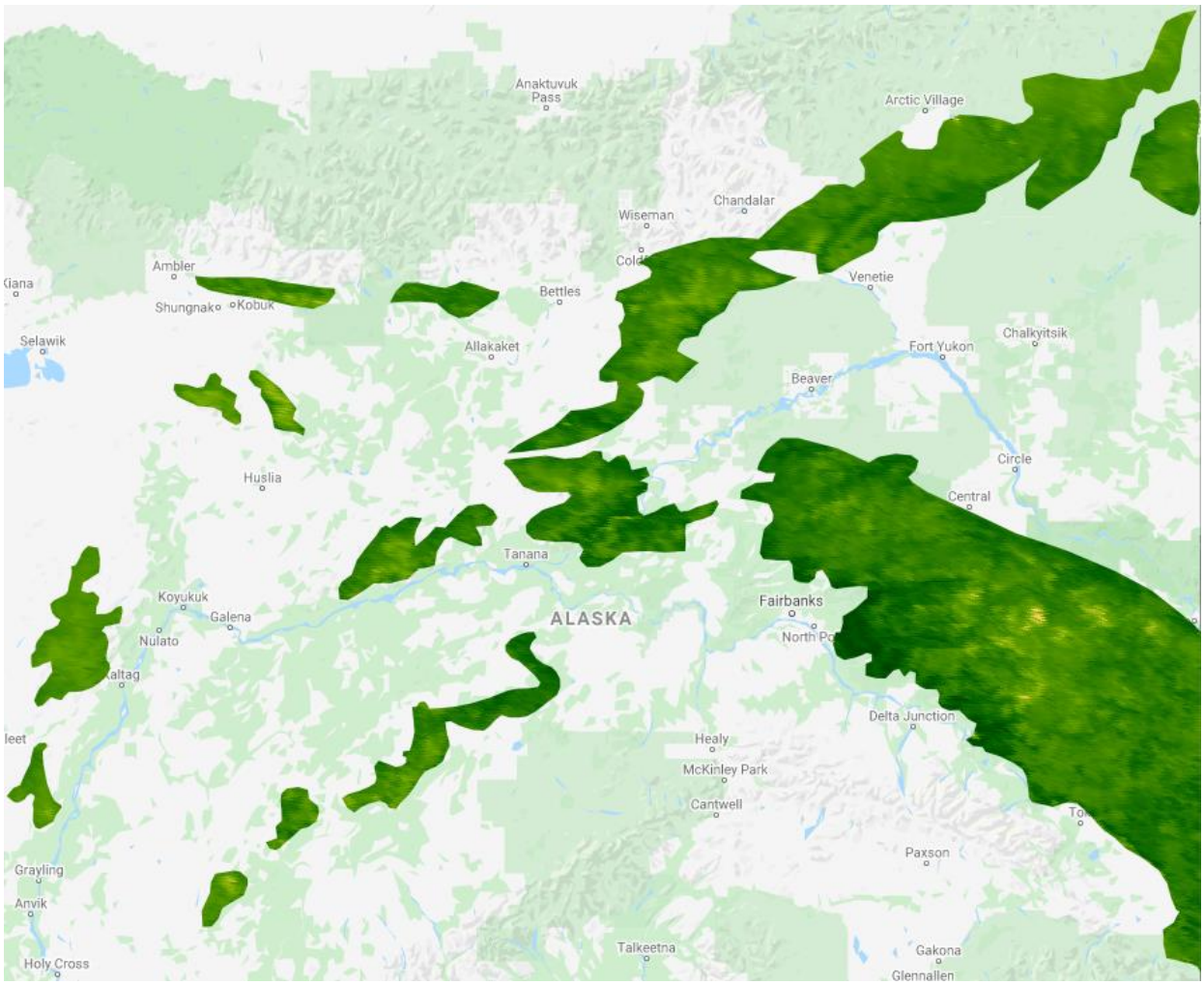

Figure 58: Eco-105: Average Vegetation (NDVI) in 2010 (April – July) (Average Melt)

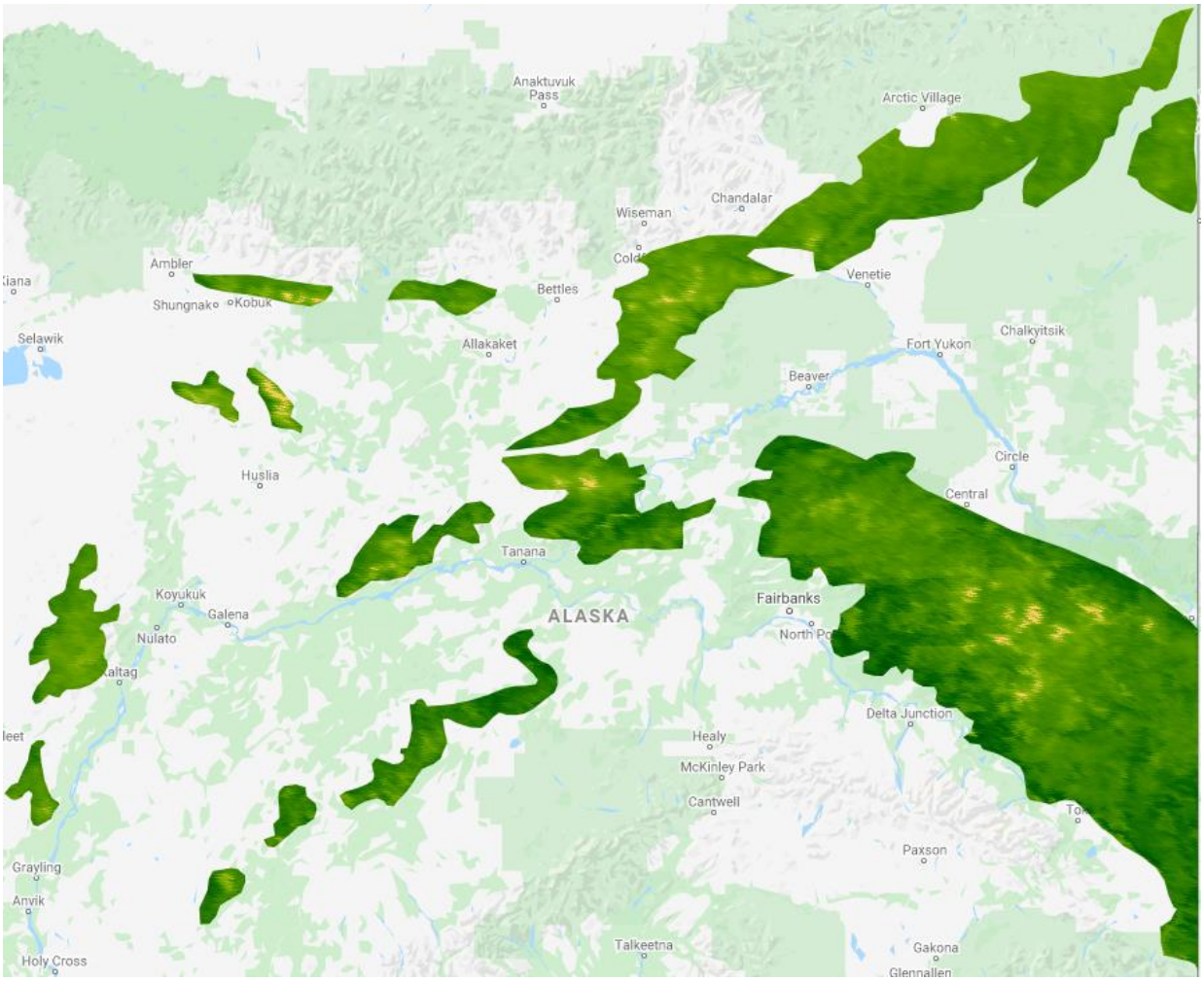

Figure 59: Eco-105: Average Vegetation (NDVI) in 2014 (April – July) (Earliest Melt)

From the vegetation index map visualizations, the picture painted by the BSA image is mostly reciprocated. Low-density vegetation areas are limited to the highest hilltops. Dense forest vegetation is located at the edge of the region where it runs into the adjacent lowland areas. Greening is observed over time. Interestingly, this effect is not most pronounced in chronological order, but by onset of vegetation growth. Of the three years highlighted, 2010 showed the earliest growth, and this is reflected by the minimal yellow coloration. Meanwhile, the year 2000 shows the most yellow, because the vegetation bloom occurred latest. 2014 sits in the middle. As vegetation here is modest, (alpine tundra and isolated spruce stands), the darkest shades of green should be considered atypical for the region, and their inroads a sign that the vegetation of the adjacent lowlands is encroaching upwards in altitude as temperatures and surface conditions become more hospitable. In 2010, the early onset greening year, vegetation covers all the hilltops north of the Yukon river.

6. Conclusion

After analyzing five regions, across twelve years, for three variables, what conclusions can be drawn? There are three questions which can be reflected upon with confidence after this study.

What is the impact of vegetation on snowmelt?

Throughout the study, a comparison of the BSA and NDVI data shows an inverse relationship between the rate of snowmelt and the texture of a surface--expressed through topography and vegetation cover. This explains how the albedo signature of vegetation-intensive regions (i.e. the Interior Forested Lowlands and Uplands, and the Brooks Range) are uneven with numerous variations in the rate of slope. These are expressions of uneven snowmelt within these regions across different surface vegetation and topography changes. Vegetation provides a textured surface cover in which pockets of thermal insulation form. These are sustained through the bio-chemical processes of vegetation growth, with generate small amounts of thermal bi-product. By contrast, in the arctic coastal plain and foothills, which are relatively featureless environments, snowmelt occurs at a more even spatial distribution. While on the one hand vegetation prolongs melting, in also limits the peak albedo value produced by a tract of land. This is evidenced in the lower maximum albedo values in regions with denser vegetation than those without.

What is the impact of albedo and vegetation on the larger snow-albedo feedback cycle?

The historical climatological effect of the arctic has been as a mirror to reflect away large amounts of incoming electro-magnetic radiation. The efficacy of this mirror is based on its texture. A smooth surface can reflect best. As all of the regions studied are snowbound through the winter, their albedo during this early phase of the study is indicative of this effect. The arctic coastal plain and foothills, with their expansive low-profile surface, produce the highest albedo in the winter. The changes over time observed in the linear trajectory of the albedo slopes in these most northerly regions are the result not of changing topography, but increases in vegetation, altering the physical texture of the surface and lessening its reflectivity. As this shift continues the repercussions will gather momentum over time and express themselves in the global climate system.

What conclusions can be drawn about the changing surface composition of northern Alaska, with special view to its permafrost?

That the arctic climate is warming at above average rates has been beyond a doubt for some time. That this is reducing snowpack is also well-established. What has been less defined to date is the way that snow cover interacts with the surface it blankets, and how this essentially calibrates the amount of albedo that will be produced. Therefore, the thawing of permafrost—evidenced from the map visualizations—not only releases a globally destabilizing amount of carbon into the atmosphere, but it reduces the maximum albedo of a region. Vegetation gains in

these most northerly regions are therefore amplified in their significance to climate models. Such gains and changes are of significance in all regions as they pertain to albedo. The shift of dominant species in response to climate changes will also cause changes in regional albedo. In the north of Alaska, permafrost is thawing, engendering a more robust layer of vegetation cover. In the Brooks Range, vegetation is extending upward to higher altitude, replacing previously snow-bound mountain slopes. In the Interior Forested Lowlands and Uplands, the density of the forest is increasing, with albedo loss occurring at earlier annual dates. In the Interior Highlands, almost no snow-bound surface remains, even at the highest elevations. Meanwhile, the signs of forestation permeate in from neighboring ecoregions.

What is the time delay between snow-loss and vegetation growth?

With all this data in mind, the snow albedo feedback mechanism of northern Alaska is in precipitous decline, due to global warming. The active processes by which the terrestrial arctic contributes to the earth's cooling is heavily influenced by the interplay of rock, soil, vegetation, and snow. Their relations are transforming in accordance with these new climate conditions. Vegetation is "gaining" from this, albedo is "losing". For those developing finely tuned global climate models, the influential role of vegetation on albedo must be considered.

References

Journal Articles

Beatrice, John. (2019) Towards Sustainable Urban Metabolisms. From System Understanding to System Transformation. *Ecological Economics, 157*(2019) 402-414

Chapin FS, Sturm M, Serreze MC, et al. (2005) Role of land-surface changes in Arctic summer warming. Science 310(5748): 657–660.

Coakley, J.A. (2003) Reflectance and Albedo, Surface. *Encyclopedia of Atmospheric Sciences (2003)* 1914-1923

Colman RA (2013) Surface albedo feedbacks from climate variability and change. *Journal of Geophysical Research: Atmospheres 118*(April): 2827–2834.

Curry, A., & Schramm, J.L. (1995) Sea Ice-Albedo Climate Feedback Mechanism. *Journal of Climate, Vol.8* (1994)

De´ry SJ and Brown RD (2007) Recent Northern hemisphere snow cover extent trends and implications for the snow-albedo feedback. *Geophysical Research Letters 34*(22): L22504.

Derksen, C. and Brown, R. (2012) Spring snow cover extent reductions in the 2008–2012 period exceeding climate model projections. *Geophysical Research Letters 39*(19): 1–6

Essery, R., (2013) Large-scale simulations of snow albedo masking by forests. *Geophysical research letters, Vol. 4* (5521-5525)

Fernandes R, Zhao H, Wang X, et al. (2009) Controls on Northern hemisphere snow albedo feedback quantified using satellite Earth observations. *Geophysical Research Letters 36*(21): L21702

Fletcher CG, Zhao H, Kushner PJ, et al. (2012) Using models and satellite observations to evaluate the strength of snow albedo feedback. *Journal of Geophysical Research 117*(D11): D11117.

Gallant, A., Binnian, F., et al. (1995) Ecoregions of Alaska. *US Geological Survey Professional Paper 1567*

Hovi, A., *et al*. (2019) Seasonal dynamics of albedo across European boreal forests: Analysis of MODIS albedo and structural metrics from airborne LiDAR. *Remote Sensing of Environment, 224 (2019)* 365-381.

Kashiwase, H., Ohshima, K.I., Nihashi, S. et al. (2017) Evidence for ice-ocean albedo feedback in the Arctic Ocean Shifting to a seasonal ice zone. *Sci Rep* 7, 8170 (2017). https://doi.org/10.1038/s41598-017-08467-z

Kim, Y., Kimball, J., et al. (2018) Quantifying the effects of freeze-thaw transitions and snowpack melt on land surface albedo and energy exchange over Alaska and Western Canada. *Environ. Res. Lett. 13* (2018) 075009

Koffka, w., Kohler, W., Wertheimer, M. et al. (1923) Untersuchungen zur Lehre von der Gestalt II. *Zeitschrift fur Psychologie und Ihre Grenzwissenschaften* (translated title: Studies and Teachings on Forms, Pt II. The Publication for Psychology & Frontier Science).

Kussinen, N., *et al*. (2015) Structural factors driving boreal forest albedo in Finland. *Remote Sensing of Environment, 175* (2016) 43-51

Kuusinen, N., Kolari, P., Levula, J., Porcar-Castell, A., Stenberg, P., Berninger, F., (2012). Seasonal variation in boreal pine forest albedo and effects of canopy snow on forest reflectance. *Agric. For. Meteorol. 164*, 53–60.

Lukeš, P., Stenberg, P., Rautiainen, M., 2013. Relationship between forest density and albedo in the boreal zone. *Ecol. Model.* 261–262, 74–79.

Moody, E., King, M., Schaaf, C., et al. (2007) Northern Hemisphere five-year average (2000-2004) spectral albedos of surfaces in the presence of snow: Statistics computed from Terra MODIS land products. *Remote Sensing of Environment 111* (2007) 337-345

Qu, X., and A. Hall (2007), What controls the strength of snow-albedo feedback? *J.Clim., 20*,3971–3981.

Robinson, D. A., and G. Kukla (1985), Maximum surface albedo of seasonally snow-covered lands in the Northern hemisphere, *J. Clim. Appl. Meteorol., 24*,402–411.

Wang, D., Liang, S., He, T., Yu, Y., Schaaf, C., Wang, Z., 2015. Estimating daily mean land surface albedo from MODIS data. *J. Geophys. Res.-Atmos. 120*, 4825–4841. https:// doi.org/10.1002/2015JD023178.

Websites

BBC.com, (2020). “Arctic Circle sees ‘highest-ever’ recorded temperatures”. June 22, 2020. Retrieved from: https://www.bbc.com/news/science-environment-53140069

Climate.gov, (2015). “Arctic continues to be significantly warmer than average”. Retrieved from: https://www.climate.gov/news-features/featured-images/Arctic-continues-be-significantly-warmer-average

Encyclopaedia Britannica (2020) “Arctic”. Retrieved from: https://www.britannica.com/place/Arctic

Environmental Protection Agency (2017) Ecoregion Download Files by State – Region 10. Retrieved from: https://www.epa.gov/eco-research/ecoregion-download-files-state-region-10

NASA Earth Observatory, 2019. Retrieved from: https://earthobservatory.nasa.gov/images/84499/measuring-earths-albedo

NASA Goddard Fight Center, 2013. Retrieved from: https://www.nasa.gov/goddard

NOAA National Oceanic and Atmospheric Administration, (2020). “2019 was 2nd hottest year on record for Earth say NOAA, NASA”. Retrieved from: https://www.noaa.gov/news/2019-was-2nd-hottest-year-on-record-for-earth-say-noaa-nasa

National Snow and Ice Data Center (2020) “Methane and Frozen Ground”. Retrieved from: https://nsidc.org/cryosphere/frozenground/methane.html

University of Massachusetts, Boston. Albedo Measurement Scale. Retrieved from: https://www.umb.edu/spectralmass/terra_aqua_modis/modis_user_guide_v004/mod43b3_albedo_product

Appendix (Code)

Surface Temperature Charts

```
var regions = combined_eco
// select the country from the fusion table


// set start date
var startDate2020 = '2020-03-01';
var endDate2020   = '2020-05-30';

var startDate2019 = '2019-03-01';
var endDate2019   = '2019-07-30';

var startDate2018 = '2018-03-01';
var endDate2018   = '2018-07-30';

var startDate2016 = '2016-03-01';
var endDate2016   = '2016-07-30';

var startDate2016 = '2016-03-01';
var endDate2016   = '2016-07-30';

var startDate2014 = '2014-03-01';
var endDate2014   = '2014-07-30';

var startDate2012 = '2012-03-01';
var endDate2012   = '2012-07-30';

var startDate2010 = '2010-03-01';
var endDate2010   = '2010-07-30';

var startDate2008 = '2008-03-01';
var endDate2008   = '2008-07-30';

var startDate2006 = '2006-03-01';
var endDate2006   = '2006-07-30';

var startDate2004 = '2004-03-01';
var endDate2004   = '2004-07-30';
```

```
var startDate2002 = '2002-03-01';
var endDate2002   = '2002-07-30';

var startDate2000 = '2000-03-01';
var endDate2000   = '2000-07-30';


var temp_2020 = temp8d
   .filterDate(startDate2020, endDate2020)


var EcoRegion_surface_temp_2020 = ui.Chart.image.seriesByRegion(
   temp_2020, combined_eco, ee.Reducer.mean(), 'LST_Day_1km', 200, 'system:time_start',
'US_L3CODE')
       .setChartType('ScatterChart')
       .setOptions({
         title: 'Alaskan Ecoregion Average Surface Temperatures 2020',
         vAxis: {title: 'Surface Temperature'},
         lineWidth: 1,
         pointSize: 4,

         series: {
           0: {color: 'FF0000'}, // 1
           1: {color: '00FF00'}, // 2
           // 2: {color: '0000FF'}  NOTE: Additional colors automatically generated for extra regions
}});

// Display.
print(EcoRegion_surface_temp_2020);



var temp_2019 = temp8d
   .filterDate(startDate2019, endDate2019)


var EcoRegion_surface_temp_2019 = ui.Chart.image.seriesByRegion(
   temp_2019, combined_eco, ee.Reducer.mean(), 'LST_Day_1km', 200, 'system:time_start',
'US_L3CODE')
       .setChartType('ScatterChart')
       .setOptions({
         title: 'Alaskan Ecoregion Average Surface Temperatures 2019',
```

```
        vAxis: {title: 'Surface Temperature'},
        lineWidth: 1,
        pointSize: 4,

        series: {
          0: {color: 'FF0000'}, // 1
          1: {color: '00FF00'}, // 2
          // 2: {color: '0000FF'}  NOTE: Additional colors automatically generated for extra regions
}});

// Display.
print(EcoRegion_surface_temp_2019);


var temp_2018 = temp8d
   .filterDate(startDate2018, endDate2018)


var EcoRegion_surface_temp_2018 = ui.Chart.image.seriesByRegion(
   temp_2018, combined_eco, ee.Reducer.mean(), 'LST_Day_1km', 200, 'system:time_start',
'US_L3CODE')
       .setChartType('ScatterChart')
       .setOptions({
         title: 'Alaskan Ecoregion Average Surface Temperatures 2018',
         vAxis: {title: 'Surface Temperature'},
         lineWidth: 1,
         pointSize: 4,

         series: {
           0: {color: 'FF0000'}, // 1
           1: {color: '00FF00'}, // 2
           // 2: {color: '0000FF'}  NOTE: Additional colors automatically generated for extra regions
}});

// Display.
print(EcoRegion_surface_temp_2018);

var temp_2016 = temp8d
   .filterDate(startDate2016, endDate2016)


var EcoRegion_surface_temp_2016 = ui.Chart.image.seriesByRegion(
   temp_2016, combined_eco, ee.Reducer.mean(), 'LST_Day_1km', 200, 'system:time_start',
'US_L3CODE')
```

```
      .setChartType('ScatterChart')
      .setOptions({
        title: 'Alaskan Ecoregion Average Surface Temperatures 2016',
        vAxis: {title: 'Surface Temperature'},
        lineWidth: 1,
        pointSize: 4,

        series: {
          0: {color: 'FF0000'}, // 1
          1: {color: '00FF00'}, // 2
          // 2: {color: '0000FF'}  NOTE: Additional colors automatically generated for extra regions
}});

// Display.
print(EcoRegion_surface_temp_2016);


var temp_2014 = temp8d
   .filterDate(startDate2014, endDate2014)


var EcoRegion_surface_temp_2014 = ui.Chart.image.seriesByRegion(
   temp_2014, combined_eco, ee.Reducer.mean(), 'LST_Day_1km', 200, 'system:time_start',
'US_L3CODE')
      .setChartType('ScatterChart')
      .setOptions({
        title: 'Alaskan Ecoregion Average Surface Temperatures 2014',
        vAxis: {title: 'Surface Temperature'},
        lineWidth: 1,
        pointSize: 4,

        series: {
          0: {color: 'FF0000'}, // 1
          1: {color: '00FF00'}, // 2
          // 2: {color: '0000FF'}  NOTE: Additional colors automatically generated for extra regions
}});

// Display.
print(EcoRegion_surface_temp_2014);

var temp_2012 = temp8d
   .filterDate(startDate2012, endDate2012)
```

```
var EcoRegion_surface_temp_2012 = ui.Chart.image.seriesByRegion(
   temp_2012, combined_eco, ee.Reducer.mean(), 'LST_Day_1km', 200, 'system:time_start',
'US_L3CODE')
       .setChartType('ScatterChart')
       .setOptions({
         title: 'Alaskan Ecoregion Average Surface Temperatures 2012',
         vAxis: {title: 'Surface Temperature'},
         lineWidth: 1,
         pointSize: 4,

         series: {
           0: {color: 'FF0000'}, // 1
           1: {color: '00FF00'}, // 2
           // 2: {color: '0000FF'}  NOTE: Additional colors automatically generated for extra regions
}});

// Display.
print(EcoRegion_surface_temp_2012);


var temp_2010 = temp8d
   .filterDate(startDate2010, endDate2010)


var EcoRegion_surface_temp_2010 = ui.Chart.image.seriesByRegion(
   temp_2010, combined_eco, ee.Reducer.mean(), 'LST_Day_1km', 200, 'system:time_start',
'US_L3CODE')
       .setChartType('ScatterChart')
       .setOptions({
         title: 'Alaskan Ecoregion Average Surface Temperatures 2010',
         vAxis: {title: 'Surface Temperature'},
         lineWidth: 1,
         pointSize: 4,

         series: {
           0: {color: 'FF0000'}, // 1
           1: {color: '00FF00'}, // 2
           // 2: {color: '0000FF'}  NOTE: Additional colors automatically generated for extra regions
}});

// Display.
print(EcoRegion_surface_temp_2010);
```

```
var temp_2008 = temp8d
   .filterDate(startDate2008, endDate2008)


var EcoRegion_surface_temp_2008 = ui.Chart.image.seriesByRegion(
   temp_2008, combined_eco, ee.Reducer.mean(), 'LST_Day_1km', 200, 'system:time_start',
'US_L3CODE')
       .setChartType('ScatterChart')
       .setOptions({
         title: 'Alaskan Ecoregion Average Surface Temperatures 2008',
         vAxis: {title: 'Surface Temperature'},
         lineWidth: 1,
         pointSize: 4,

         series: {
           0: {color: 'FF0000'}, // 1
           1: {color: '00FF00'}, // 2
           // 2: {color: '0000FF'}  NOTE: Additional colors automatically generated for extra regions
}});

// Display.
print(EcoRegion_surface_temp_2008);



var temp_2006 = temp8d
   .filterDate(startDate2006, endDate2006)


var EcoRegion_surface_temp_2006 = ui.Chart.image.seriesByRegion(
   temp_2006, combined_eco, ee.Reducer.mean(), 'LST_Day_1km', 200, 'system:time_start',
'US_L3CODE')
       .setChartType('ScatterChart')
       .setOptions({
         title: 'Alaskan Ecoregion Average Surface Temperatures 2006',
         vAxis: {title: 'Surface Temperature'},
         lineWidth: 1,
         pointSize: 4,

         series: {
           0: {color: 'FF0000'}, // 1
           1: {color: '00FF00'}, // 2
           // 2: {color: '0000FF'}  NOTE: Additional colors automatically generated for extra regions
}});
```

```
// Display.
print(EcoRegion_surface_temp_2006);


var temp_2004 = temp8d
   .filterDate(startDate2004, endDate2004)


var EcoRegion_surface_temp_2004 = ui.Chart.image.seriesByRegion(
   temp_2004, combined_eco, ee.Reducer.mean(), 'LST_Day_1km', 200, 'system:time_start',
'US_L3CODE')
       .setChartType('ScatterChart')
       .setOptions({
         title: 'Alaskan Ecoregion Average Surface Temperatures 2004',
         vAxis: {title: 'Surface Temperature'},
         lineWidth: 1,
         pointSize: 4,

         series: {
           0: {color: 'FF0000'}, // 1
           1: {color: '00FF00'}, // 2
           // 2: {color: '0000FF'}  NOTE: Additional colors automatically generated for extra regions
}});

// Display.
print(EcoRegion_surface_temp_2004);

var temp_2002 = temp8d
   .filterDate(startDate2002, endDate2002)


var EcoRegion_surface_temp_2002 = ui.Chart.image.seriesByRegion(
   temp_2002, combined_eco, ee.Reducer.mean(), 'LST_Day_1km', 200, 'system:time_start',
'US_L3CODE')
       .setChartType('ScatterChart')
       .setOptions({
         title: 'Alaskan Ecoregion Average Surface Temperatures 2002',
         vAxis: {title: 'Surface Temperature'},
         lineWidth: 1,
         pointSize: 4,

         series: {
           0: {color: 'FF0000'}, // 1
```

```
        1: {color: '00FF00'}, // 2
        // 2: {color: '0000FF'}  NOTE: Additional colors automatically generated for extra regions
}});

// Display.
print(EcoRegion_surface_temp_2002);


var temp_2000 = temp8d
   .filterDate(startDate2000, endDate2000)


var EcoRegion_surface_temp_2000 = ui.Chart.image.seriesByRegion(
   temp_2000, combined_eco, ee.Reducer.mean(), 'LST_Day_1km', 200, 'system:time_start',
'US_L3CODE')
      .setChartType('ScatterChart')
      .setOptions({
        title: 'Alaskan Ecoregion Average Surface Temperatures 2000',
        vAxis: {title: 'Surface Temperature'},
        lineWidth: 1,
        pointSize: 4,

        series: {
          0: {color: 'FF0000'}, // 1
          1: {color: '00FF00'}, // 2
          // 2: {color: '0000FF'}  NOTE: Additional colors automatically generated for extra regions
}});

// Display.
print(EcoRegion_surface_temp_2000);
```

Albedo Charts

```
var startDate2020 = '2020-03-01';
var endDate2020   = '2020-05-30';

var startDate2019 = '2019-03-01';
var endDate2019   = '2019-07-30';

var startDate2018 = '2018-03-01';
var endDate2018   = '2018-07-30';

var startDate2016 = '2016-03-01';
var endDate2016   = '2016-07-30';

var startDate2014 = '2014-03-01';
var endDate2014   = '2014-07-30';

var startDate2012 = '2012-03-01';
var endDate2012   = '2012-07-30';

var startDate2010 = '2010-03-01';
var endDate2010   = '2010-07-30';

var startDate2008 = '2008-03-01';
var endDate2008   = '2008-07-30';

var startDate2006 = '2006-03-01';
var endDate2006   = '2006-07-30';

var startDate2004 = '2004-03-01';
var endDate2004   = '2004-07-30';

var startDate2002 = '2002-03-01';
var endDate2002   = '2002-07-30';

var startDate2000 = '2000-03-01';
var endDate2000   = '2000-07-30';


// Load MODIS Albedo data for a month.
var BSA_collection2020 = ee.ImageCollection('MODIS/006/MCD43A3')
   .filterDate(startDate2020, endDate2020)

var BSA_collection2019 = ee.ImageCollection('MODIS/006/MCD43A3')
```

```
  .filterDate(startDate2019, endDate2019)

var BSA_collection2018 = ee.ImageCollection('MODIS/006/MCD43A3')
  .filterDate(startDate2018, endDate2018)

var BSA_collection2016 = ee.ImageCollection('MODIS/006/MCD43A3')
  .filterDate(startDate2016, endDate2016)

var BSA_collection2014 = ee.ImageCollection('MODIS/006/MCD43A3')
  .filterDate(startDate2014, endDate2014)

var BSA_collection2012 = ee.ImageCollection('MODIS/006/MCD43A3')
  .filterDate(startDate2012, endDate2012)

var BSA_collection2010 = ee.ImageCollection('MODIS/006/MCD43A3')
  .filterDate(startDate2010, endDate2010)

var BSA_collection2008 = ee.ImageCollection('MODIS/006/MCD43A3')
  .filterDate(startDate2008, endDate2008)

var BSA_collection2006 = ee.ImageCollection('MODIS/006/MCD43A3')
  .filterDate(startDate2006, endDate2006)

var BSA_collection2004 = ee.ImageCollection('MODIS/006/MCD43A3')
  .filterDate(startDate2004, endDate2004)

var BSA_collection2002 = ee.ImageCollection('MODIS/006/MCD43A3')
  .filterDate(startDate2002, endDate2002)

var BSA_collection2000 = ee.ImageCollection('MODIS/006/MCD43A3')
  .filterDate(startDate2000, endDate2000)


var eco_101 = ee.FeatureCollection(eco_full.filter(ee.Filter.eq('US_L3CODE', '101')))
var eco_102 = ee.FeatureCollection(eco_full.filter(ee.Filter.eq('US_L3CODE', '102')))
var eco_103 = ee.FeatureCollection(eco_full.filter(ee.Filter.eq('US_L3CODE', '103')))
var eco_104 = ee.FeatureCollection(eco_full.filter(ee.Filter.eq('US_L3CODE', '104')))
var eco_105 = ee.FeatureCollection(eco_full.filter(ee.Filter.eq('US_L3CODE', '105')))

var combined_eco =
eco_101.merge(eco_102).merge(eco_103).merge(eco_104).merge(eco_105);
```

```
var combined_eco101 =
eco_101_fid_0.merge(eco_101_fid_1).merge(eco_101_fid_2).merge(eco_101_fid_3).merge(ec
o_101_fid_4);

var regions = ak_101_105


//************************ Albedo time series chart Alaska Ecoregion 2016
var EcoRegion_Albedo_Histogram_2020 = ui.Chart.image.seriesByRegion(
   BSA_collection2020, combined_eco, ee.Reducer.mean(), 'Albedo_BSA_Band1', 200,
'system:time_start', 'US_L3CODE')
       .setChartType('ScatterChart')
       .setOptions({
         title: 'Alaskan Ecoregion Black Sky Albedo 2020',
         vAxis: {title: 'Black Sky Albedo'},
         lineWidth: 1,
         pointSize: 4,
         //labelSize: 20,
         series: {
           0: {color: 'FF0000'}, // 1
           1: {color: '00FF00'}, // 2
           // 2: {color: '0000FF'}  NOTE: Additional colors automatically generated for extra regions
}});

// Display.
print(EcoRegion_Albedo_Histogram_2020);

var EcoRegion_Albedo_Histogram_2019 = ui.Chart.image.seriesByRegion(
   BSA_collection2019, combined_eco, ee.Reducer.mean(), 'Albedo_BSA_Band1', 200,
'system:time_start', 'US_L3CODE')
       .setChartType('ScatterChart')
       .setOptions({
         title: 'Alaskan Ecoregion Black Sky Albedo 2019',
         vAxis: {title: 'Black Sky Albedo'},
         lineWidth: 1,
         pointSize: 4,
         //labelSize: 20,
         series: {
           0: {color: 'FF0000'}, // 1
           1: {color: '00FF00'}, // 2
           // 2: {color: '0000FF'}  NOTE: Additional colors automatically generated for extra regions
}});

// Display.
```

```
print(EcoRegion_Albedo_Histogram_2019);


var EcoRegion_Albedo_Histogram_2018 = ui.Chart.image.seriesByRegion(
   BSA_collection2018, combined_eco, ee.Reducer.mean(), 'Albedo_BSA_Band1', 200,
'system:time_start', 'US_L3CODE')
       .setChartType('ScatterChart')
       .setOptions({
         title: 'Alaskan Ecoregion Black Sky Albedo 2018',
         vAxis: {title: 'Black Sky Albedo'},
         lineWidth: 1,
         pointSize: 4,
         //labelSize: 20,
         series: {
           0: {color: 'FF0000'}, // 1
           1: {color: '00FF00'}, // 2
           // 2: {color: '0000FF'}  NOTE: Additional colors automatically generated for extra regions
}});

// Display.
print(EcoRegion_Albedo_Histogram_2018);


var EcoRegion_Albedo_Histogram_2016 = ui.Chart.image.seriesByRegion(
   BSA_collection2016, combined_eco, ee.Reducer.mean(), 'Albedo_BSA_Band1', 200,
'system:time_start', 'US_L3CODE')
       .setChartType('ScatterChart')
       .setOptions({
         title: 'Alaskan Ecoregion Black Sky Albedo 2016',
         vAxis: {title: 'Black Sky Albedo'},
         lineWidth: 1,
         pointSize: 4,
         //labelSize: 20,
         series: {
           0: {color: 'FF0000'}, // 1
           1: {color: '00FF00'}, // 2
           // 2: {color: '0000FF'}  NOTE: Additional colors automatically generated for extra regions
}});

// Display.
print(EcoRegion_Albedo_Histogram_2016);

// Albedo time series chart Alaska Ecoregion 2014
```

```
var EcoRegion_Albedo_Histogram_2014 = ui.Chart.image.seriesByRegion(
   BSA_collection2014, combined_eco, ee.Reducer.mean(), 'Albedo_BSA_Band1', 200,
'system:time_start', 'US_L3CODE')
       .setChartType('ScatterChart')
       .setOptions({
         title: 'Alaskan Ecoregion Black Sky Albedo 2014',
         vAxis: {title: 'Black Sky Albedo'},
         lineWidth: 1,
         pointSize: 4,
         series: {
           0: {color: 'FF0000'}, // 1
           1: {color: '00FF00'}, // 2
           // 2: {color: '0000FF'}  NOTE: Additional colors automatically generated for extra regions
}});

// Display.
print(EcoRegion_Albedo_Histogram_2014);

// Albedo time series chart Alaska Ecoregion 2012

var EcoRegion_Albedo_Histogram_2012 = ui.Chart.image.seriesByRegion(
   BSA_collection2012, combined_eco, ee.Reducer.mean(), 'Albedo_BSA_Band1', 200,
'system:time_start', 'US_L3CODE')
       .setChartType('ScatterChart')
       .setOptions({
         title: 'Alaskan Ecoregion Black Sky Albedo 2012',
         vAxis: {title: 'Black Sky Albedo'},
         lineWidth: 1,
         pointSize: 4,
         series: {
           0: {color: 'FF0000'}, // 1
           1: {color: '00FF00'}, // 2
           // 2: {color: '0000FF'}  NOTE: Additional colors automatically generated for extra regions
}});

// Display.
print(EcoRegion_Albedo_Histogram_2012);


// Albedo time series chart Alaska Ecoregion 2010

var EcoRegion_Albedo_Histogram_2010 = ui.Chart.image.seriesByRegion(
   BSA_collection2010, combined_eco, ee.Reducer.mean(), 'Albedo_BSA_Band1', 200,
'system:time_start', 'US_L3CODE')
```

```
      .setChartType('ScatterChart')
      .setOptions({
        title: 'Alaskan Ecoregion Black Sky Albedo 2010',
        vAxis: {title: 'Black Sky Albedo'},
        lineWidth: 1,
        pointSize: 4,
        series: {
          0: {color: 'FF0000'}, // 1
          1: {color: '00FF00'}, // 2
          // 2: {color: '0000FF'}  NOTE: Additional colors automatically generated for extra regions
}});

// Display.
print(EcoRegion_Albedo_Histogram_2010);


// Albedo time series chart Alaska Ecoregion 2008

var EcoRegion_Albedo_Histogram_2008 = ui.Chart.image.seriesByRegion(
   BSA_collection2008, combined_eco, ee.Reducer.mean(), 'Albedo_BSA_Band1', 200,
'system:time_start', 'US_L3CODE')
      .setChartType('ScatterChart')
      .setOptions({
        title: 'Alaskan Ecoregion Black Sky Albedo 2008',
        vAxis: {title: 'Black Sky Albedo'},
        lineWidth: 1,
        pointSize: 4,
        series: {
          0: {color: 'FF0000'}, // 1
          1: {color: '00FF00'}, // 2
          // 2: {color: '0000FF'}  NOTE: Additional colors automatically generated for extra regions
}});

// Display.
print(EcoRegion_Albedo_Histogram_2008);


// Albedo time series chart Alaska Ecoregion 2006

var EcoRegion_Albedo_Histogram_2006 = ui.Chart.image.seriesByRegion(
   BSA_collection2006, combined_eco, ee.Reducer.mean(), 'Albedo_BSA_Band1', 200,
'system:time_start', 'US_L3CODE')
      .setChartType('ScatterChart')
      .setOptions({
```

```
        title: 'Alaskan Ecoregion Black Sky Albedo 2006',
        vAxis: {title: 'Black Sky Albedo'},
        lineWidth: 1,
        pointSize: 4,
        series: {
          0: {color: 'FF0000'}, // 1
          1: {color: '00FF00'}, // 2
          // 2: {color: '0000FF'}  NOTE: Additional colors automatically generated for extra regions
}});

// Display.
print(EcoRegion_Albedo_Histogram_2006);

// Albedo time series chart Alaska Ecoregion 2004

var EcoRegion_Albedo_Histogram_2004 = ui.Chart.image.seriesByRegion(
   BSA_collection2004, combined_eco, ee.Reducer.mean(), 'Albedo_BSA_Band1', 200,
'system:time_start', 'US_L3CODE')
      .setChartType('ScatterChart')
      .setOptions({
        title: 'Alaskan Ecoregion Black Sky Albedo 2004',
        vAxis: {title: 'Black Sky Albedo'},
        lineWidth: 1,
        pointSize: 4,
        series: {
          0: {color: 'FF0000'}, // 1
          1: {color: '00FF00'}, // 2
          // 2: {color: '0000FF'}  NOTE: Additional colors automatically generated for extra regions
}});

// Display.
print(EcoRegion_Albedo_Histogram_2004);

// Albedo time series chart Alaska Ecoregion 2002

var EcoRegion_Albedo_Histogram_2002 = ui.Chart.image.seriesByRegion(
   BSA_collection2002, combined_eco, ee.Reducer.mean(), 'Albedo_BSA_Band1', 200,
'system:time_start', 'US_L3CODE')
      .setChartType('ScatterChart')
      .setOptions({
        title: 'Alaskan Ecoregion Black Sky Albedo 2002',
        vAxis: {title: 'Black Sky Albedo'},
        lineWidth: 1,
        pointSize: 4,
```

```
        series: {
          0: {color: 'FF0000'}, // 1
          1: {color: '00FF00'}, // 2
          // 2: {color: '0000FF'}  NOTE: Additional colors automatically generated for extra regions
}});

// Display.
print(EcoRegion_Albedo_Histogram_2002);

// Albedo time series chart Alaska Ecoregion 2000

var EcoRegion_Albedo_Histogram_2000 = ui.Chart.image.seriesByRegion(
   BSA_collection2000, combined_eco, ee.Reducer.mean(), 'Albedo_BSA_Band1', 200,
'system:time_start', 'US_L3CODE')
       .setChartType('ScatterChart')
       .setOptions({
         title: 'Alaskan Ecoregion Black Sky Albedo 2000',
         vAxis: {title: 'Black Sky Albedo'},
         lineWidth: 1,
         pointSize: 4,
         series: {
           0: {color: 'FF0000'}, // 1
           1: {color: '00FF00'}, // 2
           // 2: {color: '0000FF'}  NOTE: Additional colors automatically generated for extra regions
}});

// Display.
print(EcoRegion_Albedo_Histogram_2000);


//*************************************************************
```

Albedo Map Visualizations

```
var collection2020 = ee.ImageCollection('MODIS/006/MCD43A3')
              .filter(ee.Filter.date('2020-04-01', '2020-05-29'))



var blackSkyAlbedo2020 = collection2020.select('Albedo_BSA_Band1');
var blackSkyAlbedoVis = {
  min: 0.0,
  max: 1000.0, //
```

```
};

var clipped2020 = blackSkyAlbedo2020.mean().clip(combined_eco)


Map.addLayer(clipped2020, blackSkyAlbedoVis, 'BSA 2020'); //Working

var collection2019 = ee.ImageCollection('MODIS/006/MCD43A3')
                .filter(ee.Filter.date('2019-04-01', '2019-07-30'))



var blackSkyAlbedo2019 = collection2019.select('Albedo_BSA_Band1');
var blackSkyAlbedoVis = {
  min: 0.0,
  max: 1000.0, //
};

var clipped2019 = blackSkyAlbedo2019.mean().clip(combined_eco)


Map.addLayer(clipped2019, blackSkyAlbedoVis, 'BSA 2019'); //Working



var collection2018 = ee.ImageCollection('MODIS/006/MCD43A3')
                .filter(ee.Filter.date('2018-04-01', '2018-07-30'))



var blackSkyAlbedo2018 = collection2018.select('Albedo_BSA_Band1');
var blackSkyAlbedoVis = {
  min: 0.0,
  max: 1000.0, //
};

var clipped2018 = blackSkyAlbedo2018.mean().clip(combined_eco)

Map.addLayer(clipped2018, blackSkyAlbedoVis, 'BSA 2018'); //Working


// Black Sky Albedo Map Viz 2016

var collection2016 = ee.ImageCollection('MODIS/006/MCD43A3')
```

```
            .filter(ee.Filter.date('2016-04-01', '2016-07-30'))


var blackSkyAlbedo2016 = collection2016.select('Albedo_BSA_Band1');
var blackSkyAlbedoVis = {
  min: 0.0,
  max: 1000.0, //
};

var clipped2016 = blackSkyAlbedo2016.mean().clip(combined_eco)


Map.addLayer(clipped2016, blackSkyAlbedoVis, 'BSA 2016'); //Working


// Black Sky Albedo Map Viz 2014

var collection2014 = ee.ImageCollection('MODIS/006/MCD43A3')
            .filter(ee.Filter.date('2014-04-01', '2014-07-30'))



var blackSkyAlbedo2014 = collection2014.select('Albedo_BSA_Band1');
var blackSkyAlbedoVis = {
  min: 0.0,
  max: 1000.0, //
};

var clipped2014 = blackSkyAlbedo2014.mean().clip(combined_eco)


Map.addLayer(clipped2014, blackSkyAlbedoVis, 'BSA 2014'); //Working



//BSA Map Viz 2012
var collection2012 = ee.ImageCollection('MODIS/006/MCD43A3')
            .filter(ee.Filter.date('2012-04-01', '2012-07-30'))


var blackSkyAlbedo2012 = collection2012.select('Albedo_BSA_Band1');
var blackSkyAlbedoVis = {
```

```
  min: 0.0,
  max: 1000.0, //
};

var clipped2012 = blackSkyAlbedo2012.mean().clip(combined_eco)


Map.addLayer(clipped2012, blackSkyAlbedoVis, 'BSA 2012'); //Working


//BSA Map Viz 2010
var collection2010 = ee.ImageCollection('MODIS/006/MCD43A3')
                .filter(ee.Filter.date('2010-04-01', '2010-07-30'))



var blackSkyAlbedo2010 = collection2010.select('Albedo_BSA_Band1');
var blackSkyAlbedoVis = {
  min: 0.0,
  max: 1000.0, //
};

var clipped2010 = blackSkyAlbedo2010.mean().clip(combined_eco)


Map.addLayer(clipped2010, blackSkyAlbedoVis, 'BSA 2010'); //Working

//BSA Map Viz 2008
var collection2008 = ee.ImageCollection('MODIS/006/MCD43A3')
                .filter(ee.Filter.date('2008-04-01', '2008-07-30'))


var blackSkyAlbedo2008 = collection2008.select('Albedo_BSA_Band1');
var blackSkyAlbedoVis = {
  min: 0.0,
  max: 1000.0, //
};

var clipped2008 = blackSkyAlbedo2008.mean().clip(combined_eco)


Map.addLayer(clipped2008, blackSkyAlbedoVis, 'BSA 2008'); //Working

//BSA Map Viz 2006
```

```
var collection2006 = ee.ImageCollection('MODIS/006/MCD43A3')
                .filter(ee.Filter.date('2006-04-01', '2006-07-30'))


var blackSkyAlbedo2006 = collection2006.select('Albedo_BSA_Band1');
var blackSkyAlbedoVis = {
  min: 0.0,
  max: 1000.0, //
};

var clipped2006 = blackSkyAlbedo2006.mean().clip(combined_eco)


Map.addLayer(clipped2006, blackSkyAlbedoVis, 'BSA 2006'); //Working

//BSA Map Viz 2004
var collection2004 = ee.ImageCollection('MODIS/006/MCD43A3')
                .filter(ee.Filter.date('2004-04-01', '2004-07-30'))


var blackSkyAlbedo2004 = collection2004.select('Albedo_BSA_Band1');
var blackSkyAlbedoVis = {
  min: 0.0,
  max: 1000.0, //
};

var clipped2004 = blackSkyAlbedo2004.mean().clip(combined_eco)

Map.addLayer(clipped2004, blackSkyAlbedoVis, 'BSA 2004'); //Working

//BSA Map Viz 2002
var collection2002 = ee.ImageCollection('MODIS/006/MCD43A3')
                .filter(ee.Filter.date('2002-04-01', '2002-07-30'))


var blackSkyAlbedo2002 = collection2002.select('Albedo_BSA_Band1');
var blackSkyAlbedoVis = {
  min: 0.0,
  max: 1000.0, //
};

var clipped2002 = blackSkyAlbedo2002.mean().clip(combined_eco)

Map.addLayer(clipped2002, blackSkyAlbedoVis, 'BSA 2002'); //Working
```

```
//BSA Map Viz 2000
var collection2000 = ee.ImageCollection('MODIS/006/MCD43A3')
                .filter(ee.Filter.date('2000-04-01', '2000-07-30'))


var blackSkyAlbedo2000 = collection2000.select('Albedo_BSA_Band1');
var blackSkyAlbedoVis = {
  min: 0.0,
  max: 1000.0, //
};

var clipped2000 = blackSkyAlbedo2000.mean().clip(combined_eco)

Map.addLayer(clipped2000, blackSkyAlbedoVis, 'BSA 2000'); //Working
```

NDVI Charts

```
var startDate2020 = '2020-03-01';
var endDate2020   = '2020-05-30';

var startDate2019 = '2020-03-01';
var endDate2019   = '2020-05-30';

var startDate2018 = '2018-03-01';
var endDate2018   = '2018-07-30';

var startDate2016 = '2016-03-01';
var endDate2016   = '2016-07-30';

var startDate2014 = '2014-03-01';
var endDate2014   = '2014-07-30';

var startDate2012 = '2012-03-01';
var endDate2012   = '2012-07-30';

var startDate2010 = '2010-03-01';
var endDate2010   = '2010-07-30';

var startDate2008 = '2008-03-01';
var endDate2008   = '2008-07-30';
```

```
var startDate2006 = '2006-03-01';
var endDate2006   = '2006-07-30';

var startDate2004 = '2004-03-01';
var endDate2004   = '2004-07-30';

var startDate2002 = '2002-03-01';
var endDate2002   = '2002-07-30';

var startDate2000 = '2000-03-01';
var endDate2000   = '2000-07-30';


// Load MODIS Albedo data for a month.

var eco_101 = ee.FeatureCollection(ak_101_105.filter(ee.Filter.eq('US_L3CODE', '101')))
var eco_102 = ee.FeatureCollection(ak_101_105.filter(ee.Filter.eq('US_L3CODE', '102')))
var eco_103 = ee.FeatureCollection(ak_101_105.filter(ee.Filter.eq('US_L3CODE', '103')))
var eco_104 = ee.FeatureCollection(ak_101_105.filter(ee.Filter.eq('US_L3CODE', '104')))
var eco_105 = ee.FeatureCollection(ak_101_105.filter(ee.Filter.eq('US_L3CODE', '105')))

var combined_eco =
eco_101.merge(eco_102).merge(eco_103).merge(eco_104).merge(eco_105);

var regions = ak_101_105

var m_veg_2020 = m_veg.filter(ee.Filter.date('2020-03-01', '2020-07-30'));
var m_veg_2019 = m_veg.filter(ee.Filter.date('2019-03-01', '2019-07-30'));
var m_veg_2018 = m_veg.filter(ee.Filter.date('2018-03-01', '2018-07-30'));
var m_veg_2016 = m_veg.filter(ee.Filter.date('2016-03-01', '2016-07-30'));
var m_veg_2014 = m_veg.filter(ee.Filter.date('2014-03-01', '2014-07-30'));
var m_veg_2012 = m_veg.filter(ee.Filter.date('2012-03-01', '2012-07-30'));
var m_veg_2010 = m_veg.filter(ee.Filter.date('2010-03-01', '2010-07-30'));
var m_veg_2008 = m_veg.filter(ee.Filter.date('2008-03-01', '2008-07-30'));
var m_veg_2006 = m_veg.filter(ee.Filter.date('2006-03-01', '2006-07-30'));
var m_veg_2004 = m_veg.filter(ee.Filter.date('2004-03-01', '2004-07-30'));
var m_veg_2002 = m_veg.filter(ee.Filter.date('2002-03-01', '2002-07-30'));
var m_veg_2000 = m_veg.filter(ee.Filter.date('2000-03-01', '2000-07-30'));


var NDVI_Merge2020_TimeSeriesChart = ui.Chart.image.seriesByRegion(
   m_veg_2020, eco_merge, ee.Reducer.mean(), 'NDVI', 250, undefined, 'US_L3CODE')
      .setChartType('ScatterChart')
      .setOptions({
```

```
        title: 'NDVI by Ecoregion, 2020',
        vAxis: {title: 'NDVI'},
        lineWidth: 1,
        pointSize: 4,
        series: {
          0: {color: 'FF0000'},
          1: {color: '00FF00'},

}});
print(NDVI_Merge2020_TimeSeriesChart);

var NDVI_Merge2019_TimeSeriesChart = ui.Chart.image.seriesByRegion(
   m_veg_2019, eco_merge, ee.Reducer.mean(), 'NDVI', 250, undefined, 'US_L3CODE')
      .setChartType('ScatterChart')
      .setOptions({
        title: 'NDVI by Ecoregion, 2019',
        vAxis: {title: 'NDVI'},
        lineWidth: 1,
        pointSize: 4,
        series: {
          0: {color: 'FF0000'},
          1: {color: '00FF00'},

}});
print(NDVI_Merge2019_TimeSeriesChart);

var NDVI_Merge2018_TimeSeriesChart = ui.Chart.image.seriesByRegion(
   m_veg_2018, eco_merge, ee.Reducer.mean(), 'NDVI', 250, undefined, 'US_L3CODE')
      .setChartType('ScatterChart')
      .setOptions({
        title: 'NDVI by Ecoregion, 2018',
        vAxis: {title: 'NDVI'},
        lineWidth: 1,
        pointSize: 4,
        series: {
          0: {color: 'FF0000'},
          1: {color: '00FF00'},

}});
print(NDVI_Merge2018_TimeSeriesChart);

var NDVI_Merge2016_TimeSeriesChart = ui.Chart.image.seriesByRegion(
   m_veg_2016, eco_merge, ee.Reducer.mean(), 'NDVI', 250, undefined, 'US_L3CODE')
      .setChartType('ScatterChart')
```

```
      .setOptions({
        title: 'NDVI by Ecoregion, 2016',
        vAxis: {title: 'NDVI'},
        lineWidth: 1,
        pointSize: 4,
        series: {
          0: {color: 'FF0000'},
          1: {color: '00FF00'},

}});
print(NDVI_Merge2016_TimeSeriesChart);

var NDVI_Merge2014_TimeSeriesChart = ui.Chart.image.seriesByRegion(
   m_veg_2014, eco_merge, ee.Reducer.mean(), 'NDVI', 250, undefined, 'US_L3CODE')
      .setChartType('ScatterChart')
      .setOptions({
        title: 'NDVI by Ecoregion, 2014',
        vAxis: {title: 'NDVI'},
        lineWidth: 1,
        pointSize: 4,
        series: {
          0: {color: 'FF0000'},
          1: {color: '00FF00'},

}});
print(NDVI_Merge2014_TimeSeriesChart);

var NDVI_Merge2012_TimeSeriesChart = ui.Chart.image.seriesByRegion(
   m_veg_2012, eco_merge, ee.Reducer.mean(), 'NDVI', 250, undefined, 'US_L3CODE')
      .setChartType('ScatterChart')
      .setOptions({
        title: 'NDVI by Ecoregion, 2012',
        vAxis: {title: 'NDVI'},
        lineWidth: 1,
        pointSize: 4,
        series: {
          0: {color: 'FF0000'},
          1: {color: '00FF00'},
}});
print(NDVI_Merge2012_TimeSeriesChart);

var NDVI_Merge2010_TimeSeriesChart = ui.Chart.image.seriesByRegion(
   m_veg_2010, eco_merge, ee.Reducer.mean(), 'NDVI', 250, undefined, 'US_L3CODE')
      .setChartType('ScatterChart')
```

```
      .setOptions({
        title: 'NDVI by Ecoregion, 2010',
        vAxis: {title: 'NDVI'},
        lineWidth: 1,
        pointSize: 4,
        series: {
          0: {color: 'FF0000'},
          1: {color: '00FF00'},
}});
print(NDVI_Merge2010_TimeSeriesChart);

var NDVI_Merge2008_TimeSeriesChart = ui.Chart.image.seriesByRegion(
   m_veg_2008, eco_merge, ee.Reducer.mean(), 'NDVI', 250, undefined, 'US_L3CODE')
      .setChartType('ScatterChart')
      .setOptions({
        title: 'NDVI by Ecoregion, 2008',
        vAxis: {title: 'NDVI'},
        lineWidth: 1,
        pointSize: 4,
        series: {
          0: {color: 'FF0000'},
          1: {color: '00FF00'},
}});
print(NDVI_Merge2008_TimeSeriesChart);

var NDVI_Merge2006_TimeSeriesChart = ui.Chart.image.seriesByRegion(
   m_veg_2006, eco_merge, ee.Reducer.mean(), 'NDVI', 250, undefined, 'US_L3CODE')
      .setChartType('ScatterChart')
      .setOptions({
        title: 'NDVI by Ecoregion, 2006',
        vAxis: {title: 'NDVI'},
        lineWidth: 1,
        pointSize: 4,
        series: {
          0: {color: 'FF0000'},
          1: {color: '00FF00'},

}});
print(NDVI_Merge2006_TimeSeriesChart);

var NDVI_Merge2004_TimeSeriesChart = ui.Chart.image.seriesByRegion(
   m_veg_2004, eco_merge, ee.Reducer.mean(), 'NDVI', 250, undefined, 'US_L3CODE')
      .setChartType('ScatterChart')
      .setOptions({
```

```
        title: 'NDVI by Ecoregion, 2004',
        vAxis: {title: 'NDVI'},
        lineWidth: 1,
        pointSize: 4,
        series: {
          0: {color: 'FF0000'},
          1: {color: '00FF00'},

}});
print(NDVI_Merge2004_TimeSeriesChart);

var NDVI_Merge2002_TimeSeriesChart = ui.Chart.image.seriesByRegion(
   m_veg_2002, eco_merge, ee.Reducer.mean(), 'NDVI', 250, undefined, 'US_L3CODE')
      .setChartType('ScatterChart')
      .setOptions({
        title: 'NDVI by Ecoregion, 2002',
        vAxis: {title: 'NDVI'},
        lineWidth: 1,
        pointSize: 4,
        series: {
          0: {color: 'FF0000'},
          1: {color: '00FF00'},

}});
print(NDVI_Merge2002_TimeSeriesChart);

var NDVI_Merge2000_TimeSeriesChart = ui.Chart.image.seriesByRegion(
   m_veg_2000, eco_merge, ee.Reducer.mean(), 'NDVI', 250, undefined, 'US_L3CODE')
      .setChartType('ScatterChart')
      .setOptions({
        title: 'NDVI by Ecoregion, 2000',
        vAxis: {title: 'NDVI'},
        lineWidth: 1,
        pointSize: 4,
        series: {
          0: {color: 'FF0000'},
          1: {color: '00FF00'},

}});
print(NDVI_Merge2000_TimeSeriesChart);

//*************************************************************************
```

NDVI Map Visualizations

```
//NDVI Time Series Map Viz 2020


var dataset2020 = m_veg.filter(ee.Filter.date('2020-04-01', '2020-06-30'));



var ndvi = dataset2020.select('NDVI');

var ndviVis_v1 = {
  min: -2000.0,
  max: 10000.0,
  palette: [
    'FFFFFF', 'CE7E45', 'DF923D', 'F1B555', 'FCD163', '99B718', '74A901',
    '66A000', '529400', '3E8601', '207401', '056201', '004C00', '023B01',
    '012E01', '011D01', '011301'
  ],
};


var clipped0 = ndvi.mean().clip(eco_104)

Map.addLayer(clipped0, ndviVis_v1, 'NDVI 2020');

var dataset2019 = m_veg.filter(ee.Filter.date('2019-04-01', '2019-07-30'));



var ndvi = dataset2018.select('NDVI');

var ndviVis_v1 = {
  min: -2000.0,
  max: 10000.0,
  palette: [
    'FFFFFF', 'CE7E45', 'DF923D', 'F1B555', 'FCD163', '99B718', '74A901',
    '66A000', '529400', '3E8601', '207401', '056201', '004C00', '023B01',
    '012E01', '011D01', '011301'
  ],
};
```

```
var clipped0 = ndvi.mean().clip(eco_104)

Map.addLayer(clipped0, ndviVis_v1, 'NDVI 2018'); // WORKING


var dataset2018 = m_veg.filter(ee.Filter.date('2018-04-01', '2018-07-30'));



var ndvi = dataset2018.select('NDVI');

var ndviVis_v1 = {
  min: -2000.0,
  max: 10000.0,
  palette: [
    'FFFFFF', 'CE7E45', 'DF923D', 'F1B555', 'FCD163', '99B718', '74A901',
    '66A000', '529400', '3E8601', '207401', '056201', '004C00', '023B01',
    '012E01', '011D01', '011301'
  ],
};



var clipped0 = ndvi.mean().clip(eco_104)

Map.addLayer(clipped0, ndviVis_v1, 'NDVI 2018'); // WORKING

//NDVI Time Series Map Viz 2016

var dataset2016 = ee.ImageCollection('MODIS/MOD13A1')
                  .filter(ee.Filter.date('2016-04-01', '2016-07-30'));

var ndvi = dataset2016.select('NDVI');

var ndviVis_v1 = {
  min: -2000.0,
  max: 10000.0,
  palette: [
    'FFFFFF', 'CE7E45', 'DF923D', 'F1B555', 'FCD163', '99B718', '74A901',
    '66A000', '529400', '3E8601', '207401', '056201', '004C00', '023B01',
    '012E01', '011D01', '011301'
  ],
};
```

```
var clipped0 = ndvi.mean().clip(combined_eco)

Map.addLayer(clipped0, ndviVis_v1, 'NDVI 2016');


//**************NDVI Time Series Map Viz 2014

var dataset2014 = ee.ImageCollection('MODIS/006/MOD13A1')
                .filter(ee.Filter.date('2014-04-01', '2014-07-30'));

var ndvi = dataset2014.select('NDVI');

var ndviVis_v1 = {
  min: -2000.0,
  max: 10000.0,
  palette: [
    'FFFFFF', 'CE7E45', 'DF923D', 'F1B555', 'FCD163', '99B718', '74A901',
    '66A000', '529400', '3E8601', '207401', '056201', '004C00', '023B01',
    '012E01', '011D01', '011301'
  ],
};


var clipped0 = ndvi.mean().clip(combined_eco)

Map.addLayer(clipped0, ndviVis_v1, 'NDVI 2014');

//************************************NDVI Time Series Map Viz 2012

var dataset2012 = ee.ImageCollection('MODIS/006/MOD13A1')
                .filter(ee.Filter.date('2012-04-01', '2012-07-30'));

var ndvi = dataset2012.select('NDVI');

var ndviVis_v1 = {
  min: -2000.0,
  max: 10000.0,
  palette: [
    'FFFFFF', 'CE7E45', 'DF923D', 'F1B555', 'FCD163', '99B718', '74A901',
    '66A000', '529400', '3E8601', '207401', '056201', '004C00', '023B01',
    '012E01', '011D01', '011301'
  ],
};
```

```
var clipped0 = ndvi.mean().clip(combined_eco)

Map.addLayer(clipped0, ndviVis_v1, 'NDVI 2012'); // WORKING

//************************************NDVI Time Series Map Viz 2010

var dataset2010 = ee.ImageCollection('MODIS/006/MOD13A1')
                .filter(ee.Filter.date('2010-04-01', '2010-07-30'));

var ndvi = dataset2010.select('NDVI');

var ndviVis_v1 = {
  min: -2000.0,
  max: 10000.0,
  palette: [
    'FFFFFF', 'CE7E45', 'DF923D', 'F1B555', 'FCD163', '99B718', '74A901',
    '66A000', '529400', '3E8601', '207401', '056201', '004C00', '023B01',
    '012E01', '011D01', '011301'
  ],
};


var clipped0 = ndvi.mean().clip(combined_eco)

Map.addLayer(clipped0, ndviVis_v1, 'NDVI 2010'); // WORKING

//************************************NDVI Time Series Map Viz 2008

var dataset2008 = ee.ImageCollection('MODIS/006/MOD13A1')
                .filter(ee.Filter.date('2008-04-01', '2008-07-30'));

var ndvi = dataset2008.select('NDVI');

var ndviVis_v1 = {
  min: -2000.0,
  max: 10000.0,
  palette: [
    'FFFFFF', 'CE7E45', 'DF923D', 'F1B555', 'FCD163', '99B718', '74A901',
    '66A000', '529400', '3E8601', '207401', '056201', '004C00', '023B01',
    '012E01', '011D01', '011301'
  ],
};
```

```
var clipped0 = ndvi.mean().clip(combined_eco)

Map.addLayer(clipped0, ndviVis_v1, 'NDVI 2008');

//************************************NDVI Time Series Map Viz 2006

var dataset2006 = ee.ImageCollection('MODIS/006/MOD13A1')
                .filter(ee.Filter.date('2006-04-01', '2006-07-30'));

var ndvi = dataset2006.select('NDVI');

var ndviVis_v1 = {
  min: -2000.0,
  max: 10000.0,
  palette: [
    'FFFFFF', 'CE7E45', 'DF923D', 'F1B555', 'FCD163', '99B718', '74A901',
    '66A000', '529400', '3E8601', '207401', '056201', '004C00', '023B01',
    '012E01', '011D01', '011301'
  ],
};


var clipped0 = ndvi.mean().clip(combined_eco)

Map.addLayer(clipped0, ndviVis_v1, 'NDVI 2006');

//************************************NDVI Time Series Map Viz 2004

var dataset2004 = ee.ImageCollection('MODIS/006/MOD13A1')
                .filter(ee.Filter.date('2004-04-01', '2004-07-30'));

var ndvi = dataset2004.select('NDVI');

var ndviVis_v1 = {
  min: -2000.0,
  max: 10000.0,
  palette: [
    'FFFFFF', 'CE7E45', 'DF923D', 'F1B555', 'FCD163', '99B718', '74A901',
    '66A000', '529400', '3E8601', '207401', '056201', '004C00', '023B01',
    '012E01', '011D01', '011301'
  ],
};
```

```
var clipped0 = ndvi.mean().clip(combined_eco)

Map.addLayer(clipped0, ndviVis_v1, 'NDVI 2004'); // WORKING

//************************************NDVI Time Series Map Viz 2002

var dataset2002 = ee.ImageCollection('MODIS/006/MOD13A1')
                .filter(ee.Filter.date('2002-04-01', '2002-07-30'));

var ndvi = dataset2002.select('NDVI');

var ndviVis_v1 = {
  min: -2000.0,
  max: 10000.0,
  palette: [
    'FFFFFF', 'CE7E45', 'DF923D', 'F1B555', 'FCD163', '99B718', '74A901',
    '66A000', '529400', '3E8601', '207401', '056201', '004C00', '023B01',
    '012E01', '011D01', '011301'
  ],
};


var clipped0 = ndvi.mean().clip(combined_eco)

Map.addLayer(clipped0, ndviVis_v1, 'NDVI 2002'); // WORKING

//************************************NDVI Time Series Map Viz 2000

var dataset2000 = ee.ImageCollection('MODIS/006/MOD13A1')
                .filter(ee.Filter.date('2000-04-01', '2000-07-30'));

var ndvi = dataset2000.select('NDVI');

var ndviVis_v1 = {
  min: -2000.0,
  max: 10000.0,
  palette: [
    'FFFFFF', 'CE7E45', 'DF923D', 'F1B555', 'FCD163', '99B718', '74A901',
    '66A000', '529400', '3E8601', '207401', '056201', '004C00', '023B01',
    '012E01', '011D01', '011301'
  ],
};
```

```
var clipped0 = ndvi.mean().clip(combined_eco)

Map.addLayer(clipped0, ndviVis_v1, 'NDVI 2000');
```

Postscript

You who have lived in the land,
You who have trusted the trail,
You who are strong to withstand,
You who are swift to assail:
Songs have I sung to beguile,
Vintage of desperate years,
Hard as a harlot's smile,
Bitter as unshed tears.

Little of joy or mirth,
Little of ease I sing;
Sagas of men of earth
Humanly suffering,
Such as you all have done;
Savagely faring forth,
Sons of the midnight sun,
Argonauts of the North.

Far in the land God forgot
Glimmers the lure of your trail;
Still in your lust are you taught
Even to win is to fail.
Still you must follow and fight
Under the vampire wing;
There in the long, long night
Hoping and vanquishing.

Husbandman of the Wild,
Reaping a barren gain;
Scourged by desire, reconciled
Unto disaster and pain;
These, my songs, are for you,
You who are seared with the brand.
God knows I have tried to be true;
Please God you will understand.

—Robert W. Service (L'Envoi, 1907)